Start-up Optimization of Uniper RoCa3 Power Station

Alessandro Nannarone

TU Delft

Start-up Optimization of Uniper RoCa3 Power Station

by

A. Nannarone

to obtain the degree of Master of Science
at the Delft University of Technology,
to be defended publicly on Monday October 30, 2017 at 01:30 PM.

Student number:	4509048	
Project duration:	November 28, 2016 – October 30, 2017	
Thesis committee:	Prof. dr. ir. S. A. Klein,	TU Delft, supervisor
	Prof. dr. ir. B. J. Boersma,	TU Delft
	Dr. ir. R. Pecnik,	TU Delft
	Dr. ir. M. Langelaar,	TU Delft
	Ing. J. J. Honcoop,	Uniper Benelux N.V.

This thesis is confidential and cannot be made public until April 30, 2017.

TU Delft

Abstract

The rapid growth of renewable generation has modified the role of combined cycle power stations in the energy industry. Due to the strong increase of intermittent renewable sources, (solar, wind) the key feature for the operational excellence of combined cycle power stations is flexibility. In particular, the capability to start an installation quickly and efficiently after a shutdown period leads to lower operational cost and a higher capacity factor. However, most of existing thermal power stations worldwide are designed for continuous operation, with no special focus on an efficient start-up process.

In most current start-up procedures the GT controls ensure maximum heat flow to the HRSG, without feedback from the steam cycle. The steam cycle start-up controls work independently, with as main control parameter: the limitation of the thermal stresses in the steam turbine rotor. In this paper, a novel philosophy for the start-up optimization of an existing 200 MW CCGT power station is presented. In this new start-up procedure, a feedback loop is established between the steam turbine, the boiler and the gas turbine start-up controls. This feedback loop ensures that the steam turbine can be started up more quickly together with a significant reduction in stresses.

The methodology implied the creation of a flexible and accurate dynamic model in the Simulink^{TM} environment. The full detailed model consists of more than 100 component blocks (heat exchangers, valves, meters and sensors, turbines, controls etc). The mathematical submodels in the component blocks are mainly based on physical models and for a lesser part on experimental correlations. This makes the model generally applicable to other power plant installations. The model was validated against real process data related to the three start-up types (cold start, warm start, hot start). The start up model was extended in order to establish feedback loops between the steam cycle, boiler and gas turbine start-up controls. These feedback loops control for example the exit temperature of the gas turbine based on the actual steam turbine housing temperature, resulting in a smoother heating up of the steam turbine.

The extended model was used to define the optimal trends for the most important operating variables for cold and warm start-up types. These optimization actions were tested real power station start-ups, leading to a start-up time reduction of more than 30%, and a reduction in thermal stresses above 10% for cold starts.

Acknowledgements

First of all, I would like to thank my supervisor, Prof. Sikke Klein, for the guidance he has given me during these 11 months. I consider myself lucky to have worked with such a talented researcher and manager, whom I will always consider as an example for my professional career.

I am also truly grateful to my company supervisor, Ing. Jacques Honcoop, for the opportunity he gave concerning this master thesis project, and for his support in my daily life at Uniper Benelux. His trust on my potential strongly motivated me in putting all my efforts in this project, in order to obtain the best results and exceed his initial expectations. Furthermore, I would like to express my deepest appreciation to all the people of Uniper Benelux, who made this experience fantastic under any point of view. No words can describe how much I have learnt as a member of the Uniper family, and they have played an important role in my personal and professional growth.

I would also like to thank the other members of my Master's Exam committee, Prof. Bendiks Jan Boersma, Dr. Rene Pecnik, and Dr. Matthijs Langelaar, for the time they will spend in reading this report, and assessing my preparation in my thesis defense.

In the end, I would like to express my gratitude to all the people who have supported me in these two years journey at TU Delft. To them I dedicate this project, and every success I can achieve in my life.

Contents

1 Introduction

1.0.1. Changes in the world of energy

The increasing penetration of renewable energy to the power market is reshaping the role of the combined cycle gas turbine (CCGT) technology in the industry. The variable costs of renewable systems are lower, due to the absence of fuel costs, making combined cycle installations less competitive. However, as soon as the sky becomes dark and no wind is available, combined cycle power stations are asked to go online or ramp up, in order to supply the power previously produced by renewables. As an example, Figure 1.1 depicts the load trends by source in California, USA, on April 9^{th} 2017 [1]. During the day, the PV systems account for nearly half of the total load, and only the cheapest power stations run with profit. As soon as the sunlight starts reducing, more power is requested from thermal generation: the base-load plants are quickly ramped up, and the ones previously in shut-down are started. This new operational strategy is called cycling, and it relies on the capability of thermal installations to adapt to the power market. The total and thermal generation load curves resemble a duck profile, whose size increases on varying of the renewables penetration in the region.

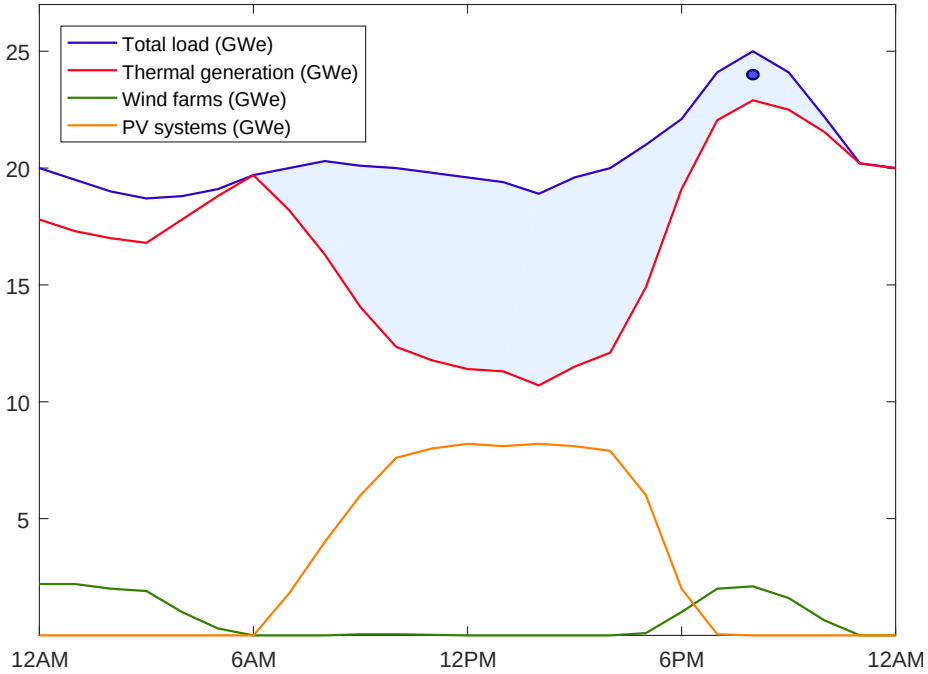

Figure 1.1: Load and supply curves for California, USA, on April 9^{th} 2017

1.0.2. Research questions

In the new energy world, the key for the operational excellence of CCGT power stations is flexibility. In particular, the high operational cost leads to frequent shut-downs of the installations, and the attention is accordingly focused on how long they take to go back supplying power to the grid. This period, also known as start-up time, is very important for the profitable operation of combined cycle power stations, since installations characterized by shortest start-up time can adapt quicker to the market and remain competitive. However, most of CCGT installations worldwide are designed for a base-load operation, which involves just few start-ups during a year. In The Netherlands, many utility companies currently focus their attention on this operational issue, by investing time and resources on the start-up optimization of their combined cycle power stations. Among these companies, Uniper Benelux was motivated to carry out an optimization of its largest installation, Uniper RoCa3, depicted in Figure 1.2.

Figure 1.2: Uniper RoCa3 power station in 2013 (E.ON RoCa3 prior to 2016)

The aim of the start-up process is to bring the installation from standstill to minimum part-load operation. This implies the gradual heating up of the equipments until their operational temperature. Being designed as a base-load power station, the control systems carry out the start-up process according to an old, standard procedure. As a result, the start-up time due to several bottlenecks concerning the control setpoints of the main operational variables. Furthermore, the heating up leads to the generation of thermal stress in the materials, which has to be controlled in order to prevent the necessary slowing down of the process. As a consequence, the research questions accordingly address the previous problems, and they are presented in the list provided below.

1. Identify the bottlenecks which hinder a fast start-up for the RoCa3 power station;
2. Develop and test potential optimization actions within the control systems capability;
3. Conceive and assess innovative start-up strategies as recommendations for future optimization.

1.0.3. Methodology

The methodology used to carry out the RoCa3 start-up optimization embraces multiple stages, as shown in Figure 1.3. Real start-up processes are monitored real-time from the control room together with process operators, kept involved in the work from beginning to end. The physical reality within the components of the power station is thoroughly analysed. In this way, it is possible to study and understand the dynamics of all the transients involved in the process, and to identify the bottlenecks to be solved. Meanwhile, the multi-domain dynamic modelling of the RoCa3 installation is carried out, capable to reproduce the start-up process in an accurate and reliable way. The RoCa3 model is validated against real process data, and is extended in order to be used as optimization tool. Based on the start-up analysis and extended model results, a set of potential optimization actions is identified and tested in real start-ups, and the impact of innovative start-up strategies is evaluated.

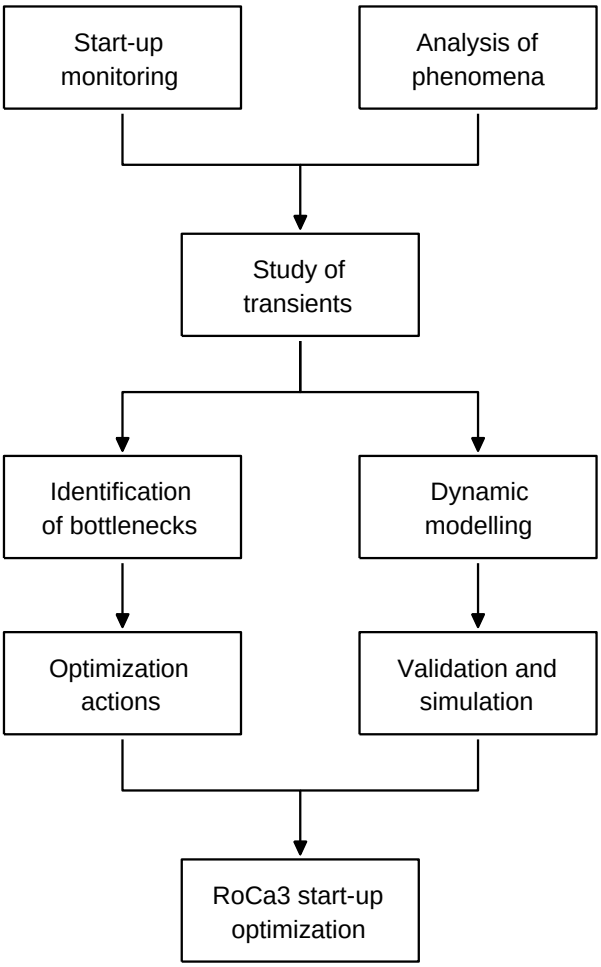

Figure 1.3: Methodology used for the RoCa3 start-up optimization

1.0.4. Chapters summary

The present report includes 5 Chapters. After the introduction presented in this Chapter, the RoCa3 start-up process is analysed in Chapter 2, providing also the theory and the description of the installation. Chapter 3 describes the modelling of the power station, the implementation to the Simulink^{TM} software and the validation results. Chapter 4 deals with the start-up optimization, presenting the optimization actions proposed and the significant results achieved in terms of start-up time, fuel consumption, and stress reduction. In the end, the conclusions of the work are included in Chapter 5.

2

RoCa3 Start-up Process

2.1. Theory

Before introducing the start-up process of the existing installation, it is important to briefly describe the thermodynamic cycles according to which the power station operates. For a more specific description of the combined cycles theory, the reader can refer to [].

2.1.1. The Joule-Brayton cycle

The Joule-Brayton cycle is the reference cycle of gas turbine engines. The working fluid is air, which is continuously drawn from the environment and discharged back into it in the form of flue gas. The cycle is open, and it consists of four thermodynamic processes: air compression (a-b), heat addition (b-c), flue gas expansion (c-d) and heat discharge (d-a), as shown in Figure 2.1.

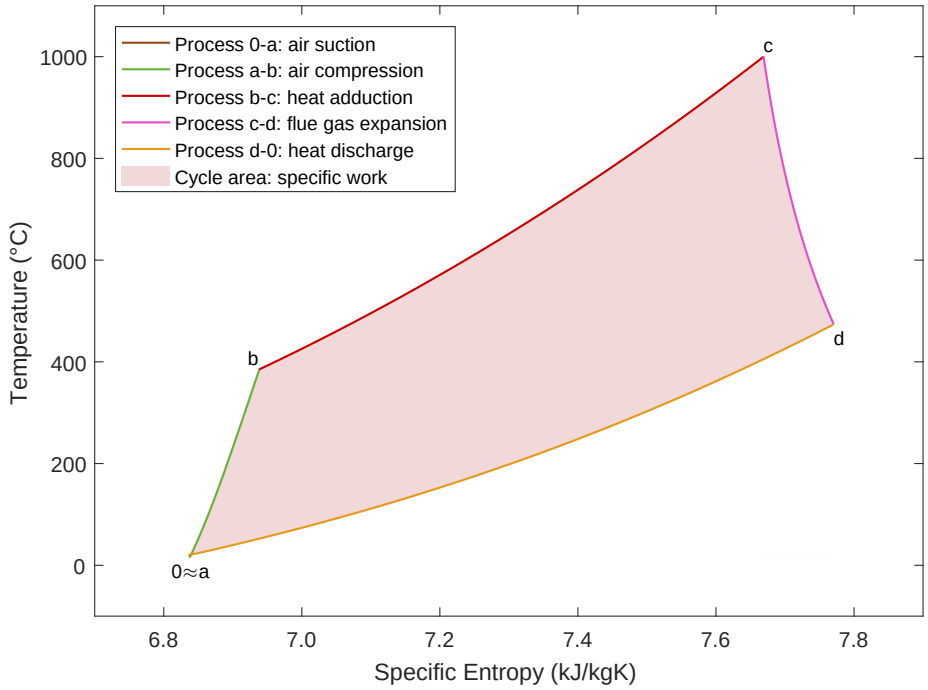

Figure 2.1: The Joule-Brayton cycle in the T-s diagram

The cycle starts with the air suction at the environment conditions (0). The first thermodynamic process is the air compression (a-b). It can be considered adiabatic, since the heat transfer with the surroundings is negligible, and irreversible, due to the entropy production. The compression leads to the increase of the air pressure, whose ratio between outlet and inlet is called overall pressure ratio. A temperature increase is linked to the pressure rise, which is also function of the compression efficiencies. External power is needed to carry out the compression, and, for an industrial gas turbine engine, it is commonly equal to two thirds the one extracted in the expansion.

The second thermodynamic process is the heat addition (b-c). The compressed air mixes with the fuel and the mixture conditions trigger a combustion reaction. The process can be considered quasi-isobar, due to a pressure loss linked to the heat addition and mixing, and it is irreversible, involving an entropy increase. The fuel is usually a gaseous or liquid hydrocarbon, characterized by low impurities. The combustion reaction converts the air oxygen and the fuel compounds into carbon dioxide and water, releasing heat in the process. The combustion products absorb the heat and the flue gas temperature increases. However, in order to keep the temperature below the maximum acceptable value, some air does not join the reaction and is used to cool down the hot flue gas.

The third thermodynamic process is the flue gas expansion (c-d). The negligible heat transfer to the surroundings makes the process adiabatic. On the other hand, it is irreversible due to the entropy production. The flue gas pressure decreases during expansion, and the pressure ratio between inlet and outlet is nearly equal to the one for the compression. The quality of the process is expressed by the expansion efficiencies, which also determine the temperature drop for a specified pressure ratio. The expansion enables the extraction of specific work from the fluid, and the related power is partly absorbed by the cycle in the compression process. The remaining power can be converted into the desired form: electricity (power generation) or thrust (propulsion).

The fourth thermodynamic process is the heat discharge (d-0). The exhaust flue gas reaches the environment, where it cools down until the environment temperature. The heat discharged to the environment air is large, due to the high temperature of the exhaust flue gas. The heat discharge is quasi-isobar, due to a pressure loss existing during the process, and irreversible. After a certain period in the environment, the thermodynamic and chemical properties of the flue gas are considered to coincide with the ones of the inlet air.

The cycle performance can be analysed by evaluating net power output $\dot{W}_{JBr}$, and the cycle efficiency η_{JBr}. Neglecting the mechanical efficiency of the equipments, the former is obtained by subtracting the compression power $\dot{W}_{ab}$ and auxiliaries power $\dot{W}_{au}$ to the power extracted during expansion $\dot{W}_{cd}$. Regarding the cycle efficiency η_{JBr}, it is obtained by dividing the previous value of the net power output by the heat flow added to the cycle $\dot{Q}_{bc}$.

$$\dot{W}_{JBr} = \dot{W}_{cd} - \dot{W}_{ab} - \dot{W}_{au}; \qquad \text{Joule-Brayton cycle: net power output} \quad (2.1)$$

$$\eta_{JBr} = \frac{\dot{W}_{JBr}}{\dot{Q}_{bc}}; \qquad \text{Joule-Brayton cycle: efficiency} \quad (2.2)$$

2.1.2. The Rankine cycle

The Rankine cycle is the reference cycle of conventional steam plants. It is a closed cycle, and the working fluid is water, which undergoes a phase change in the heat transfer processes. Like the Joule-Brayton, the standard Rankine cycle is composed by four processes, depicted in Figure 2.2: water compression (1-2), heat addition (2-5), steam expansion (5-6) and heat discharge (6-1).

The first thermodynamic process is the water compression (1-2). Like the air compression in the Joule-Brayton cycle, the negligible heat transfer makes the process adiabatic, and the irreversibility

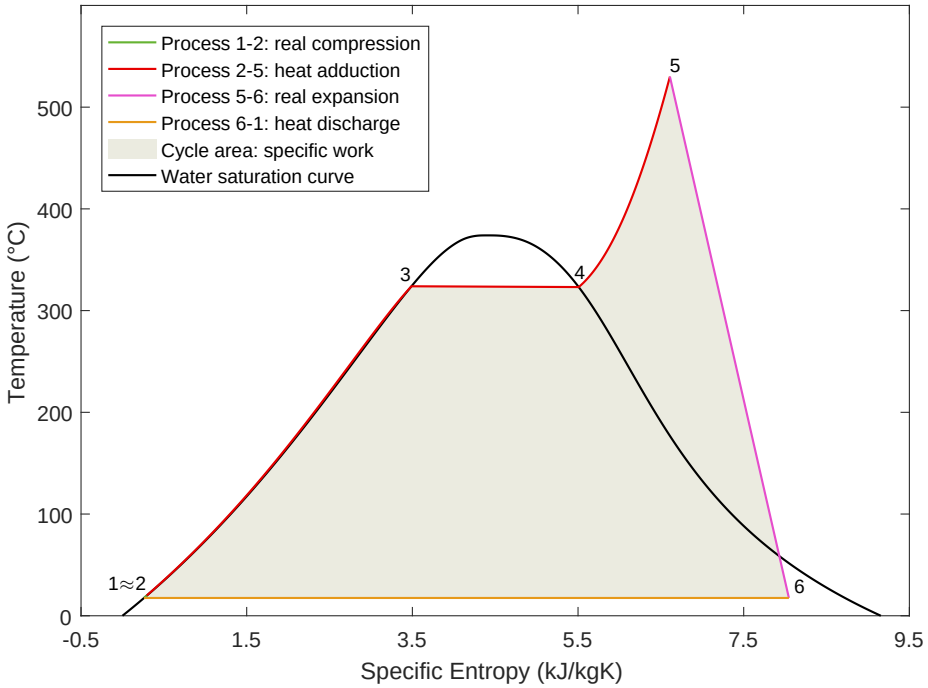

Figure 2.2: The Rankine cycle in the T-s diagram

is measured by the entropy increase. The pressure increase can still be expressed by the overall pressure ratio, commonly higher than the air compression. Furthermore, the high density of the liquid water leads to a very low power consumption in the process, and the temperature increase in the fluid is very small. As a result, the water compression is hardly visible in the T-s diagram.

The second thermodynamic process is the heat addition (2-5). It is divided into three sub-processes: water preheating (2-3), water evaporation (3-4) and steam superheating (4-5). The sub-processes are characterized by a pressure loss, and are accordingly considered quasi-isobaric. Furthermore, they are irreversible, due to the entropy production during the processes. After the water preheating, the liquid reaches the saturation temperature at the existing pressure. During the water evaporation, the largest heat flow is absorbed by the water, which turns isothermally into vapour. The steam superheating concludes the heat addition process, after which the steam reaches its maximum temperature.

The third thermodynamic process is the steam expansion (5-6), which can be considered adiabatic and irreversible, like the flue gas expansion in the Joule-Brayton cycle. The steam pressure and temperature decrease, and part of the steam enthalpy is converted into specific work. The expansion efficiency measures the quality of the process. The expansion ends at saturated conditions, with the exhaust vapour having quality above 0.9. Like the Joule-Brayton cycle, the extracted work can be converted into electricity (power generation).

The cycle ends with the heat discharge (6-1), which involves the vapour condensation at a slightly decreasing pressure and temperature. In order to maximize the work extractable in the steam turbine, the condensation pressure is kept as low as possible. However, the heat is commonly discharged to the environment, due to the very low saturation temperature at low pressure. At the end of the heat discharge process, the saturated liquid is compressed again, closing the cycle.

It is possible to determine the performance of the Rankine cycle by considering the energy flows related to the 4 processes. Like the Joule-Brayton cycle, the net power output $\dot{W}_R$ is obtained by subtracting the power absorbed by the pumps $\dot{W}_{12}$ and auxiliaries $\dot{W}_{au}$ to the power extracted by the steam turbine $\dot{W}_{56}$. The mechanical efficiencies of the equipments are neglected in the calculation. In

the end, the efficiency of the cycle η_R is equal to the net power output divided by the heat flow added $\dot{Q}_{25}$.

$$\dot{W}_R = \dot{W}_{56} - \dot{W}_{12} - \dot{W}_{au}; \qquad \text{Rankine cycle: net power output} \quad (2.3)$$

$$\eta_R = \frac{\dot{W}_R}{\dot{Q}_{25}}; \qquad \text{Rankine cycle: efficiency} \quad (2.4)$$

It is important to mention that the advanced Rankine cycles currently adopted in the industry always differ from the standard one. In order to maximize the performance, several solutions have been developed and implemented. The shape of an advanced Rankine cycle is shown in Figure 2.3.

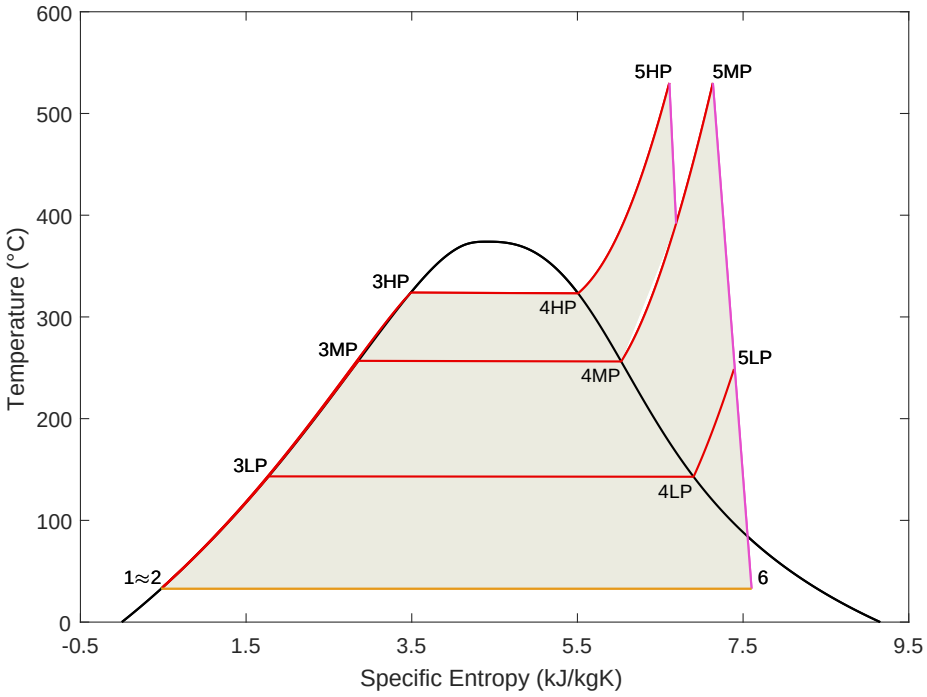

Figure 2.3: A three-pressure level reheated Rankine cycle in the T-s diagram

The main features of the current advanced Rankine cycles are:

- the water is compressed at three different pressures levels, conveniently called High Pressure (HP), Medium Pressure (MP) and Low Pressure (LP). This solution leads to a more efficient use of the heat added to the steam cycle, minimizing the temperature differences during heat transfer;
- the steam expansion is fractionated into three processes, obtaining higher expansion efficiencies. Furthermore, the exhaust HP is reheated with the MP steam by adding additional heat to the cycle, leading to a net power output increase.
- A small quantity of steam is extracted during the expansions, in order to partially preheat the liquid water. This solution leads to a decrease in the net power produced, which is compensated by a significant improvement in terms of efficiency.

2.1.3. The combined cycle

The Joule-Brayton and Rankine cycles can be coupled into one combined cycle, characterized by higher performance compared to the individual ones. In this way, it is possible to extract more power

from the same heat flow added to the gas turbine cycle, by using its exhaust heat in the steam cycle. Figure 2.4 shows a flow diagram of the combined cycle aimed at the combined production of heat and power (CHP).

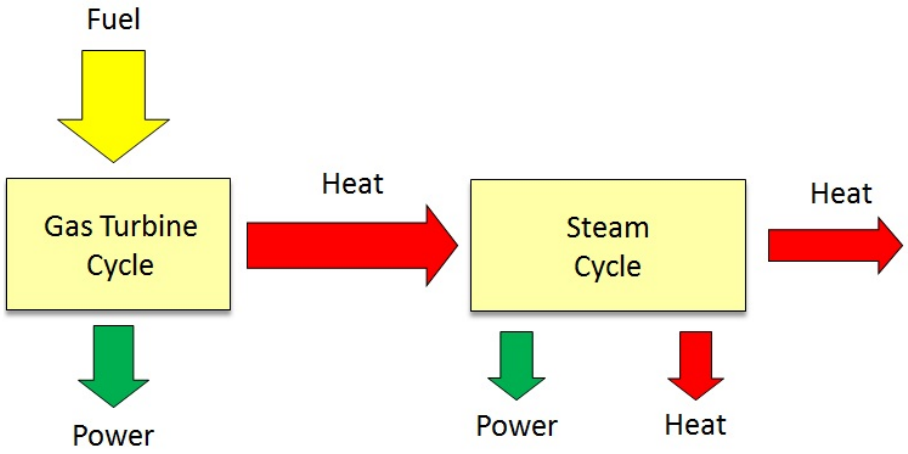

Figure 2.4: Process flow diagram of a CHP combined cycle

In order to use the heat discharged by the Joule-Brayton cycle, the hot flue gas is cooled down by transferring heat to the steam cycle. The temperature differences at which the heat transfer occurs are minimized by dividing heat into different processes, as shown in Figure 2.5.

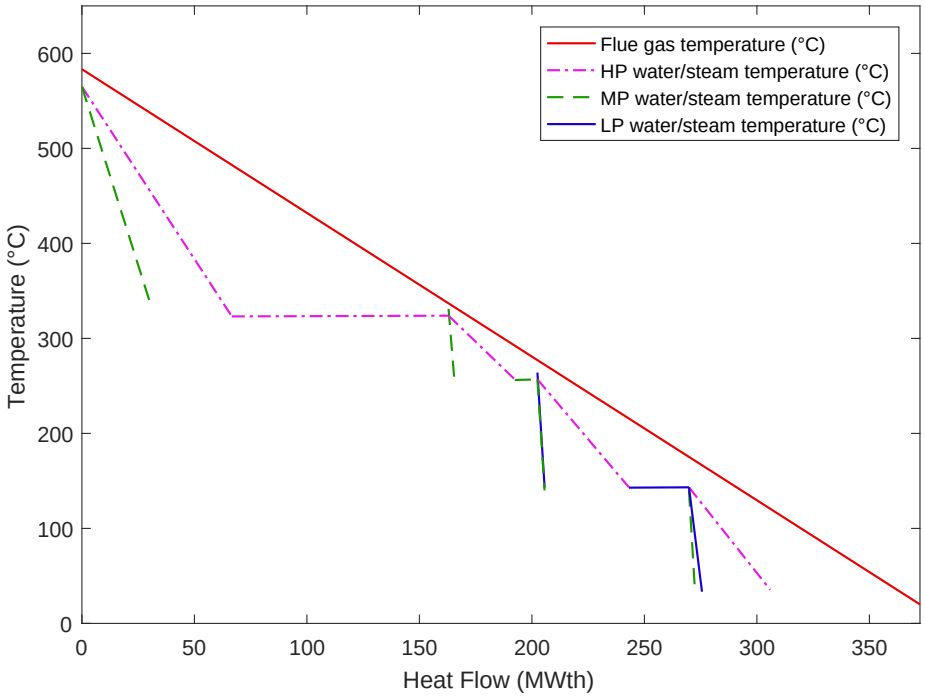

Figure 2.5: The flue gas cooling in the T-Q diagram

At the beginning of the flue gas cooling, the heat is used for the superheating and reheating processes, which are commonly carried out in parallel. Afterwards, the largest amount of heat is absorbed during the evaporation of the HP steam. At this point, also called pinch point, the flue gas temperature

is only a few degrees above the HP saturation temperature. The flue gas temperature keeps decreasing, and its heat flow is absorbed by the sub-cooled water during the preheating processes. Once the water preheating is complete, the flue gas concludes its cooling process in the environment.

Regarding the combined cycle performance, the overall net power output $\dot{W}_{CC}$ is the sum of the net power outputs related to the individual cycles. Furthermore, the overall efficiency η_{CC} can be obtained by dividing the overall net power output by the heat flow $\dot{Q}_{bc}$ added to the Joule-Brayton cycle. The values of both these performance parameters are higher than the ones related to the individual cycles.

$$\dot{W}_{CC} = \dot{W}_{JBr} + \dot{W}_R; \qquad \text{Combined cycle: net power output} \quad (2.5)$$

$$\eta_{CC} = \frac{\dot{W}_{CC}}{\dot{Q}_{bc}} > max\left(\eta_{JBr}; \eta_R\right); \qquad \text{Combined cycle: efficiency} \quad (2.6)$$

2.2. RoCa3 power station

The RoCa3 power station operates according to a CHP combined cycle, and is composed by a gas turbine plant and a steam plant. The flue gas cooling takes place in the Heat Recovery Steam Generator (HRSG). The installation produces up to 220 MWe, with an overall efficiency above 48%.

2.2.1. Gas turbine plant

The gas turbine plant is a General Electric MS PG9161E, which operates according to the Joule-Brayton cycle shown in Figure 2.6.

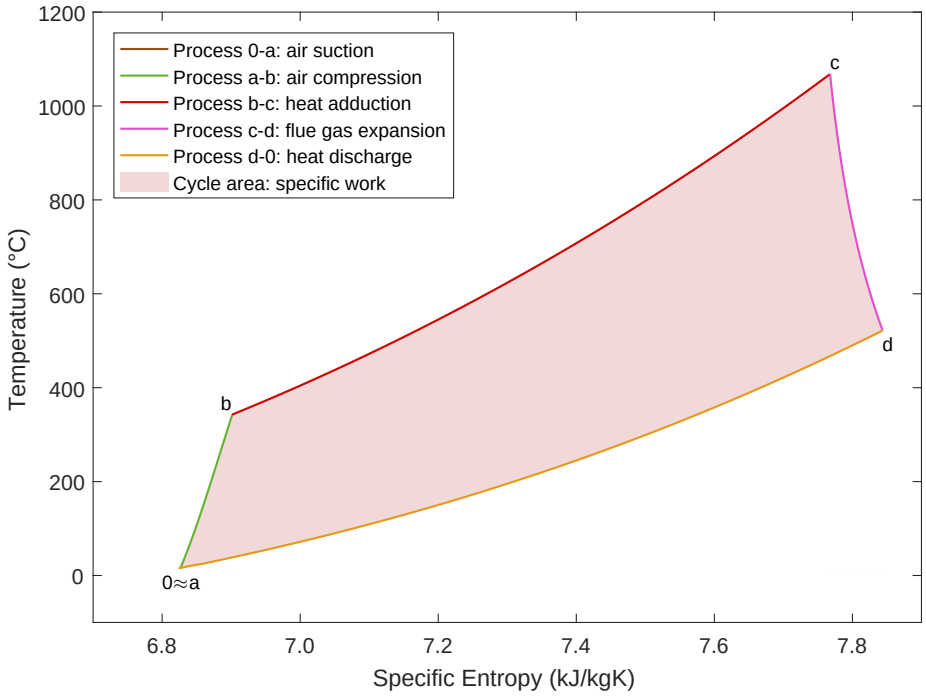

Figure 2.6: Joule-Brayton cycle of the MS PG9161E gas turbine plant

The overall pressure ratio of the cycle is 13, and the air temperature after compression is around 340°C. The flue gas expansion starts at a temperature above 1060°C, and ends at 529°C. The plant

specified power output is 123 MW, with a thermal efficiency of 32.9%. The gas-turbine plant is composed by an intake duct, an axial compressor, a can-anular combustion chamber, an axial turbine, and an exhaust duct. The exhaust duct is connected to the HRSG, where the heat transfer between flue gas and steam cycle takes place. A representation of the the MS PG9161E is shown in Figure 2.7.

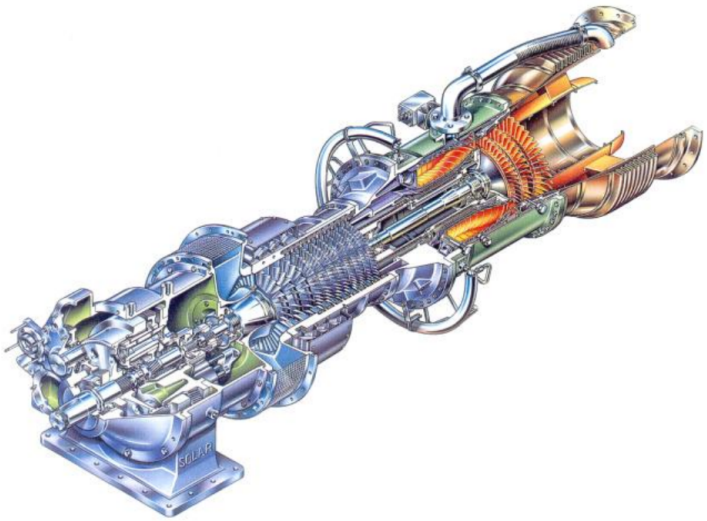

Figure 2.7: The General Electric MS PG9161E plant

The air intake is responsible for drawing and filtering the air, preparing it for the compression. It is composed by a demister and filters, which involve a pressure loss. The end of the intake duct is connected to the compressor inlet, where a row of adjustable blades is installed. These blades, also called Inlet Guide Vanes (IGV), allow to control the inlet air mass flow by modifying its opening angle. A picture depicting the IGV blades of the gas turbine plant is provided in Figure 2.8.

Figure 2.8: The IGV blades

The air compression is carried out by the axial compressor. The machine is composed by 17 stages, each composed by a row of stator and rotor blades. The rotor blades are located before the stator

blades, and they are respectively installed to the rotor wheels and compressor housing. The rotor wheels are mounted to the GT shaft. The shaft rotates allowing the rotor blades to transfer mechanical power to the air, whose kinetic energy increases. The kinetic energy is converted into a pressure increase in the stator. The pressure increase within the stages is kept small in order to avoid flow separation from the blades. The air density increases along the stages, and, in order to keep the mass flow rate constant, the blades length decreases. The trends of the velocity, pressure and temperature of air along the compressor stages are depicted in Figure 2.9. The decrease of the air velocity at compressor outlet is due to the presence of a diffuser installed after the last stage. By reducing the flow speed, the diffuser allows to minimize the pressure loss in the combustion chamber.

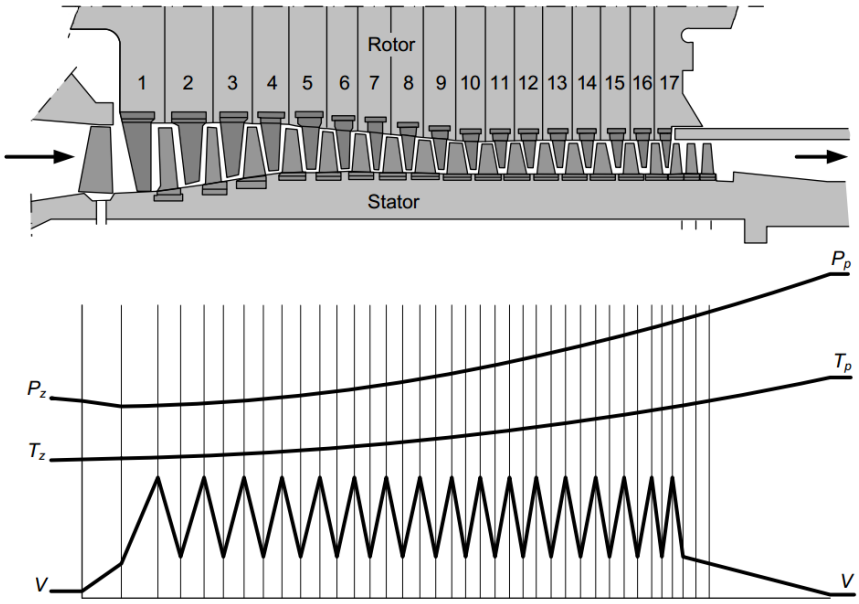

Figure 2.9: Trend of the main physycal variables during air compression

The compressed air flows into the combustion chamber of the plant, where the heat addition process takes place. It consists in a combustion between Slochteren natural gas and the compressed air, during which the chemical energy of the gas is converted into heat. The combustion chamber is composed of 14 interconnected tubular liners located inside a single anular casing. Each liner is characterized by 6 primary burners which surround 1 secondary burner, both of the GE Dry-Low NOx 1 (DLN 1) type. This type of burners enable the minimization of the NOx emissions during design operation, and operate according to 4 different combustion modes: primary, lean-lean, secondary and premix. Each combustion mode implies specific fuel admissions in the primary and secondary burners, as shown in Figure 2.10. Only part of the air burns with fuel, while the rest flows in the anulus and is gradually admitted into the liner through three bands of cooling holes. In this way, the flue gas temperature is conveniently lowered, in order to prevent high temperature oxidation and creep in the turbine blades.

The axial turbine carries out the flue gas expansion. The turbine, more compact than the compressor, counts 3 stages only. The stator vanes, located before the rotor blades, convert the flue gas enthalpy into kinetic energy, which is transferred to the rotor blades in the form of mechanical power. As a result, the power is transferred to the shaft, and it is absorbed by both the compressor and the electrical generator. Despite the dilution of the flue gas with the excess air, the high temperature can still lead to oxidation and creep. As further preventive action, the stator blades of the first two stages have small holes from which a small amount of compressed air comes out, and creates a protective film between blades and flue gas. The pressure decrease during the expansion leads to a density increase along the stages. As a consequence, the blades height conveniently increases and, in order to account for

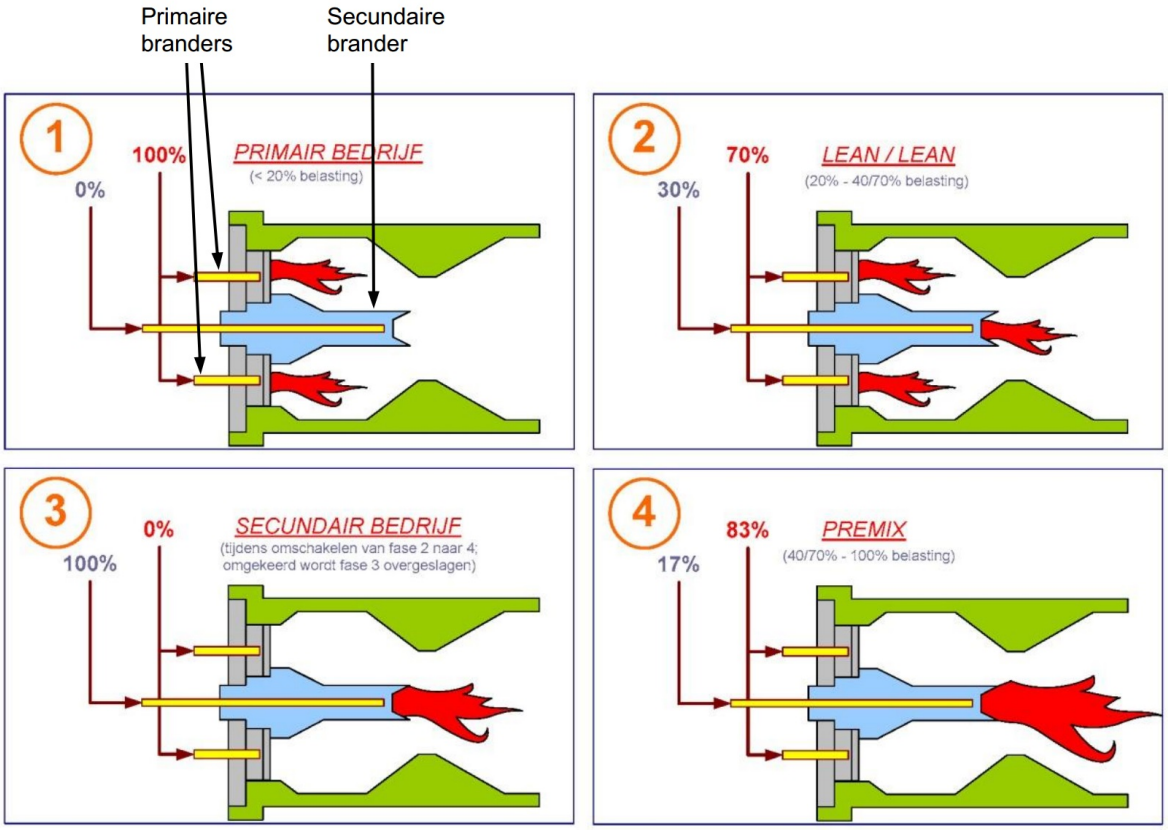

Figure 2.10: Sketch of the fuel admissions in the burners in the 4 combustion modes

the change in circumferential velocity and ensure an optimum flow path, the blades are twisted. Figure 2.11 provides a picture of the twisted rotor blades in the third stage of the axial turbine.

Figure 2.11: Twisted blades in the third turbine stage

The exhaust flue gas flows through the exhaust duct, which connects the turbine outlet to the bottom of the HRSG. After the heat transfer with the water, the flue gas exits the HRSG through its stack.

2.2.2. Steam turbine plant

The steam plant operates according to the reheated Rankine cycle shown in Figure 2.12. The three pressure levels are 112 bar (HP), 41 bar (MP) and 5 bar (LP), and the maximum steam temperature is 520°C. The steam condenses at a temperature of 17.5°C, corresponding to a pressure of 0.02 bar. The specified off-combined values for the power output and efficiency are 104 MWe and 35.9 %.

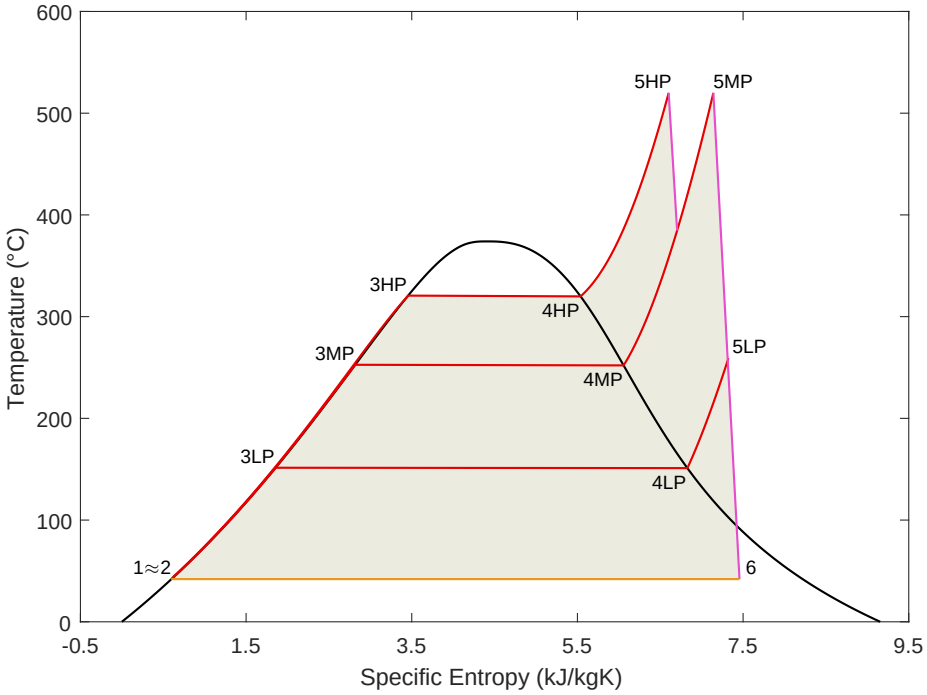

Figure 2.12: Rankine cycle of the RoCa3 steam plant

The steam plant is composed by three main systems, which are the feed water system, the HRSG, and the steam turbines system. The first two, manufactured by Stork B.V., include the main condenser, condenser pumps, deaerator, feed water pumps, heat exchangers, drums and bypass valves. The steam turbines system, manufactured by ABB, comprehend the stop valves, control valves, HP turbine, MP turbine, and LP turbine. A schematic diagram of the RoCa3 steam plant is provided in Figure 2.13.

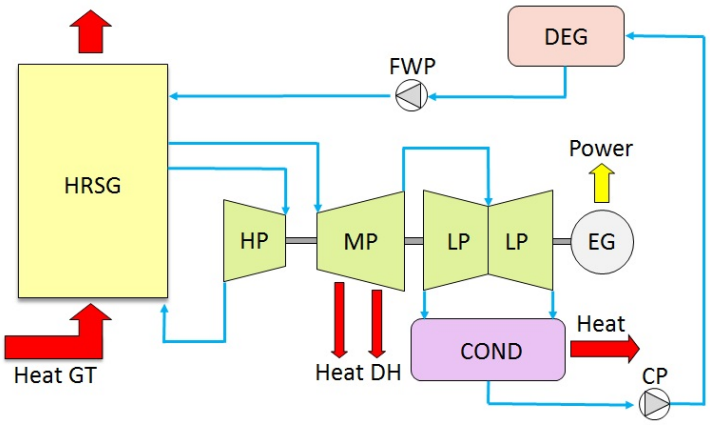

Figure 2.13: Rankine cycle of the RoCa3 steam plant

The saturated water exits the main condenser and is compressed in 3 centrifugal pumps, until the pressure existing in the deaerator. Due to the saturated conditions of the inlet water, the pumps are located a few meters below the main condenser, in order to prevent cavitation in the machines. The liquid reaches the deaerator, a large cylindrical tank equipped with vent holes on its top surface. It is normally operated at a pressure of 1.3 bar, and saturated conditions are ensured by injecting LP steam from the HRSG. The non-condensable gas separated from the water exit the tank through the vent holes. The feed water flows into the 3 HRSG circuits, one per pressure level, where the feed water pumps are installed. Like the condenser pumps, they are centrifugal, and located around 10 m below the deaerator. There are 2 pumps for the LP and MP feed water circuits, while 3 pumps are installed to the HP circuit. A picture of the HP feed water pump B is provided in Figure 2.14.

Figure 2.14: View of the HP feedwater pump B

The heat addition process of the cycle is carried out in the HRSG, by using the heat discharged by the exhaust flue gas. The heat transfer takes place in 4 types of heat exchangers: economizers (flue gas/liquid water), evaporators (flue gas/saturated mixture), superheaters (flue gas/steam) and reheaters (flue gas/steam). The heat exchangers consist of a number of bundles composed by finned pipes, whose outer surface is shown in Figure 2.15.

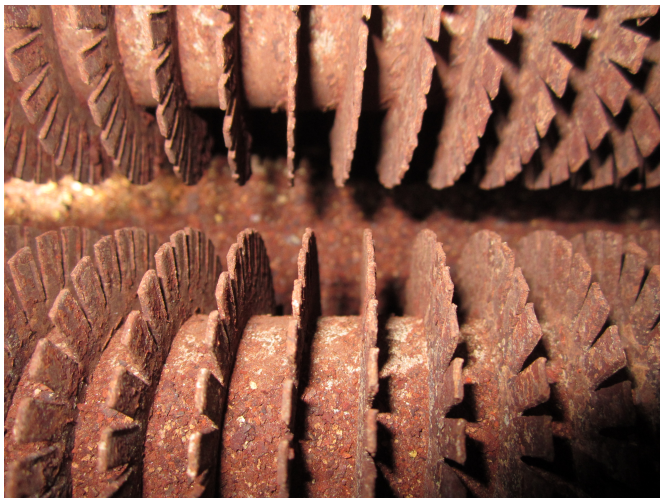

Figure 2.15: View of the HP economizer 4 pipes

The position of the heat exchangers in the HRSG depends on the design temperature range. As a consequence, the superheaters and reheaters are located close to the HRSG inlet, while the first economizer bundles are installed close to the stack. The heat exchangers characterized by the same temperature range are located in the same HRSG level, so that the heat transfer between flue gas and steam/water occurs in parallel. Figure 2.16 depictes the arrangement of the heat exchangers in the RoCa3 HRSG. The abbreviations adopted in the sketch are ECO (economizer), VERD (evaporator), OVO (superheater), her-OVO (reheater).

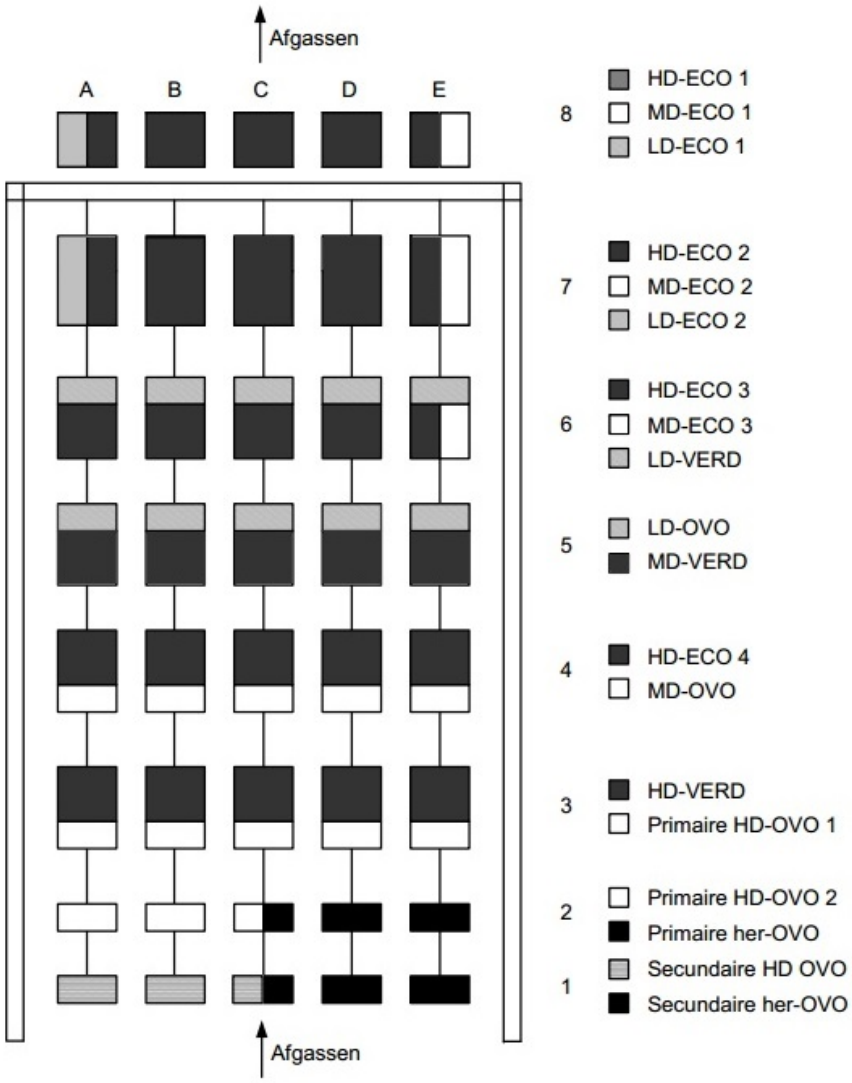

Figure 2.16: Heat exchangers arrangement inside th RoCa3 HRSG

The economizers carry out the water preheating, and they are respectively 4 in the HP circuit, 3 in the MP circuit, and 2 in the LP circuit. The water exits the last economizers at saturated conditions, and enters the boiler drums. The boiler drums, shown in Figure 2.17, are cylindrical tanks connected to the boiler evaporators, which contain the vapour-water mixture. In the evaporators, composed by a higher number of tubes compared to the economizers, the saturated water turns into vapour. A number of cyclones in the drums remove the water droplets from the vapour, which is superheated in a sequence of superheaters: 3 for the HP circuits, and 1 for the MP and LP circuits. The reheaters are 2, and they installed in parallel with the last 2 HP superheaters.

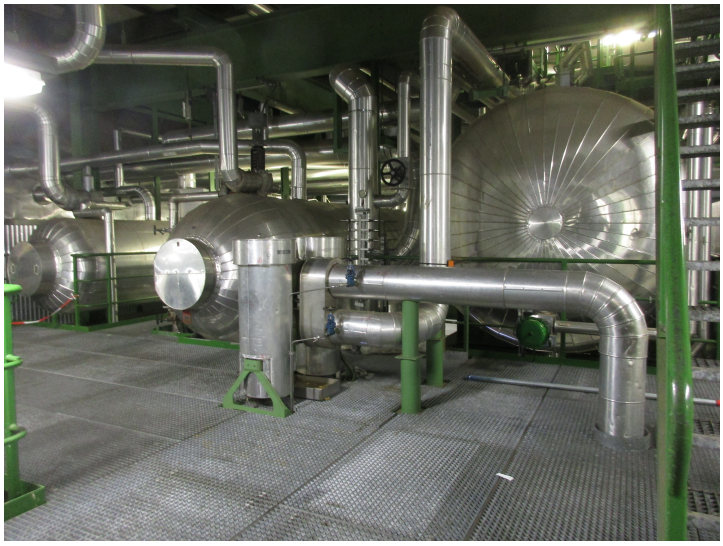

Figure 2.17: Frontal view of the LD drum (left), HD drum (center) and degasser (right)

The superheated and reheated steam expands in the steam turbines, built on the same shaft and connected to the electrical generator. The HP turbine rotor counts 22 reaction stages, along which the steam pressure decreases from 112 bar to 41 bar. The access to the steam turbines is controlled by one stop valve and two control valves. The exhaust steam is reheated together with the MP superheated steam, and flows into the MP turbine. The machine, larger than the previous one, is composed by 34 reaction stages, along which the steam pressure decreases from 40 bar to 1.7 bar. The MP turbine is characterized by the highest power production, thanks to the higher enthalpy difference between inlet and outlet. Furthermore, two extractions enable the drawing of hot steam from the turbine for district heating purposes. The extracted steam is condensed in two different district heating condensers, where the latent heat of condensation is transferred to a large flow of liquid water to be sent to the municipality of Rotterdam. The MP turbine and its inlet circuits are shown in Figure 2.18: unlike the HP circuits, two stop valves allow the steam to reach the machine.

Figure 2.18: View of the MP turbine inlet, with stop valve B (right) and control valves A and B (top)

In the end, the MP exhaust steam flows into the LP steam turbine, composed by a 8 stages two-flow rotor. The steam expands until the condenser pressure, leaving the turbine at saturated conditions.

The exhaust vapour flows into the main condenser, where it turns into liquid. The condenser is a shell-and-tube heat exchanger: cooling water flows inside its tubes, while the two-phase mixture occupies the shell. The condensation heat is removed from the cooling water thanks to hybrid cooling towers, enabling the closed circulation of the fluid.

2.3. The RoCa3 start-up process

After the short description of the RoCa3 power station, it is possible to introduce the start-up process of the installation. The aim of the start-up process is to bring the CCGT installation from standstill to minimum part-load operation. The transients phenomena characterizing the process, such as the heating up of the steam plant equipments and the turbines shaft acceleration, are controlled by means of specific components. In particular, the heating up of the steam turbines leads to high thermal stress in the machines, which has to be controlled in order to prevent damages in the machines.

2.3.1. Thermal stress in the steam turbines

During the start-up process, the flue gas transfers heat to the steam cycle, and the high temperature steam produced flows into the steam turbines. Inside the machines, heat transfer occurs between the steam and the turbine blades, mainly driven by the temperature difference existing between the fluid and the metal. The heat propagates inside the rotor wheels, but it gradually decreases going from surface to center, due to gradual heat absorption by the metal. As a result, the closer the metal is to the rotor center, the slower it heats up. As an example, Figures 2.19 and 2.20 respectively depict a 600MW supercritical steam turbine rotor modelled in [3] and the related temperature distribution.

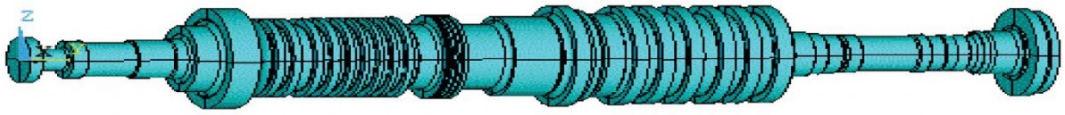

Figure 2.19: A 600MW supercritical steam turbine rotor modelled in [3]

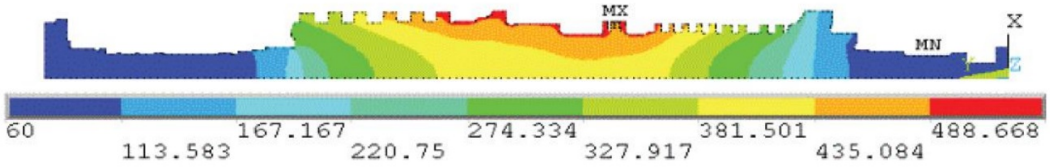

Figure 2.20: Temperature distribution in the steam turbine rotor modelled in [3]

The temperature increase leads to a thermal expansion of the metal, but it is restrained by the neighboring metal. As a result, thermal stress develops in the rotor metal. According to [4], the thermal stress can be expressed as function of the temperature difference between the metal temperature and the volumetric mean temperature of the rotor wheel, under the assumptions provided below:

1. The turbine wheels are considered to be thin solid disks of external radius R_o;
2. The temperature distribution within the rotor wheels is axial-symmetric;
3. The rotor material is homogeneous, isotropic, and compressible;
4. The physical properties of the rotor material are only temperature-dependent;

The expressions of the thermal stress along the three cylindrical coordinates (r,θ,z) are provided below.

$$\sigma_r(R) = \frac{E\alpha}{1-\nu}\left(\frac{1}{R_o^2}\int_0^{R_o} T(r)\ r\ dr - \frac{1}{R^2}\int_0^{R} T(r)\ r\ dr\right); \quad \text{Radial stress (2.7)}$$

$$\sigma_\theta(R) = \frac{E\alpha}{1-\nu}\left(\frac{1}{R_o^2}\int_0^{R_o} T(r)\ r\ dr + \frac{1}{R^2}\int_0^{R} T(r)\ r\ dr - T(R)\right); \quad \text{Circumferential stress (2.8)}$$

$$\sigma_z(R) = \frac{E\alpha}{1-\nu}\left(\frac{2}{R_o^2}\int_0^{R_o} T(r)\ r\ dr - T(R)\right); \quad \text{Axial stress (2.9)}$$

By analysing the previous expressions it is possible to conclude that the maximum thermal stress occurs at the rotor wheels surface, since it is characterized by the highest temperature. The heat transfer to the surface must be accordingly controlled, since the surface temperature $T(R_o)$ increases much faster than the volumetric mean temperature. In particular, the steam condensation in the machines leads to a very strong increase of $T(R_o)$, to which the highest thermal stress is linked. As an example, Figure 2.21 provide the stress distribution for the same steam turbine rotor modelled in [3].

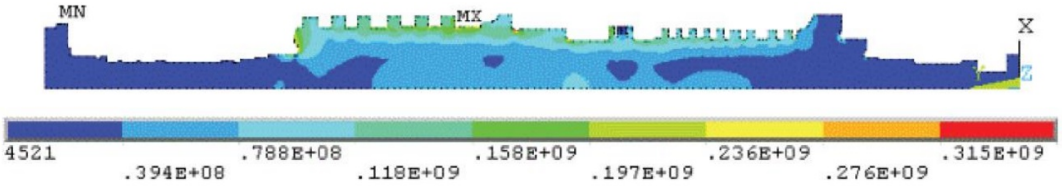

Figure 2.21: Stress distribution in the steam turbine rotor modelled in [3]

2.3.2. Key components

The most important processes furing start-up are carried out by a few components only. It is accordingly important to briefly describe their operation, if it has not already been described in the previous section. The key components in the start-up process are the stop valves, control valves, bypass valves, desuperheaters and drain ducts, which are introduced below.

- The stop valves either completely block or completely open the access of the steam to the steam turbine circuits. As a consequence, they are characterized by an on/off operation, which is commanded by the HRSG control system. When the stop valves are closed, the steam turbines are totally isolated from the steam circuits.
- The control valves regulate the steam flow to the turbines. They fix the maximum steam flow, equal to the choked value, which is dependent on their opening position. When closed, the control valves cannot completely block the steam flow. As a result, some steam flows into the machines as soon as the stop valves are open, and the heating up of the turbines begins.
- The bypass valves are extremely important in the start-up process, since they allow the water circulation in the plant as long as the access to the turbines is limited. The HP bypass circuit commonly discharges the steam to the cold reheater inlet, while the MP and LP bypass circuits are usually connected to the main condenser. Furthermore, they enable the pressure control by regulating the steam accumulation/discharge in the circuits (drums, pipes), due to the mismatch between the steam production and valves flow.
- The steam temperature control is carried out by the desuperheaters, installed in the HP and MP circuits between first and second HRSG rows. The temperature control is carried out by spraying

liquid water into the steam flow entering the last heat exchanger. The water is drawn from the economizers by means of an auxiliary circuit, equipped with stop and control valves.

- The drain ducts are aimed at the removal of the steam condensate produced during the heat transfer with the cold metal from the steam circuits and turbine. The ducts are commonly connected either to the main condenser or to a flash tank, and include one stop valve each. The drain ducts are commonly operated during start-ups after a long shut-down period, characterized by metal temperatures lower than the saturation value at the design pressure.

2.3.3. Types of start-up

The steam turbine control systems are programmed to keep the thermal stress within the acceptable ranges. If the maximum permissible value for the thermal stress is approached, the control valves start automatically closing in order to reduce the heat flow to the turbine wheels. On the other hand, the control valves can quickly open if the thermal stress level in the turbines is low. The rate at which the control valves open influences the start-up time. In order to select the best control strategy before the beginning of a start-up, a classification of the processes is implemented to the control systems, based on the turbines surface temperatures. According to this classification, the control system knows in advance whether the thermal stress will be high, medium, or low. As an example, the start-up classification in the steam turbines control system of the RoCa3 steam plant is provided in Table 2.1. The average start-up time is calculated from the start of the GT shaft acceleration (starting motor IN), until the bypass valves are steadily closed and the GT operates at minimum part-load.

Table 2.1: Start-up classification in the Turbomax^{TM} 6 control system

Type of start-up	Thermal stress level	HP turbine surface temperature	Average start-up time
Cold	High	$\leq 240°C$	240 min
Warm	Medium	$> 240°C$ and $\leq 420°C$	90 min
Hot	Low	$> 420°C$	40 min

The values of the turbines surface temperatures depend on the shut-down period, whose duration determines the metal cooling process. Regarding the RoCa3 power station, a start is cold after a shut-down period of 40 hours, while it is warm within a shut-down period between 5.5 and 40 hours. Due to the very high surface temperatures, the hot starts occur after trips only, within a shut-down period lower than 5.5 hours. The start-up process of the RoCa3 power station divides into two sub-processes: the GT start-up and steam plant start-up. The sub-processes are described in the next subsections, highlighting the main steps and providing the trends for the main operating variables.

2.3.4. GT start

The start-up of the MS PG9161E gas turbine is governed by the Speedtronic^{TM} Mark V control system. The main steps of the process are presented in Table 2.2, while the trends of the main operating variables is shown in Figure 2.22.

The start-up begins with the start of the auxiliary motor, which drives the first acceleration of the shaft until 540 rpm. The acceleration takes around 3 minutes, after which a ventilation period of 5 minutes is started. This period is needed to vent the GT components and HRSG, before the ignition triggered by the opening of the fuel stop valve. The natural gas starts flowing into the combustion chambers, and the fuel-air mixture ignites. At this point, the starting motor gradually increases the shaft speed until 1600 rpm, and the cycle pressure ratio increases. This enables the GT to produce net mechanical power: at this point, the motor is disconnected and the shaft quickly reaches the synchronization speed of 3000 rpm. After around 17 minutes from the motor start, the GT generator synchronizes to the grid and starts delivering electrical power. The IGV are kept constant by the Mark V at the minimum anti-surge value,

Table 2.2: Main steps of the gas turbine start-up process

Step number	Step name	Control system
0	GT Aux. motor start	Speedtronic^{TM} Mark V
1	GT Ventilation start	Speedtronic^{TM} Mark V
2	GT Ignition	Speedtronic^{TM} Mark V
3	GT Acceleration start	Speedtronic^{TM} Mark V
4	GT Synchronization	Speedtronic^{TM} Mark V
5	GT Ramp-up start	Speedtronic^{TM} Mark V or MANUAL

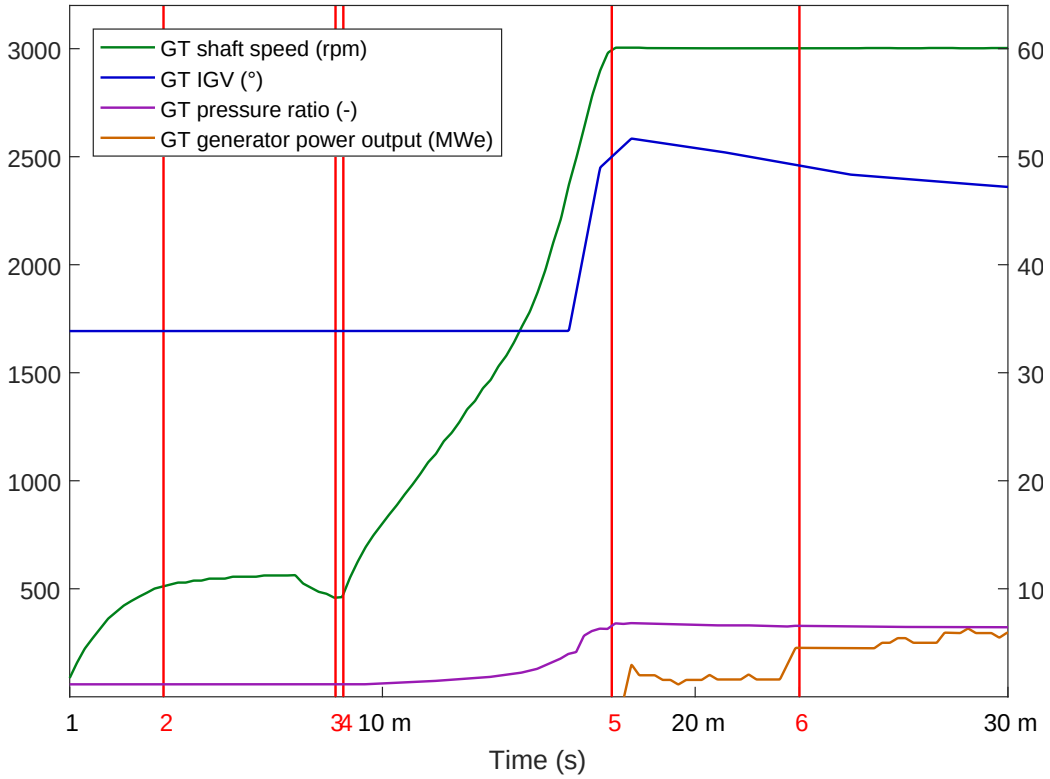

Figure 2.22: Trends of IGV, rpm, pressure ratio and GT generator output during start-up

which depends on the ambient conditions. After the synchronization to the grid, two different options are available for the GT ramp-up: the predefined DCS control and the manual control. The trends of power output and flue gas temperature for both the options are provided in Figure 2.23.

The predefined DCS control is programmed in order to maximize the heat supply to the steam plant. As a consequence, it implies a constant GT ramp-up of around 0.3 MWe/min, leading to a fast increase of the flue gas temperature. On the other hand, the process operators can manually control the GT power output, in order to adapt the flue gas temperature to the steam plant conditions. No manual control is available for the IGV opening. However, the operators can modify this variable by selecting the bleed-heat off mode in the Speedtronic^{TM} Mark V. Due to the lower temperature at compressor inlet, the control system keeps the IGV at 57°, with a consequent decrease in the flue gas temperature.

2.3.5. Steam cycle start

The start-up process of the steam plant is carried out by the FG Blokprogramma^{TM} and the Turbomax^{TM} 6 control systems. Although they work independently from each other, it is possible to identify an overall sequence characterized by the main steps of the two control systems, presented in Table 2.3. These

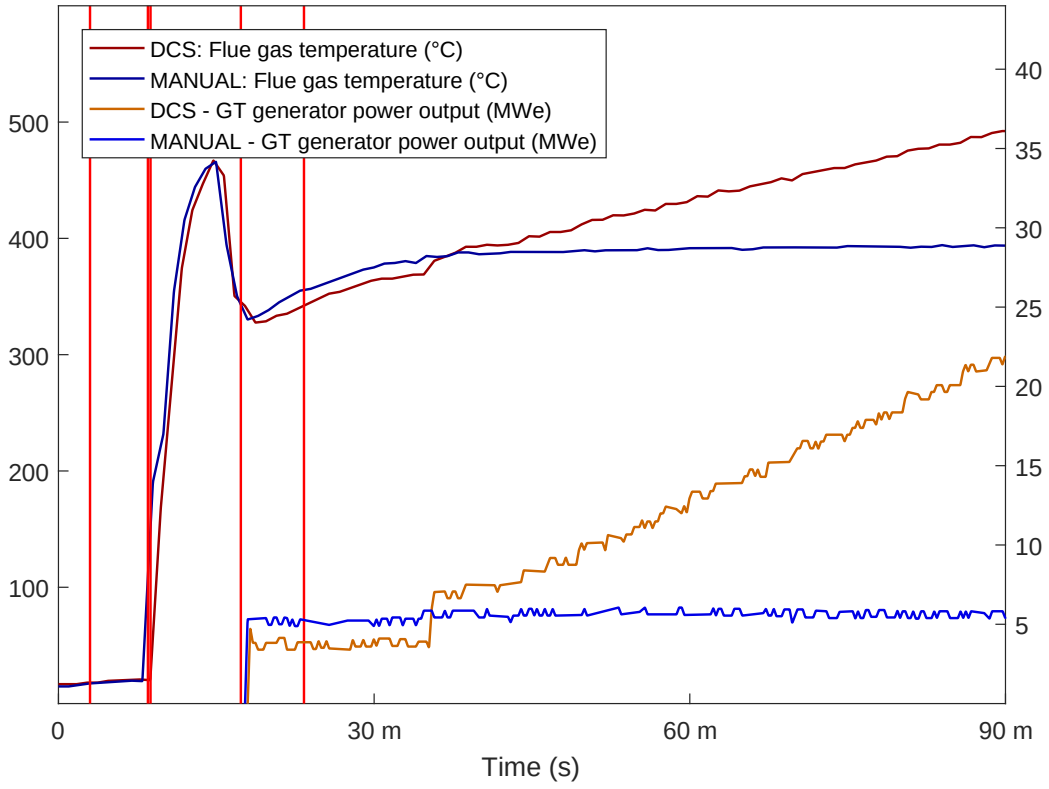

Figure 2.23: The DCS and MANUAL control modes in the first hour of start-up

steps are valid for all the three start-up types: cold, warm and hot. The start-ups differ only on the duration of the start-up phases, which mainly depends on the stress in the steam turbines. The process is considered to be concluded once the HP and MP bypass valves are steadily closed.

Table 2.3: Steps of the steam plant overall start-up program

Step number	Step name	Control system	Step end condition
1	Bypass valves: OPEN	FG Blokprogramma^{TM}	MP Bypass > 10%
2	Pressure control: AUTO	FG Blokprogramma^{TM}	Metal superheating > 20°C
3	Stop valves: OPEN	Turbomax^{TM} 6	Time after opening > 5 min
4	Control valves: AUTO	Turbomax^{TM} 6	Depends on the start-up type
5	ST Acceleration	Turbomax^{TM} 6	ST shaft speed = 3000 rpm
6	ST Synchronization	Turbomax^{TM} 6	ST generator output > 0 MWe
End	Bypass valves: CLOSED	FG Blokprogramma^{TM}	Bypass valves opening < 1%

The HP and MP bypass open as soon as GT ignites, and their opening positions gradually increase respectively to 40% and 96%. These values ensure a pressure gradient in the HP circuit above 1.0 bar/min, and the FG Blokprogramma^{TM} waits until the metal temperature before the HP stop valve to be at least 20°C above the steam saturation temperature (*minimum superheating*). Once this condition occurs, the Turbomax^{TM} 6 control system opens the HP and MP stop valves. At this point, a waiting period of 5 min is required in the control logics before setting the control valves on AUTO. The automatic control determines the opening position of the valves, in function of the thermal stress in the turbines. The trends of the previous variables during a cold start are shown in Figure 2.24. Regarding warm and hot starts, the trends are the same except for the ”metal superheating”, which is higher due to the higher initial temperature. As a result, the stop valves open earlier than in a cold start.

As soon as the steam starts flowing into the machines, the shaft acceleration and the turbines heating up start. Meanwhile, the HP bypass opening decreases, in order to increase the pressure gradient to 2.5 bar/min until a pressure of 80 bar is reached. However, the HP bypass closing leads to

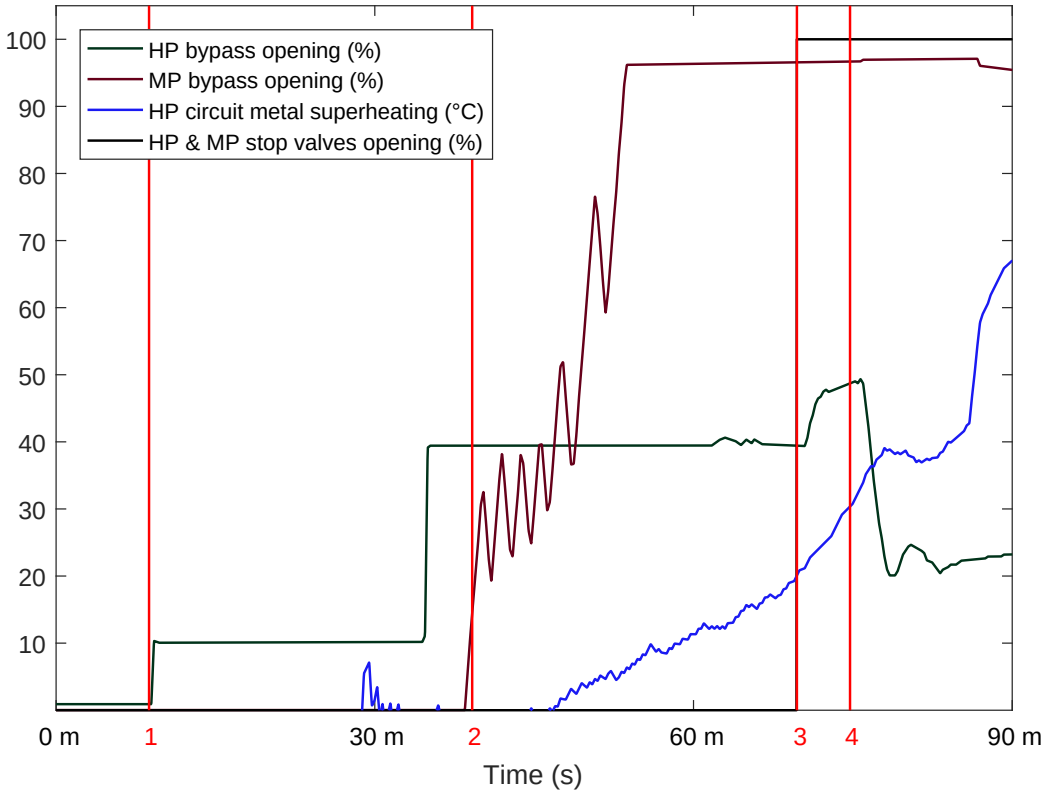

Figure 2.24: Bypass opening and pressure trends until stop valves opening

a reduction of the flow in the MP circuit, and a consequent drop of the MP pressure. The rate at which the acceleration and heating up take place depends on the steam flow. For this reason, the control valves (CV) play a main role in this phase, and 3 different strategies are adopted by Turbomax^{TM} 6 depending on the type of start-up.

- cold start: after 750 rpm shaft speed, the CV ensure an acceleration of 75 rpm/min for 30 minutes;
- warm start: after the waiting period, the CV ensure an acceleration of 300 rpm/min for 10 minutes;
- hot start: after the waiting period, the CV ensure an acceleration of 600 rpm/min for 5 minutes.

Furthermore, the strategy ensures a very fast acceleration when the shaft approaches the critical speeds. These speeds correspond to the resonance frequency speeds of the rotors, and are accordingly four: 920 rpm (generator), 1350 rpm (LP turbine), 1700 rpm (HP turbine) and 2250 rpm (MP turbine). The generator switches to the grid as soon as the shaft reaches 3000 rpm. At this point, the control valves are further opened by the automatic control and the turbines are ramped up. As a result, the pressure in the HP circuits slowly decreases to 57 bar. The ramp-up of the control valves is carried out according to 3 different strategies, based on the type of start-up.

- cold start: the CV ensure a ramp-up of 0.5 MW/min;
- warm start: the CV ensure a ramp-up of 1.0 MW/min;
- hot start: the CV ensure a ramp-up of 3.75 MW/min;

The bypass valves gradually close in function of the control valves opening. Once they are steadily closed, the start-up process can be considered to be concluded. Figure 2.25 shows the trends of shaft speed for the three types of start-up, identifying the end of the process in the three cases.

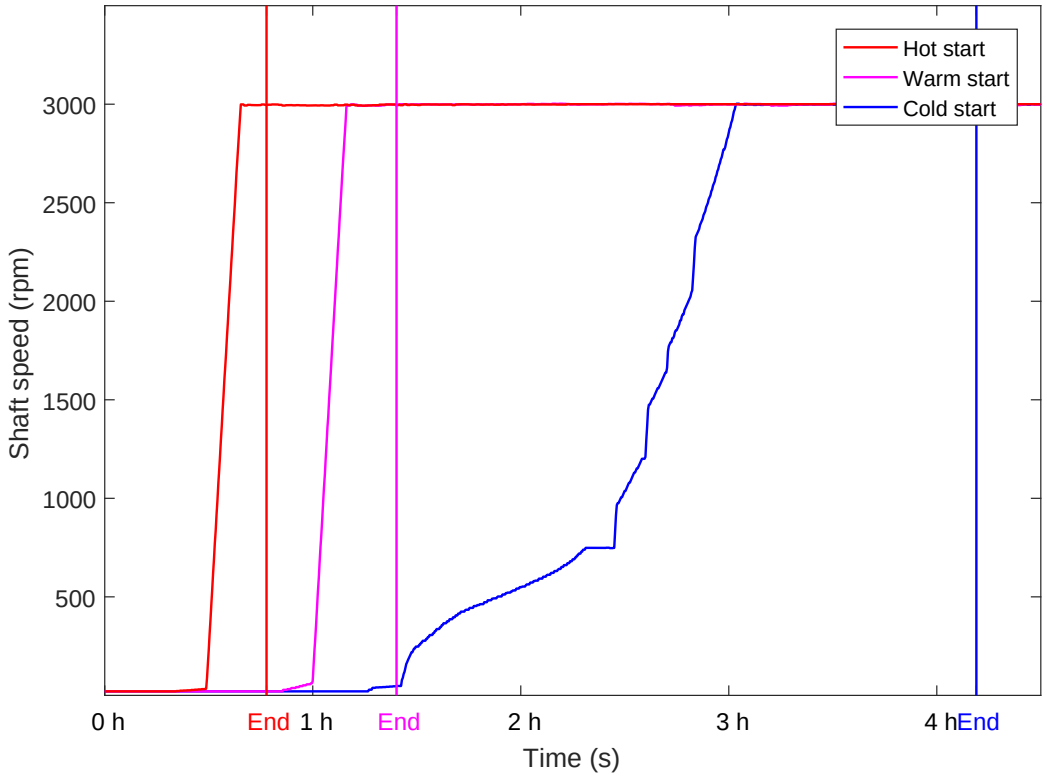

Figure 2.25: Trends of the leading control valves in the three types of start-up

2.4. Main bottlenecks

The previous description of the start-ups highlights 3 main bottlenecks, which produce unnecessary delays and fuel waste. They are presented in the list below, and discussed in the following paragraphs.

- HP pressure control;
- Steam turbines start-up;
- Steam condensation in the turbines.

The first bottleneck involves the imprecise control of the steam pressure in the HP and MP circuits. The fast pressure increase during the step 2 of the steam plant start-up delays the opening of the stop valves, and consequently slows down the process. This negative result is produced by the quick rise of the steam saturation temperature, which delays the reaching of the metal minimum superheating condition. Furthermore, the fast HP pressure ramp-up to 80 bar is not needed.

The second bottleneck regards the GT ramp-up, which takes place independently from any operating variable of the steam plant. Both the DCS and the experienced manual control are carried out according to no exact strategies. As a consequence, the high flue gas temperature leads to a high steam temperature during start-up, which results in a too severe heating up of the steam turbines. In order to control the stress in the steam turbines, the control system keeps the valves closed to limit the steam flow, slowing down the process. As a recovery action, the desuperheaters are used to reduce the steam temperature before the turbines. However, these components are not capable to carry out an efficient temperature control during the start-up, and their operation leads to further delays.

The third bottleneck is represented by the steam condensation in the turbines during the cold starts. This phenomenon negatively affects multiple aspects of the steam plant start-up. The intense heat flow transferred to the turbines surface leads to high thermal stress, which is reached a short time after the

opening of the stop valves. Furthermore, the condensation limits the exchange of mechanical power from the steam to the blades, and the initial shaft speed of 750 rpm is reached after longer time. In the end, the formation of droplets on the blades surface can damage the material, reducing the life-time of the machines.

3

Modelling

3.1. General structure

The aim of the modelling is to develop a dynamic model capable to reproduce the start-up process of CCGT installations. In order to simplify the problem, it is possible to decompose the installation in its main sub-systems, which are the gas turbine plant, the HRSG, the plant valves and the steam turbine system. As a consequence, the model can be represented by the block diagram provided in Figure 3.1. No controls are modelled in this phase, since the prediction of the physical reality of the start-ups must be validated first.

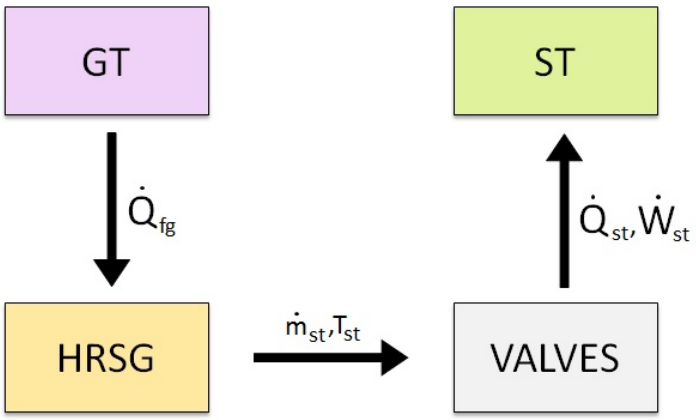

Figure 3.1: Scheme of the general structure of the dynamic model

The gas turbine plant represents the heat source of the steam cycle. The heat flow is determined by the flue gas mass flow and temperature, set as model inputs. The HRSG uses the previous heat flow to produce a certain amount of superheated steam, which is sent to the plant valves. Depending on the valves opening, part of the steam reaches the steam turbine system, leading to the heating up, stress and acceleration of the machines. The four sub-models form a network of 110 physical elements, which represents exactly the lay-out of the RoCa3 installation. Two streams, water and gas, are necessary to describe the physical flows in the model.

3.2. Sub-models

The four sub-models previously introduced are described in this section. The operation of their main physical elements is described, and the most important equations are discussed.

3.2.1. Gas turbine plant

The sub-model includes three main components: the environment, the fuel supply system, and the gas turbine plant. All the three components operate as data sources of data: in particular, since the flue gas mass flow and temperature are given, the sub-model controls the heat output to the HRSG. The structure of the sub-model is depicted in Figure 3.2.

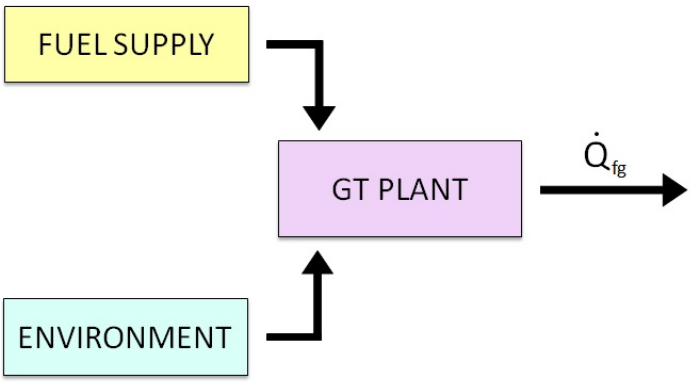

Figure 3.2: Scheme of the structure of the GT sub-model

The environment component reads the data from convenient data-sheets and modifies the properties of the air required by the GT plant. The operation of the environment component can be described by the equations provide below. However, it is important to first mention the assumptions considered for the modelling of the component:

1. the environment conditions are assumed to be the ones measures in the vicinity of the GT air intake;

$$p_{env} = p_a; \quad \text{Air pressure} \quad (3.1)$$

$$T_{env} = T_a; \quad \text{Air temperature} \quad (3.2)$$

The fuel supply system reads the data concerning the fuel mass flow rate and adjusts the related value sent to the GT plant. The equations which defines the previous relation assumes the shape of the ones for the previous component. Furthermore, the component records the fuel volumetric consumption $V_{fu,c}$ in Nm^3. It is calculated by integrating the fuel volumetric flow during the start-up, which is obtained by multiplying the fuel mass flow rate by the gas constant k_g and dividing the product by the fuel molecular weight M_{fu}. The computation is carried out considering the following assumptions:

1. the start-up process starts at t_0;
2. the default fuel type is assumed to be the Groningen ”Slochteren” natural gas;

$$\dot{m}_{su} = \dot{m}_{fu}; \quad \text{Fuel mass flow rate} \quad (3.3)$$

$$V_{fu,c} = \int_{t_0}^{t} \frac{\dot{m}_{fu} k_g}{M_{fu}}\, dt; \quad \text{Fuel volumetric consumption} \quad (3.4)$$

In the end, the GT plant component is described. It is responsible for importing data from real start-ups and setting the heat flow delivered to the HRSG by the flue gas. Under this aspect, only one assumption is made for modelling the process, and the operation of the component is described by the following equations.

1. the flue gas is assumed to lose no heat in its path to the HRSG.

$$T_{fg,r} = T_{fg}; \qquad \text{Flue gas temperature} \quad (3.5)$$

$$\dot{m}_{fg,r} = \dot{m}_{fg}; \qquad \text{Flue gas mass flow rate} \quad (3.6)$$

In addition, the component returns interesting data concerning the operation of the plant: air mass flow rate through the IGV $\dot{m}_a$, overall shaft-to-grid loss $l_{\%}$, overall efficiency η_{GT}, overall fuel-to-air ratio far and specific fuel consumption spc. Starting from the first output, it is calculated by subtracting the fuel mass flow rate from the flue gas mass flow rate.

$$\dot{m}_a = \dot{m}_{fg} - \dot{m}_{fu}; \qquad \text{Air mass flow rate} \quad (3.7)$$

In order to determine the shaft-to-grid loss, it is necessary first to calculate the net mechanical power available on the plant shaft. The computation is based on the energy balance of the component, which considers the following assumptions:

1. the air intake process is assumed to take place with no pressure and heat loss;
2. the air recirculated through the bleed heat valve is assumed to be negligible;
3. the fuel-air combustion is assumed to take place with no pressure and heat loss;
4. the fuel-air combustion is assumed to be complete;
5. the air used for the blade cooling in the gas turbine is assumed to be negligible;
6. the composition of the flue gas is assumed to be constant during the start-up;
7. the power absorbed by the gas turbine plant auxiliaries is assumed to be a power loss.

As a result, the expression of the net mechanical power $\dot{W}_{net}$ is provided below. The properties of the gas flows are determined through customized thermodynamic tables implemented to the component.

$$\dot{W}_{net} = \dot{m}_a\, h_a + \dot{m}_{fu}\left(h_{fu} + LHV_{fu}\right) - \dot{m}_{fg}\, h_{fg}; \qquad \text{Shaft net mechanical power} \quad (3.8)$$

Once the value of the net mechanical power is known, it is possible to find the shaft-to-grid loss by subtracting the value of the generator output to $\dot{W}_{net}$, and dividing the result by the same $\dot{W}_{net}$. The output of the electrical generator is also imported from experimental data-sheets. An assumption regarding the minimum generator output is made, and it is conveniently mentioned below.

1. the minimum generator output is assumed to be 3 MW, under which the loss is not determined.

$$l_{\%} = \begin{cases} 0; & [MWe < 3MW] \\ = 100 \cdot \left(\dfrac{\dot{W}_{net} - MWe}{\dot{W}_{net}}\right); & [MWe \geq 3MW] \end{cases} \qquad \text{Overall shaft-to-grid loss} \quad (3.9)$$

The second output parameter is the overall efficiency η_{GT}. It is computed by dividing the generator output value by the product of the fuel mass flow rate and its lower heating value.

$$\eta_{GT} = 100 \left(\frac{MWe}{\dot{m}_{fu}\ LHV_{fu}} \right); \qquad \text{GT plant overall efficiency} \quad (3.10)$$

The third output parameter is the overall fuel-to-air ratio far of the gas turbine plant, easily obtained by dividing the fuel mass flow rate by the air flow previously calculated.

$$far = \frac{\dot{m}_{fu}}{\dot{m}_a}; \qquad \text{Overall fuel-to-air ratio} \quad (3.11)$$

In the end, the specific fuel consumption is calculated by subtracting the characteristic fuel flow at GT ignition $\dot{m}_{fu,i}$ to the actual fuel mass flow rate, and dividing it by the generator output.

$$spc = \frac{\dot{m}_{fu} - \dot{m}_{fu,i}}{MWe}; \qquad \text{Specific fuel consumption} \quad (3.12)$$

3.2.2. HRSG

The sub-model of the HRSG includes the heat exchangers of the first 5 HRSG rows, as well as the drums and the desuperheaters. All the heat exchanger components operate according to physical models of the heat transfer, based on the logarithmic mean temperature difference and adimensional numbers. The drums operate only as flow separators, and set the pressure in the circuits according to the experimental data. The desuperheaters operate according to physical models based on energy balance equations. Due to the size of the sub-model, the portion representing the HRSG hot section is depicted only in Figure 3.3. To keep the narrative clear and concise, the characteristic equations of 3 types of components are discussed only: superheaters/reheaters, desuperheaters, and evaporators.

The superheaters/reheaters components receive the data concerning the steam and flue gas inlet flows as inputs. The physical models implemented to the components allow to obtain the temperatures of the outlet steam and flue gas, as well as the pipes wall temperature, overall heat transfer coefficient, and the heat flows. In order to do that, the heat transfer splits in two separate processes: heat transfer between flue gas and pipes wall, and heat transfer between pipe wall and steam. Starting from the former, the adimensional numbers are calculated first, based on [7]. The assumptions made for the calculation and the expressions of the final coefficients are provided below.

1. the flue gas heat transfer is assumed to take place in complete cross flow;
2. the pipes wall temperature is assumed to be constant spatially in the heat exchanger pipes;
3. the thermodynamic properties are assumed to be equal to the ones at the mean temperature;
4. the thermodynamic properties are assumed to be constant in the whole heat exchanger;
5. the effect of external fouling is assumed to be negligible.

$$Nu_{fg} = f_A \frac{T_{fg,i} + T_{fg,o}}{2\ T_m} \left(0.3 + \sqrt{Nu_{lam}^2 + Nu_{turb}^2} \right); \qquad \text{Flue gas Nusselt number} \quad (3.13)$$

$$U_{fg} = \frac{Nu_{fg}\ \lambda_{fg}}{l_{str}}; \qquad \text{Flue gas heat transfer coeff.} \quad (3.14)$$

The heat transfer coefficient is multiplied by the external heat transfer surface area A_o and the external logarithmic mean temperature difference, in order to obtain the external heat flow Q_o. No heat loss is assumed to take place in the process.

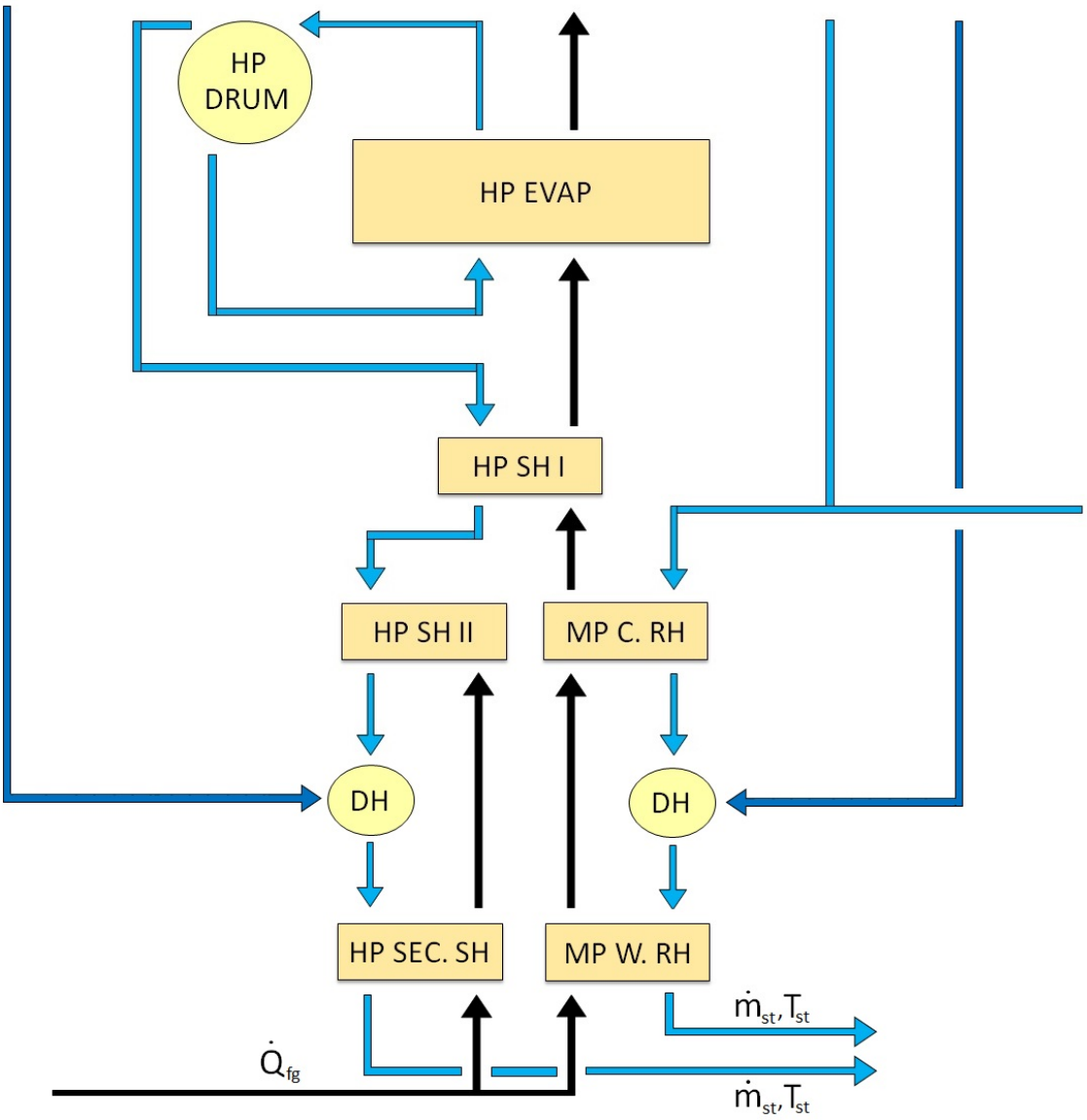

Figure 3.3: Scheme of the structure of the hot section of the HRSG sub-model

$$Q_o = U_{fg}\, A_o\, \frac{\left(T_{fg,i} - T_m\right) - \left(T_{fg,o} - T_m\right)}{\log \frac{T_{fg,i} - T_m}{T_{fg,o} - T_m}}; \qquad \text{External heat flow} \quad (3.15)$$

At this point, it is possible to find the flue gas specific enthalpy drop through the flue gas mass and energy balance equations.

$$\dot{m}_{fg,o} = \dot{m}_{fg,i}; \qquad \text{Flue gas mass balance} \quad (3.16)$$

$$Q_o = \dot{m}_{fg}\left(h_{fg,i} - h_{fg,o}\right); \qquad \text{Flue gas energy balance} \quad (3.17)$$

In the end, the flue gas outlet temperature is computed by means of the implemented p-h thermodynamic table. The pressure drop of the flue gas is also considered.

$$p_{fg,o} = p_{fg,i} - dp_{fg};$$ Outlet flue gas pressure (3.18)

$$T_{fg,o} = T\left(p_{fg,o}, h_{fg,o}\right);$$ Outlet flue gas temperature (3.19)

The same procedure applies to the heat transfer between pipe wall and steam. All the parameters needed for the calculation of the heat transfer coefficient U_{st} are obtained according to [6]. The assumptions made for the modelling are provided below, as well as the final expressions of the steam Nusselt number and heat transfer coefficient.

1. the pipes wall temperature is assumed to be constant spatially in the heat exchanger pipes;
2. the thermodynamic properties are assumed to be equal to the ones at the mean temperature;
3. the thermodynamic properties are assumed to be constant in the whole heat exchanger;
4. the steam flow is assumed to be in full hydrodynamical and thermal development;
5. the effect of internal fouling is assumed to be negligible.

$$Nu_{st} = \left(Nu_{st,1}^3 + 0.7^3 + \left(Nu_{st,2} - 0.7\right)^3 + Nu_{st,3}\right)^{\frac{1}{3}}; \qquad [Re_{st} < 2300]$$

$$= (1 - \gamma_{st})\left(Nu_{st,1}^3 + 0.7^3 + \left(Nu_{st,2} - 0.7\right)^3 + Nu_{st,3}\right)^{\frac{1}{3}} +$$

$$+ \gamma_{st}\ \frac{\epsilon_{st}}{8}\ 10^4\ Pr_{st}\ \frac{\left(1 + \left(\frac{d_i}{l_p}\right)^{\frac{2}{3}}\right)}{\left(1 + 12.7\ \sqrt{\frac{\epsilon_{st}}{8}}\ \left(Pr_{st}^{\frac{2}{3}} - 1\right)\right)} \qquad \left[Re_{st} \geq 2300 \wedge Re_{st} < 10^4\right]$$

$$= \frac{\epsilon_{st}}{8}\ Re_{st}\ Pr_{st}\ \frac{\left(1 + \left(\frac{d_{int}}{l_p}\right)^{\frac{2}{3}}\right)}{\left(1 + 12.7\ \sqrt{\frac{\epsilon_{st}}{8}}\ \left(Pr_{st}^{\frac{2}{3}} - 1\right)\right)}; \qquad \left[Re_{st} \geq 10^4\right]$$ Steam Nusselt number (3.20)

$$U_{st} = \frac{Nu_{st}\ \lambda_{st}}{d_i};$$ Metal-steam heat transfer coefficient (3.21)

Due to simulation stability problems, the internal heat flow is computed by replacing the internal logarithmic mean temperature difference with the temperature difference between metal and outlet steam. However, the loss in the prediction accuracy is very low, since it plays a minor role compared to the flue gas heat transfer coefficient. No heat loss is assumed to take place in the process.

$$Q_i = U_{st}\ A_i\ \left(T_m - T_{st,o}\right);$$ Metal-steam heat transfer (3.22)

The calculation of the outlet steam temperature follows the steps already presented for the flue gas.

$$\dot{m}_{st,o} = \dot{m}_{st,i};$$ Steam mass balance (3.23)

$$Q_i = \dot{m}_{st}\left(h_{st,o} - h_{st,i}\right);$$ Steam energy balance (3.24)

$$p_{st,o} = p_{st,i} - dp_{st};$$ Steam outlet pressure (3.25)

$$T_{st,o} = T\left(p_{st,o}, h_{st,o}\right); \qquad \text{Superheating steam temperature} \quad (3.26)$$

In the end, the expressions of the pipe wall heating up and the overall heat transfer coefficient are provided. The heat absorbed by the metal is equal to the difference between the external and internal heat flows. The heating up of the metal is described by an ordinary differential equation with the pipe wall temperature as dynamic variable, multiplied by the metal thermal inertia. Regarding the overall heat transfer coefficient, it is calculated by considering the overall logarithmic mean temperature difference and the mean surface area. The following assumptions are made:

1. the pipe wall heating up is assumed to be a uniform process in all the heat exchanger pipes;
2. only the heat flow to the steam is assumed to count in the overall heat transfer coefficient;
3. the effect of external and internal fouling is assumed to be negligible.

$$\dot{Q}_o - \dot{Q}_i = V_m\, \rho_m\, c_m\, \frac{\partial T_m}{\partial t} \qquad \text{Metal heating up} \quad (3.27)$$

$$LMTD = \frac{\left(T_{fg,i} - T_{st,o}\right) - \left(T_{fg,o} - T_{st,i}\right)}{\log \dfrac{T_{fg,i} - T_{st,o}}{T_{fg,o} - T_{st,i}}}; \qquad \text{Overall log. mean temperature diff.} \quad (3.28)$$

$$U = \frac{\dot{Q}_i}{A\, LMTD}; \qquad \text{Overall heat transfer coefficient} \quad (3.29)$$

The desuperheaters decrease the temperature of the steam before the last row of heat exchangers, and determine the amount of sub-cooled water to be drawn from the economizers. The data concerning the inlet steam and the desuperheating water conditions are set by the other components of the sub-model, while the steam outlet temperature is controlled by an external source. The amount of sub-cooled water needed is calculated through energy and mass balance equations. The assumptions made for the modelling of the component are provided below.

1. the steam-water mixing is assumed to take place with no heat loss;
2. the steam-water mixing is assumed to be complete, with no liquid at desuperheater exit;
3. the outlet steam temperature must be higher than the minimum superheating value;
4. the steam temperature distribution at desuperheater exit is assumed to be uniform.

The steam thermodynamic properties are calculated thanks to the set of implemented tables. The most important thermodynamic parameter is the specific enthalpy at the minimum superheating temperature, customizable depending on the type of desuperheater. The customizable mixing pressure drop is considered by the physical model as well.

$$p_{st,o} = p_{st,i} + dp_{mix}; \qquad \text{Outlet steam pressure} \quad (3.30)$$

$$h_{st,m} = h\left(p_{st,o}, T_{sat} + dT_{sh,m}\right); \qquad \text{Outlet steam minimum specific enthalpy} \quad (3.31)$$

Once the thermodynamic properties of the streams are known, it is possible to solve the balance equations. These equations vary depending on the controlled desuperheating temperature T_o, which cannot be higher than the steam inlet temperature nor lower than the minimum superheating. The

expressions through which the water mass flow rate $\dot{m}_{w,i}$ and steam outlet temperature $T_{st,o}$ are found are provided below.

$$\dot{m}_{st,o} = \dot{m}_{st,i} + \dot{m}_{w,i}; \qquad \text{Desuperheater mass balance} \quad (3.32)$$

$$\begin{aligned} \dot{m}_{w,i} &= 0; && \left[T_{st,i} \le T_o\right] \\ &= \frac{\dot{m}_{st,o} h_{st,m} - \dot{m}_{st,i} h_{st,i}}{h_{w,i}}; && \left[T_{st,i} > T_o \wedge T_o \le \left(T_{sat} + dT_{sh,m}\right)\right] \\ &= \frac{\dot{m}_{st,o} h_{st,o} - \dot{m}_{st,i} h_{st,i}}{h_{w,i}}; && \left[T_{st,i} > T_o \wedge T_o > \left(T_{sat} + dT_{sh,m}\right)\right] \end{aligned} \qquad \text{Liquid water mass flow rate} \quad (3.33)$$

$$\begin{aligned} T_{st,o} &= T_{st,i}; && \left[T_{st,i} \le T_o\right] \\ &= T_{sat} + dT_{sh,m}; && \left[T_{st,i} > T_o \wedge T_o \le \left(T_{sat} + dT_{sh,m}\right)\right] \\ &= T_o; && \left[T_{st,i} > T_o \wedge T_o > \left(T_{sat} + dT_{sh,m}\right)\right] \end{aligned} \qquad \text{Steam outlet temperature} \quad (3.34)$$

The evaporators components calculate the steam production in the circuits, and the outlet conditions of the flue gas exiting the heat exchanger. The thermodynamic properties of saturated water and vapour are calculated in function of the pressure existing in the circuits, by means of the tables implemented to the component. Furthermore, the flue gas data at evaporator inlet are determined by the previous heat exchangers. Except for the different approach to the computation of the boiling heat transfer coefficient, the physical models developed are very similar to the ones implemented to the superheaters. In order to avoid repetitions, the modelling of the water evaporation is described only, which required several assumptions to be considered due to the complexity of the process. The list of modelling assumptions and the final expressions for the Nusselt number and the boiling heat transfer coefficient are provided below.

1. the drums are assumed to supply as much water as the quantity of vapour produced.
2. the liquid water is assumed to enter the evaporator at uniform, saturated conditions;
3. the vapour is assumed to leave the evaporator at uniform, saturated conditions;
4. the evaporation is assumed to take place according to convective flow boiling in vertical tubes;
5. the evaporator pipes are assumed to be completely wetted;
6. a liquid layer thickness of 7.5 mm is assumed to be constant in all the pipes of the heat exchanger;
7. the boiling heat transfer coefficient is assumed to be constant in the whole heat exchanger;
8. the effect of external and internal fouling is assumed to be negligible;

$$U_l = \frac{Nu_l \, \lambda_l}{d_{int}}; \qquad \text{Liquid heat transfer coefficient} \quad (3.35)$$

$$U_v = \frac{Nu_v \, \lambda_v}{d_{int}}; \qquad \text{Vapour heat transfer coefficient} \quad (3.36)$$

$$A_b = (1 - x_{av})^{\frac{1}{100}} \left((1 - x_{av})^{\frac{3}{2}} + 1.9 \, x_{av}^{\frac{3}{5}} \left(\frac{\rho_l}{\rho_v} \right)^{\frac{7}{20}} \right)^{-\frac{11}{5}} \qquad \text{A factor} \quad (3.37)$$

$$B_b = x_{av}^{\frac{1}{100}} \left(\frac{U_v}{U_l} \left(1 + 8\,(1 - x_{av})^{\frac{7}{10}} \left(\frac{\rho_l}{\rho_v} \right)^{\frac{67}{100}} \right) \right)^{-2} \qquad \text{B factor} \quad (3.38)$$

$$U_b = U_l\,(A_b + B_b)^{-\frac{1}{2}}\,; \qquad \text{Boiling heat transfer coefficient} \quad (3.39)$$

Due to the constant pipe wall and water temperatures, no logarithmic mean temperature difference is required in the calculation of the heat flow absorbed by the two-phase mixture. Considering no heat loss in the heat transfer process, the value for the variable is obtained through the convective heat transfer equation already mentioned for the superheaters.

$$Q_i = U_b\ A_i\ \ (T_m - T_{sat})\,; \qquad \text{Metal-mixture heat transfer} \quad (3.40)$$

The amount of vapour produced during the process and the water supplied by the drums are obtained by considering the energy and mass balance equations for the water. The related expressions are provided below.

$$Q_i = \dot{m}_{v,o}\left(h_{v,o} - h_{w,i}\right); \qquad \text{Mixture energy balance} \quad (3.41)$$

$$\dot{m}_{v,o} = \dot{m}_{w,i}; \qquad \text{Mixture mass balance} \quad (3.42)$$

The last equations of the physical model are aimed at the computation of the heating up of the pipes metal and the overall heat transfer coefficient. Their shape is equal to the ones proposed for the superheaters, but are mentioned again for a matter of clearness.

$$\dot{Q}_o - \dot{Q}_i = V_m\ \rho_m\ c_m\ \frac{\partial T_m}{\partial t} \qquad \text{Metal heating up} \quad (3.43)$$

$$LMTD = \frac{\left(T_{fg,i} - T_{v,o}\right) - \left(T_{fg,o} - T_{w,i}\right)}{\log \dfrac{T_{fg,i} - T_{v,o}}{T_{fg,o} - T_{w,i}}}; \qquad \text{Overall logarithmic heat transfer coefficient} \quad (3.44)$$

$$U = \frac{\dot{Q}_i}{A\ LMTD}; \qquad \text{Overall heat transfer coefficient} \quad (3.45)$$

3.2.3. Plant valves

The sub-model comprehends the valves installed between HRSG and turbines, which control the steam flow to the machines during start-up. Except for the stop valves, the opening position of the valves is controlled by the experimental data imported by the components. However, the control valves reproduce the steam flow limitation according to physical models, which also include experimental correlations. Regarding the bypass valves, their opening positions actually determine the pressure in the circuits: although, the physical models predict the steam expansion through the valves only. A schematic representation of the valves sub-model is provided in Figure 3.4. The operation of the stop valves and control valves is described in the next paragraphs.

The stop valves operate on/off depending on whether the opening condition is satisfied. The steam conditions at valves inlet are determined in the last heat exchangers of the HRSG, and the mass flow rates are set equal to 0 as long as the valves are closed. The opening conditions usually coincides with a certain temperature to be reached in the pipe right before the HP stop valve. However, the difficulty in accurately reproducing the heating up of the pipe implies the use of a different variable as a measure of the pipe wall temperature. This variable is chosen to be the steam pressure in the HP circuit. As a

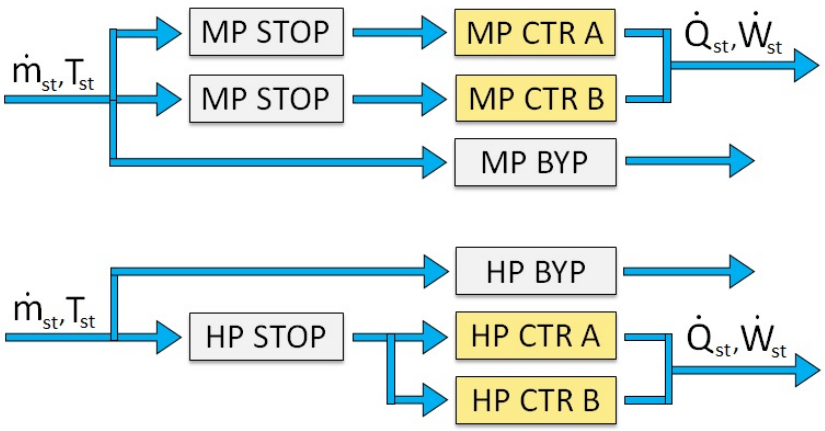

Figure 3.4: Scheme of the structure of the VALVES sub-model

result, as soon as the pressure exceeds a customizable minimum value, all the stop valves open at the same time. The modelling of the stop valves relies on the following assumptions:

1. no condensation is assumed to take place at stop valves inlet;
2. the upstream effect of the stop valves opening is assumed to be negligible;
3. the steam expansion during the fast opening is assumed to be function of the opening time;
4. the heating up of the downstream pipes is assumed to be negligible.
5. the pressure in the downstream pipes is assumed to be equal to the environment pressure;
6. the temperature in the downstream pipes is assumed to be equal to the environment temperature.

$$o_{\%} = 0; \quad [p_{st,i} < p_{min}]$$
$$= 100; \quad [p_{st,i} \geq p_{min}] \qquad \text{Stop valve position} \quad (3.46)$$

$$\dot{m}_{st,i} = 0; \quad [p_{st,i} < p_{min}]$$
$$= \dot{m}_{st,o}\left(1 - \frac{1}{1 + \left(\int_{t0}^{t} o_{\%}\, dt\right)}\right); \quad [p_{st,i} \geq p_{min}] \qquad \text{Steam outlet mass flow rate} \quad (3.47)$$

$$p_{st,o} = p_{env}; \quad [p_{st,i} < p_{min}]$$
$$= p_{env} + \left(p_{st,i} - p_{env}\right)\left(1 - \frac{1}{1 + \left(\int_{t0}^{t} o_{\%}\, dt\right)}\right); \quad [p_{st,i} \geq p_{min}] \qquad \text{Steam outlet pressure} \quad (3.48)$$

$$T_{st,o} = T_{env}; \quad [p_{st,i} < p_{min}]$$
$$= T_{env} + \left(T_{st,i} - T_{env}\right)\left(1 - \frac{1}{1 + \left(\int_{t0}^{t} o_{\%}\, dt\right)}\right); \quad [p_{st,i} \geq p_{min}] \qquad \text{Steam outlet temperature} \quad (3.49)$$

The control valves dictate the steam flow to the turbines, which depend on the valves opening, controlled by external sources, and the upstream and downstream conditions. As long as the turbines internal pressure is lower than the critical value, the steam flow is equal to the one at choking conditions. As a consequence, the physical models for the choked flow analysed in [5] are implemented to the valves, in addition to a simple steam expansion model. The parameters of the valves flow coefficients are customizable, in order to adapt the model to different valves sizes. The list of assumptions made for the modelling of the control valves is provided below.

1. the effect of the pipes bends is assumed to be negligible;
2. the steam expansion in the control valves is assumed to be isentalpic;
3. the flow coefficients of the valves are assumed to have a parabolic shape;
4. the pressure drop between valves and turbines inlet are assumed to be negligible;
5. the critical pressure ratio is assumed to be function of the adiabatic coefficient only;
6. the adiabatic coefficient and steam density are assumed to be equal to the values at valves inlet;
7. the pressure at turbines inlet is assumed to be function of the leading control valve opening;
8. the pressure in the downstream pipes is assumed to be equal to the environment pressure;
9. the temperature in the downstream pipes is assumed to be equal to the environment temperature.

The flow coefficient of the valve is obtained by using a 2-degree polynomial expression having the current opening position as variable.

$$Cv = a\ o_{\%}^2 + b\ o_{\%} + c; \qquad \text{Control valve flow coefficient} \quad (3.50)$$

The value of the downstream pressure determines whether choked flow conditions occur or not. As a consequence, it is very important to accurately predict this variable during the simulation, in order to exactly reproduce the control valves operation. The downstream pressure is assumed to be equal to the pressure in the first stage of the turbines, which depends on the thermodynamic conditions inside the machine. Due to the difficulty in reproducing the flow dynamics inside the machines, the pressure ratio between downstream and upstream pressures is expressed by an experimental correlation. The correlations are developed by analysing the data of 15 different start-ups, as shown in Figure 3.5 for the HP circuit, and 3.6. The experimental correlations are implemented to the physical model, ensuring high accuracy during the simulation.

$$\begin{aligned}\frac{p_{st,o}}{p_{st,i}} &= \frac{1}{2500}\ o_{\%}^2 + \frac{11}{1000}\ o_{\%} + \frac{1}{5}; && [o_{\%} \le 20\%] \\ &= \frac{2}{5}\sin\left(\frac{31}{625}o_{\%} - \frac{124}{125}\right) + \frac{29}{50}; && [o_{\%} > 20\% \wedge o_{\%} \le 52\%] \\ &= \frac{3}{10000}o_{\%} + \frac{3011}{3125}; && [o_{\%} > 52\%]\end{aligned} \qquad \text{HP valves pressure ratio} \quad (3.51)$$

$$\begin{aligned}\frac{p_{st,o}}{p_{st,i}} &= \frac{1}{5000}\ o_{\%}^2 + \frac{43}{5000}\ o_{\%} + \frac{1}{20}; && [o_{\%} \le 30\%] \\ &= \frac{2}{5}\sin\left(\frac{133}{2500}o_{\%} - \frac{799}{500}\right) + \frac{11}{20}; && [o_{\%} > 30\% \wedge o_{\%} \le 59\%] \\ &= \frac{11}{10000}o_{\%} + \frac{177}{200}; && [o_{\%} > 59\%]\end{aligned} \qquad \text{MP valves pressure ratio} \quad (3.52)$$

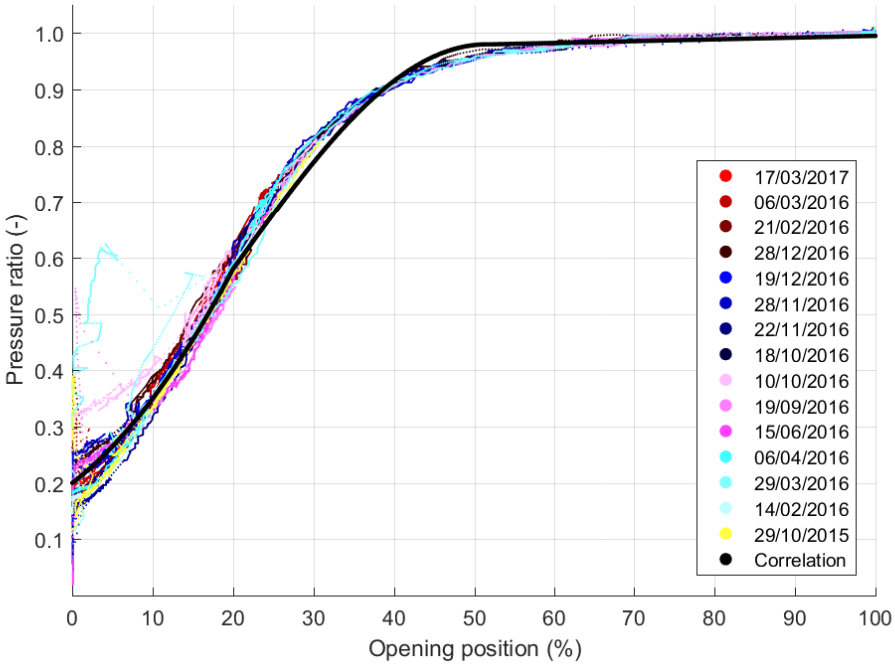

Figure 3.5: Experimental correlation for the HP control valves pressure ratio

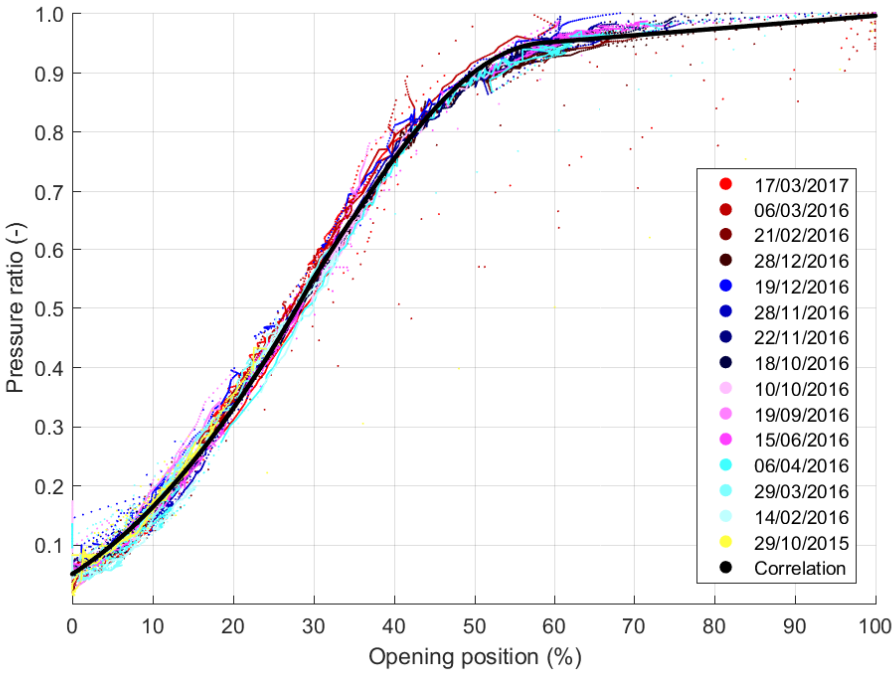

Figure 3.6: Experimental correlation for the MP control valves pressure ratio

In order to evaluate the parameters needed for the determination of the steam choked flow value, the steam thermodynamic tables are used. As a result, the critical downstream pressure is obtained as a function of the steam adiabatic coefficient.

$$\frac{p_{st,cr}}{p_{st,i}} = \left(\frac{2}{k_{st,i}+1}\right)^{\frac{k_{st,i}}{k_{st,i}-1}}; \qquad \text{Critical pressure ratio (3.53)}$$

According to the valves pressure ratio, the valves pressure drop ratio x and expansion factor y are computed. The first one provides the ratio between the pressure difference between valves inlet and outlet and the upstream pressure. It depends on the valves pressure ratio: if it is lower than the critical value, its is expressed in function of the adiabatic coefficient. The expansion factor represents the limitation factor due to the steam expansion through the valve, and it is important for the determination of the steam flow. It is obtained by dividing the actual pressure drop ratio by the maximum value at critical conditions, and the ratio is subtracted to the unity. The value for the expansion factor y is also available as component output.

$$x = k_{st,i}1.4\left(1-\frac{2}{k_{st,i}+1}\right)^{\frac{k_{st,i}}{k_{st,i}-1}}; \qquad \left[\frac{p_{st,o}}{p_{st,i}} < \frac{p_{st,cr}}{p_{st,i}}\right]$$

$$= 1-\frac{p_{st,o}}{p_{st,i}}; \qquad \left[\frac{p_{st,o}}{p_{st,i}} \geq \frac{p_{st,cr}}{p_{st,i}}\right] \qquad \text{Valve expansion factor (3.54)}$$

$$y = 1-\frac{1-\frac{p_{st,o}}{p_{st,i}}}{\frac{3k_{st,i}}{1.4}\left(1-\frac{2}{k_{st,i}+1}\right)^{\frac{k_{st,i}}{k_{st,i}-1}}}; \qquad \text{Valve expansion factor (3.55)}$$

At this point, the maximum steam flow and the outlet steam temperature are calculated. The former is obtained through the expression provided in [**?**] for compressible flow through control valves. Regarding the latter, it is determined by means of the steam p-h thermodynamic table implemented to the component. As already mentioned in the assumptions list, the specific enthalpy at valves exit is considered equal to the one at valves inlet.

$$\dot{m}_{st,o} = \frac{27.3}{3600} Cv\ y\sqrt{x p_{st,i}\rho_{st,i}}; \qquad \text{Steam mass flow rate (3.56)}$$

$$T_{st,o} = T_{st}\left(p_{st,o}, h_{st,i}\right); \qquad \text{Steam outlet temperature (3.57)}$$

3.2.4. Steam Turbines System

The main components of the sub-model are the system composed by shaft, HP turbine and MP turbine, and the rotor stress controllers. The former uses the steam variables predicted by the previous sub-model in order to calculate the heat and power flows in the machines. As a result, the component predicts the trends of the turbines reference temperatures, the acceleration of the shaft and the electrical power produced. The values of the turbines reference temperatures are sent to the rotor stress controllers, which recreate the temperature distribution within the first stage rotor wheels. The controllers return the values of the thermal stresses along the three cylindrical directions calculated at rotor surface and center. In addition, the ST sub-model includes the electrical generator and the main condenser. The structure of the sub-model is depicted in Figure 3.7. The operation of the turbines system and stress controllers is described in the next paragraphs.

The steam turbines system component ensures a accurate prediction of the most important phenomena of the start-up process, which are the turbines heating up and the shaft acceleration. Due to the difficulty in reproducing the steam-blade interaction during start-up, the physical models implemented to the steam turbines component include experimental correlations. The time derivatives of the turbine

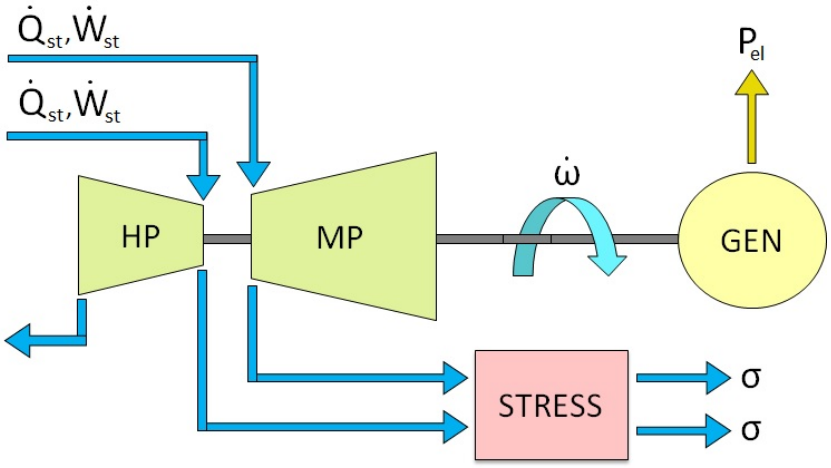

Figure 3.7: Scheme of the structure of the ST sub-model

reference temperatures and shaft speed, as well as the steam outlet conditions, depend also on the technical data of the turbines system. These data are customizable, and consist of the thermal inertias of the turbines and the system rotational inertia (turbines, shaft, generator). Several assumptions are made for the modelling of the steam turbines system. They are presented in the list below.

1. the surface temperature along the turbines stages is assumed to be constant;
2. the constant surface temperature is assumed to be equal to the reference temperature;
3. the heat transfer is assumed to take place with no thermal loss;
4. the effect of the steam flows on the heat transfer is assumed to be negligible;
5. the heat transfer is assumed to be the leading phenomenon in the turbines;
6. hence, the power flow is assumed to be function of the heat transfer in the machines;
7. if saturated conditions occur, all the steam is assumed to condense;
8. all the condense is assumed to be removes instantaneously by the drain ducts;
9. the turbines drain ducts are assumed to be steadily closed once condensation ends;
10. the power flow in the LP turbine is assumed to be negligible.

According to the previous assumptions, the mechanical power transferred by the steam to the turbines shaft is expressed in function of the heat flow. However, the difficulty in estimating the heat transfer coefficient and surface area makes an analytical description of the heat transfer non accurate. In order to solve this problem, the steam expansion in the turbines is studied, and the effects on the turbines main variables (heating up, acceleration) are assessed. As a result, it is possible to analyse the ratio between the energy flows in function of the steam-turbine temperature difference, which governs the heat transfer phenomena in the machines. Based on the data of 15 different real start-ups, two experimental correlations are developed in order to predict the heating up and the power flow in the HP and MP steam turbines. The experimental correlations developed for the HP and MP steam turbines are depicted respectively in Figure3.8 and 3.9, and the related mathematical expressions are provided.

$$r_{hp} = \frac{1}{\frac{2}{75}\left(T_{st,i} - T_{hpt}\right) - \frac{2}{3}}; \qquad \left[\left(T_{st,i} - T_{hpt}\right) \geq 100\ K\right]$$

$$= \frac{-\frac{17}{1850}\left(T_{st,i} - T_{hpt}\right) + 1}{\frac{2}{925}\left(T_{st,i} - T_{hpt}\right) - \frac{2}{37}}; \qquad \left[\left(T_{st,i} - T_{hpt}\right) < 100\ K\right] \qquad \text{HP turbine P/Q ratio} \quad (3.58)$$

$$r_{mp} = \frac{1}{\frac{1}{700}\left(T_{st,i} - T_{hpt}\right) - \frac{3}{70}}; \qquad \left[\left(T_{st,i} - T_{hpt}\right) \geq 100\ K\right]$$

$$= \frac{-\frac{17}{2400}\left(T_{st,i} - T_{hpt}\right) + 1}{\frac{1}{2400}\left(T_{st,i} - T_{hpt}\right) - \frac{1}{80}}; \qquad \left[\left(T_{st,i} - T_{hpt}\right) < 100\ K\right] \qquad \text{MP turbine P/Q ratio} \quad (3.59)$$

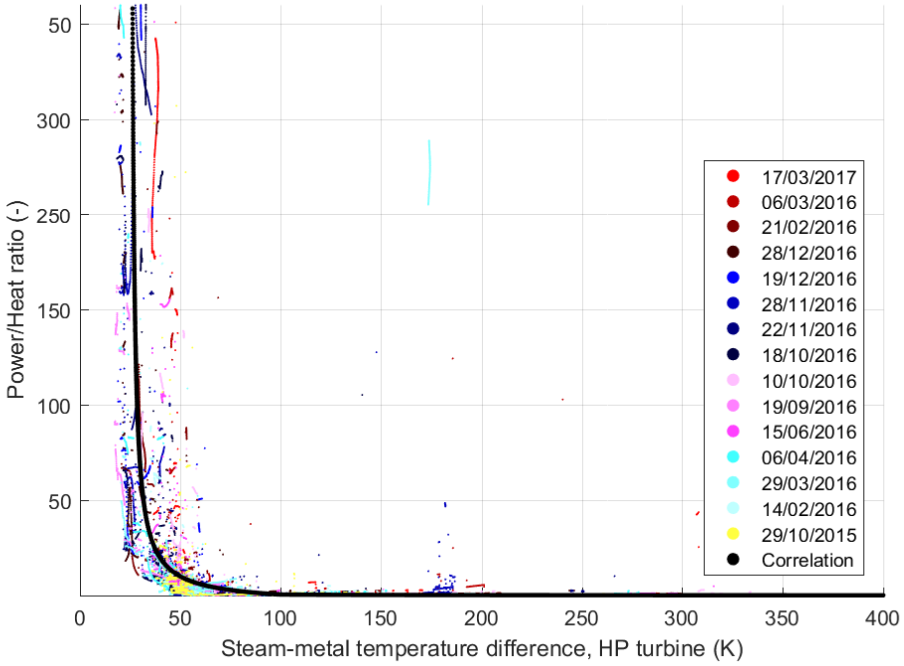

Figure 3.8: P/Q experimental correlation developed for the HP steam turbine

The time derivative of the turbines surface temperature and the mechanical power are calculated through the energy balance equations of the machines. The P/Q ratio is considered in the computation.

$$\dot{W} = r\ \dot{Q}; \qquad \text{Mechanical power} \quad (3.60)$$

$$\begin{aligned} \dot{m}_{st}\left(h_{st,i} - h_{st,o}\right) &= \dot{Q} + \dot{W}; \\ &= \dot{Q} + r\ \dot{Q}; \\ &= \dot{Q}\,(1 + r)\,; \\ &= I_{th}\,\frac{\partial T_{hpt}}{\partial t}\,(1 + r)\,; \end{aligned} \qquad \text{Turbines energy balance} \quad (3.61)$$

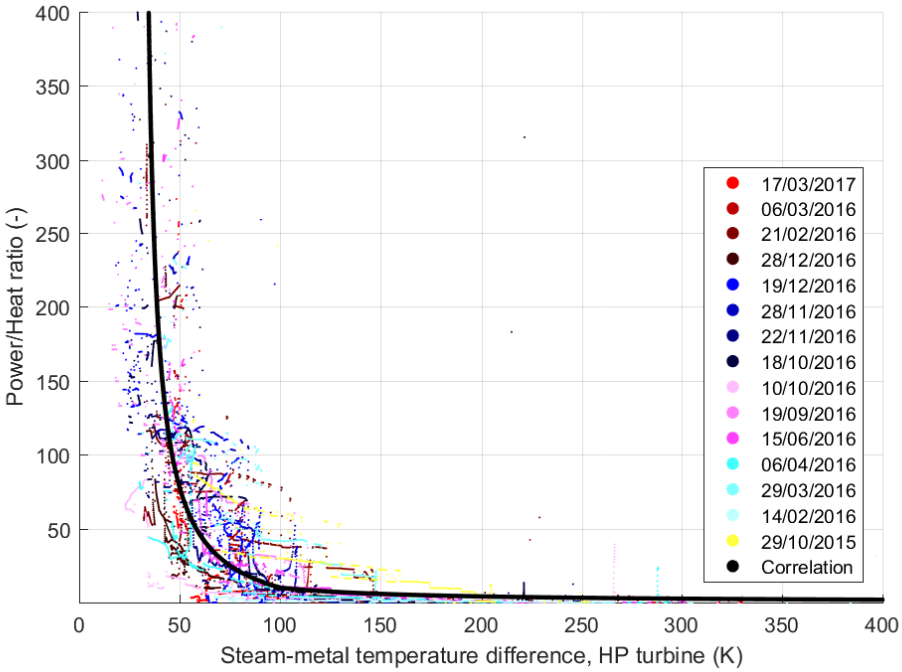

Figure 3.9: P/Q experimental correlation developed for the MP steam turbine

Once the power flows in the HP and MP turbines are known, it is possible to obtain the shaft torque by considering the energy balance equation of the shaft. The friction is considered in the energy balance as percentage of the overall mechanical power.

$$T = \frac{100 - l_{\%}}{100} \frac{\left(\dot{W}_{hp} + \dot{W}_{mp}\right)}{(2\ \pi\ \omega)}; \qquad \text{Shaft energy balance} \quad (3.62)$$

As long as the shaft speed is lower than the synchronization value, the torque produces an acceleration of the shaft. The time derivative of the angular velocity of the shaft is computed according to the conservation of the angular momentum equation. Once the shaft speed reaches the synchronization value, the generator switches on and the power produced in the steam turbines system is converted into electrical power. Like the thermal inertia of the turbines, the value of the rotational inertia of the system composed by the turbines, shaft and generator must be accurate.

$$T = J\ 2\ \pi\ \frac{\partial \omega}{\partial t}; \qquad \text{Shaft acceleration} \quad (3.63)$$

The rotor stress controllers receive the values of the turbine reference temperatures predicted by the steam turbines system component, and use them to predict the conductive heat transfer within the first stage rotor. The components operate according to pure heat transfer physical models, including no experimental correlations. The customizable material properties make the components capable to reproduce the heating up of different turbines. However, if not specified by the manufacturer, the material properties must be accurately evaluated, since the accuracy of the physical models mainly depends on these parameters. The assumptions made for the modelling of the heat transfer within the rotors are presented below.

1. the rotor wheel is considered to be a thin solid disk;
2. the left and right surfaces of the disk are assumed to by thermally isolated;
3. the temperature distribution within the rotor wheel is axial-symmetric;
4. the temperature in each shell is assumed to be equal to the one at the mean radius;
5. the material is homogeneous, isotropic and compressible;
6. the material properties are assumed constant within the rotor wheel.

The rotor disk is divided into 19 concentric shells, plus the central thin disk representing the rotor center. Each shell i is identified by a mean radius $r_{m,i}$, determined by considering a constant step equal to 5% of the rotor radius. The enumeration starts from the turbines external surface: as a consequence, the shell corresponding to the external surface is identified by the subscript 1, while the central disk is identified by the subscript 20.

$$r_{m,i} = \frac{d}{2}\frac{21-i}{20}; [i = 1:20] \qquad \text{Shell i mean radius} \quad (3.64)$$

Each concentric shell is characterized by a certain volume, enclosed between the shell inner and outer surfaces. The radius corresponding to the inner surface of the shell i can be expressed with the arithmetic mean of the radius i and $i+1$. On the other hand, the radius of the outer surface of the shell i is obtained through the arithmetic mean of the radius i and $i-1$. According to this formulation, the expressions of the shell volumes are provided below.

$$\begin{aligned} V_i &= th\,\pi\left(r_1^2 - \left(\frac{r_1+r_2}{2}\right)^2\right); && [i=1] \\ &= th\,\pi\left(\left(\frac{r_i+r_{i-1}}{2}\right)^2 - \left(\frac{r_i+r_{i+1}}{2}\right)^2\right); && [i=2:19] \\ &= th\,\pi\left(\frac{r_{20}+r_{19}}{2}\right)^2; && [i=20] \end{aligned} \qquad \text{Volume ring i} \quad (3.65)$$

At this point, it is possible to determine the temperature increase in each shell, due to the heat absorption. The shell heating up is predicted through the energy balance equation, which comprehends the Fourier's law of conduction at the outer and inner surfaces. The higher the thermal diffusivity of the material is, the faster the temperature increases within the shells. The heating up of the external shell 1 is not computed by the model, since it is determined by the steam turbines system component.

$$\begin{aligned} \frac{\partial T_i}{\partial t} &= \frac{a\;th\,\pi}{V_i}\left(\frac{r_{i-1}+r_i}{r_{i-1}-r_i}(T_{i-1}-T_i) - \frac{r_i+r_{i+1}}{r_i-r_{i+1}}(T_i-T_{i+1})\right); && [i=2:19] \\ &= \frac{a\;th\,\pi}{V_{20}}\left(\frac{r_{19}+r_{20}}{r_{19}-r_{20}}(T_{19}-T_{20})\right); && [i=20] \end{aligned} \qquad \text{Heating-up shell } i \quad (3.66)$$

It is now possible to determine the volumetric mean temperature $T_{m,vol}$ of the turbine rotor. Due to the discretization applied, it is not possible to apply the integral expression. However, the weighted average of the shell temperatures, considering the volumes as the weights, approximates well the value for this variable.

$$T_{m,vol} = \frac{\sum_{i=1}^{20} T_{hpt,i}\,V_i}{\sum_{i=1}^{20} V_i}; \qquad \text{Volumetric mean temperature} \quad (3.67)$$

In the end, the values of the thermal stresses along the radial, circumferential and axial directions are calculated at rotor surface and center. In order to keep the narrative short, only the expressions related to the maximum thermal stresses are provided. They correspond to the axial and circumferential stresses calculated at the turbine surface.

$$\sigma_{th,ax,ex}(r_{m,1}) = \frac{\alpha E}{1-\nu}\left(T_{m,vol} - Thpt1\right); \qquad \text{Surface axial thermal stress} \quad (3.68)$$

$$\sigma_{th,cir,ex}(r_{m,1}) = \frac{\alpha E}{1-\nu}\left(T_{m,vol} - Thpt1\right); \qquad \text{Surface circumferential thermal stress} \quad (3.69)$$

3.3. Modelling approach

The sub-models described so far are characterized by two types of physical objects: streams and components. The streams represent flows of substances, such as water and gas, characterized by certain properties and variables. The streams enter and exit the components, which provide the physical relations between their variables. As a result, streams and components are represented by two different types of physical models, whose structures are described in this section.

3.3.1. Stream model

A stream physical model describes the thermodynamic state of a substance flow. The thermodynamic parameters, such as tables or universal constants, and the main physical variables of the stream are declared and characterize all the flows belonging to the same stream type. In the CCGT power station model, two stream types are modelled: water and gas. They differ in the type and number of parameters, while the variables are exactly the same. This modelling choice is explained by considering the different role of the two physical objects in the model. While the thermodynamic tables and constants depend on the specific substance considered in the stream, the flows of the substances are defined by the same physical variables, such as mass flow rate, pressure, temperature, density and specific enthalpy. In particular, all the stream thermodynamic variables can be determined in function of pressure and temperature, and the mass flow rate is sufficient to describe the stream flows inside pipes and machines. According to this approach, the list of variables and parameters declared in the water and gas stream models are provided in Tables 3.1, 3.2 and 3.3.

Table 3.1: Variables declared in the water and gas stream models

Variable name	Description	Unit
$\dot{m}$	Mass flow rate	kg/s
p	Static pressure	bar
T	Static temperature	K

Table 3.2: Parameters declared in the water stream model

Parameter name	Description	Type	Unit
p_w	Pressure reference vector	Array	bar
x_w	Vapor quality reference vector	Array	-
$\rho_{w,re}$	Density reference vector	Array	kg/m^3
T_{sc}	Subcooling temperature reference vector	Array	K
T_{sh}	Superheating temperature reference vector	Array	K
h_{sc}	Subcooling spec. enthalpy reference vector	Array	kJ/kg
h_{sh}	Superheating spec. enthalpy reference vector	Array	kJ/kg
$T_{sc,hp}$	Subcooled temperature hp table	Table	K
$T_{sat,xp}$	Saturated temperature xp table	Table	K
$T_{sh,hp}$	Superheating temperature hp table	Table	K
$h_{sc,Tp}$	Subcooled spec. enthalpy Tp table	Table	kJ/kg
$h_{sat,xp}$	Saturated spec. enthalpy xp table	Table	kJ/kg
$h_{sh,Tp}$	Superheating spec. enthalpy Tp table	Table	kJ/kg
$\lambda_{sc,Tp}$	Subcooled therm. conductivity Tp table	Table	W/m K
$\lambda_{sat,xp}$	Saturated therm. conductivity xp table	Table	W/m K
$\lambda_{sh,Tp}$	Superheating therm. conductivity Tp table	Table	W/m K
$c_{sc,Tp}$	Subcooled spec. heat Tp table	Table	kJ/kg K
$c_{sat,xp}$	Saturated spec. heat xp table	Table	kJ/kg K
$c_{sh,Tp}$	Superheating spec. heat Tp table	Table	kJ/kg K
$Pr_{sc,Tp}$	Subcooled Prandtl number Tp table	Table	-
$Pr_{sat,xp}$	Saturated Prandtl number xp table	Table	-
$Pr_{sh,Tp}$	Superheating Prandtl number Tp table	Table	-
$\rho_{sc,Tp}$	Subcooled density Tp table	Table	kg/m^3
$\rho_{sat,xp}$	Saturated density xp table	Table	kg/m^3
$\rho_{sh,Tp}$	Superheating density Tp table	Table	kg/m^3
$\mu_{sc,Tp}$	Subcooled kin. viscosity Tp table	Table	Pa s
$\mu_{sat,xp}$	Saturated kin. viscosity xp table	Table	Pa s
$\mu_{sh,Tp}$	Superheating kin. viscosity Tp table	Table	Pa s
$k_{sh,Tp}$	Adiabatic coefficient Tp table	Table	-

Table 3.3: Parameters declared in the gas stream model

Parameter name	Description	Type	Unit
p_{fg}	Pressure reference vector	Array	bar
T_{fg}	Temperature reference vector	Array	K
h_{fg}	Specific enthalpy reference vector	Array	kJ/kg
$T_{fg,hp}$	Temperature hp table	Table	K
$h_{fg,Tp}$	Specific enthalpy Tp table	Table	kJ/kg
$\lambda_{fg,hp}$	Thermal conductivity hp table	Table	W/m K
$\lambda_{fg,Tp}$	Thermal conductivity Tp table	Table	W/m K
$c_{fg,hp}$	Specific heat at constant pressure hp table	Table	kJ/kg K
$c_{fg,Tp}$	Specific heat at constant pressure Tp table	Table	kJ/kg K
$Pr_{fg,hp}$	Prandtl number hp table	Table	-
$Pr_{fg,Tp}$	Prandtl number Tp table	Table	-
$\rho_{fg,hp}$	Density hp table	Table	kg/m^3
$\rho_{fg,Tp}$	Density Tp table	Table	kg/m^3
$\mu_{fg,hp}$	Kinetic viscosity hp table	Table	Pa s
$\mu_{fg,Tp}$	Kinetic viscosity Tp table	Table	Pa s

3.3.2. Component model

A component physical model reproduces the operation of an equipment installed in the CCGT installation. In order to do so, it is characterized by input and output ports, which describe the physical streams and the signals entering and exiting the component. An example of component ports is provided in Table , which described the ports of the HP Evaporator model.

Table 3.4: Ports of the HP Evaporator model

Port name	Type	Description
w_i	Water	Saturated water from the HP drum
fg_i	Gas	Flue gas from the HP Primary Superheater
T_m	Output	Constant pipes wall temperature (K)
Q_i	Output	Heat flow absorbed by the water (MWth)
Q_o	Output	Heat flow discharged by the flue gas (MWth)
U	Output	Overall heat transfer coefficient (kW/m^{2}K)
v_o	Water	Saturated vapour to the HP drum
fg_o	Gas	Flue gas to the MP Superheater

A component model can also include customizable parameters, such as technical data or additional thermodynamic tables, and internal variables. These modelling objects are declared for each type of component, which presents the same features independently from its position in the component network. In the CCGT power station model, more than 50 components are modelled and gathered in 10 different groups. The component groups are described in Table 3.5.

Table 3.5: Groups of the *Prediction* multi-domain components library

Group name	Number of Components	Streams involved
Drums	2	*Water*
Heat exchangers	15	*Water*, *Gas*
Measurements	6	*Water*, *Gas*
Mixers	6	*Water*, *Gas*
Pumps	2	*Water*
Sinks	3	*Water*, *Gas*
Sources	4	*Water*, *Gas*
Splitters	3	*Water*, *Gas*
Tables	2	*Water*, *Gas*
Turbines	5	*Water*, *Gas*
Valves	9	*Water*

The component equations define the relations existing between input, output and internal variables. They can be algebraic or differential, depending on whether the time derivative of the variables appears in the expression. The known quantities, like parameters and input data, are considered as boundary conditions by the solver. The shape of the model equations can adapt to different operating conditions, thanks to the conditional expressions already provided for the characteristic equations discussed in the previous section.

3.4. Implementation in Simulink^{TM}

The physical models developed for the streams and components are implemented in the dynamic simulation software Simulink^{TM} as a custom component library. This choice relies on the possibility to make the dynamic model of the power station easily accessible by the users, thanks to the object-oriented environment and the customizable user-friendly interfaces of the components. Furthermore, Simulink^{TM} is integrated in the MATLAB^{TM} software, and this simplifies the conversion of the physical model codes, written in MATLAB^{TM}, into Simulink^{TM} blocks. However, the physical models have to be modified according to the Simscape^{TM} modelling language, through which it is possible to customize the user-friendly interfaces of the blocks. The stream models must be declared as *Domain* class models, which allow the declaration of parameters and variables only. They characterize the physical ports of the component blocks, and are represented in Simulink^{TM} as coloured lines. In the dynamic model, the *Water* streams appear as blue lines, while the *Gas* streams appear as green lines, as shown respectively in Figures 3.10 and 3.11.

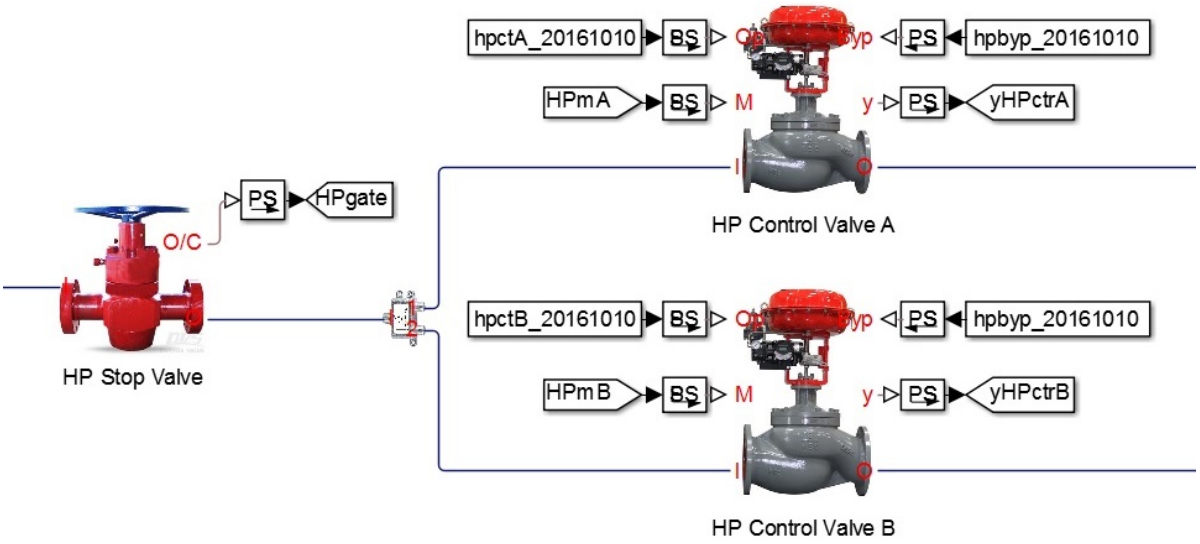

Figure 3.10: *Water* physical streams representing the steam flow after the *HP Stop Valve*

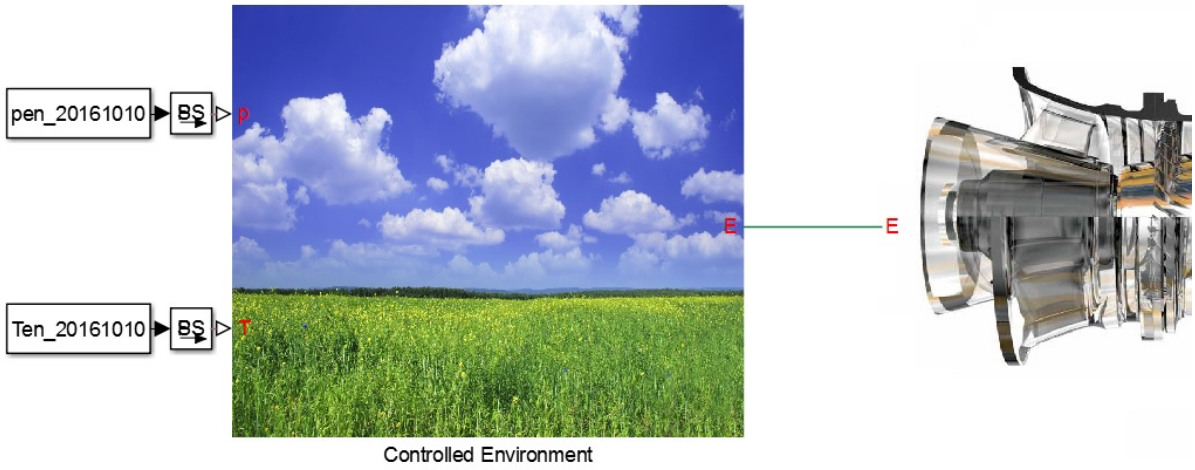

Figure 3.11: *Gas* physical stream representing the air flow to the GT intake

The component models must be declared as *Component* class models, and include all the objects discussed in the previous section. The ports name and position on the component external interface can be specified in the code. Same applies for the parameter description and variables list. As an example, the ports of the *HP Control Valve A* component are described in Table 3.6 and shown in Figure 3.12 as they appear in the component external interface.

Table 3.6: Ports of the *HP Control Valve A* component block

Port name	Type	Description	Location
OP	Input	Controlled opening position (%)	Left
M	Input	HP steam mass flow at HRSG outlet (kg/s)	Left
I	*Water*	Steam from the *HP Stop Valve*	Left
Byp	Input	*HP Bypass* opening position (%)	Right
y	Output	Expansion factor (-)	Right
O	*Water*	Steam to the *Steam Turbines System*	Right

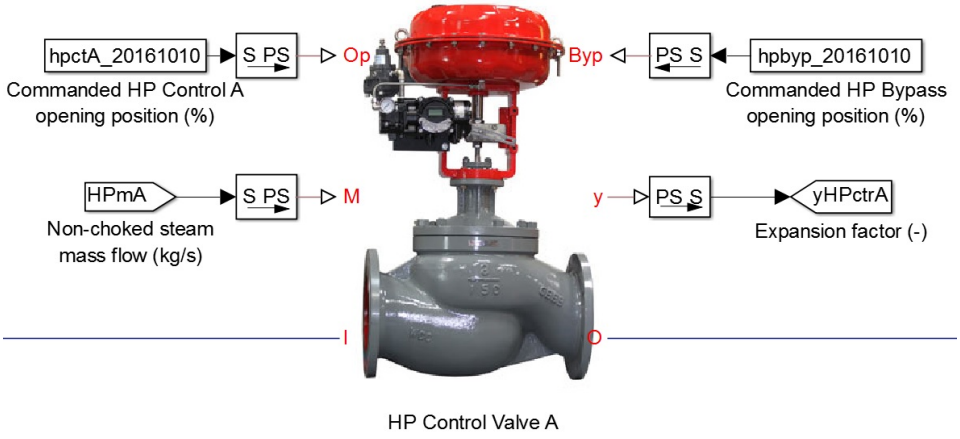

Figure 3.12: View of the *HP Control Valve A* external interface

Regarding the component parameters, the *HP Control Valve A* includes 4 different parameters, provided in Table 3.7. The parameter list in the component internal interface is shown in Figure 3.13.

Table 3.7: Parameters of the *HP Control Valve A* model

Parameter name	Description	Type	Unit
p_{op}	HP stop valve opening pressure	Value	bar
a	Coefficient a of Cv parabolic correlation	Value	m^2
b	Coefficient b of Cv parabolic correlation	Value	m^2
c	Coefficient c of Cv parabolic correlation	Value	m^2

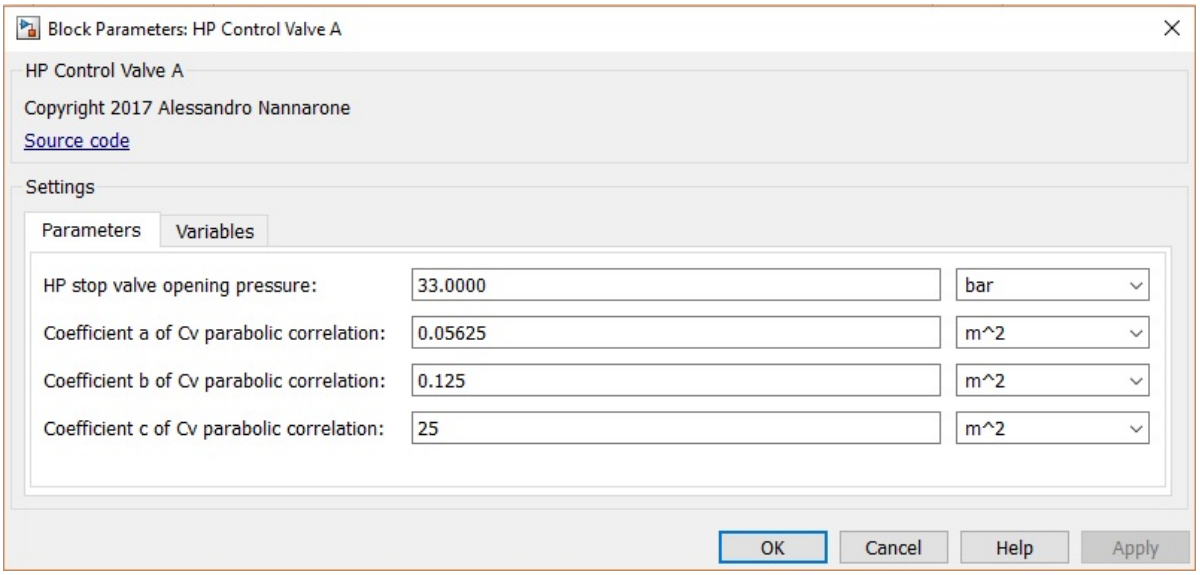

Figure 3.13: Parameters list in the *HP Control Valve A* element interface

In the end, the only internal variable implemented to the *HP Control Valve A* model is described first in Table 3.8, and shown in Figure 3.14 as it appears in the component interface.

Table 3.8: Internal variables of the *HP Control Valve A* model

Variable name	Description	Unit
dp	Valve pressure drop	bar

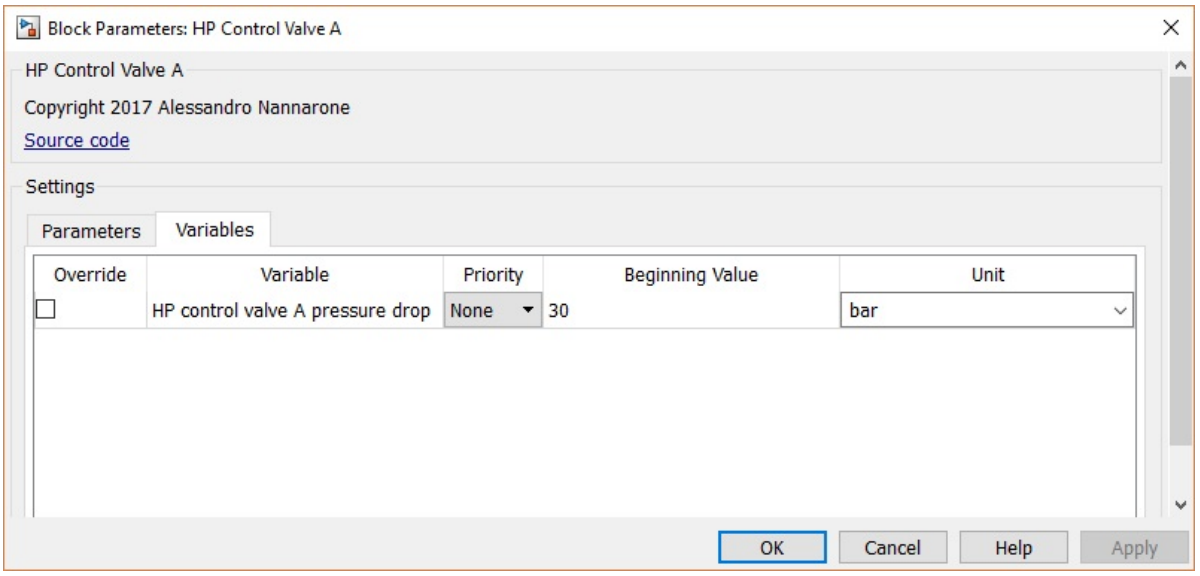

Figure 3.14: Internal variables list in the *HP Control Valve A* element interface

3.5. Model set-up

The general structure of the dynamic model presented in the first section of the Chapter is reproduced in Simulink^{TM} as a network of physical streams and components. As a result, the dynamic model includes more than 110 components, which form the four sub-models of the GT, HRSG, VALVES and ST. The details concerning the operation of the sub-models are summarized below.

- the GT operates as heat source of the steam cycle;
- the GT returns the operating cost and relevant parameters;
- the HRSG requires the pressures and desuperheating temperatures to be set;
- the HRSG returns the values of the steam flows and temperatures;
- the VALVES require the opening position to be set;
- the VALVES return the values of the steam flows and temperatures at turbines inlet;
- the ST returns the turbines heating up, stresses, shaft acceleration and power output.

Figures 3.15, 3.16, 3.17 and 3.18 respectively depict the four sub-models as they appear in Simulink^{TM}. The measurements carried out by thermocouples, manometers and flow meters are available in the model *control room*, not shown in the pictures. It reproduces the control panels installed in the control rooms of existing power stations.

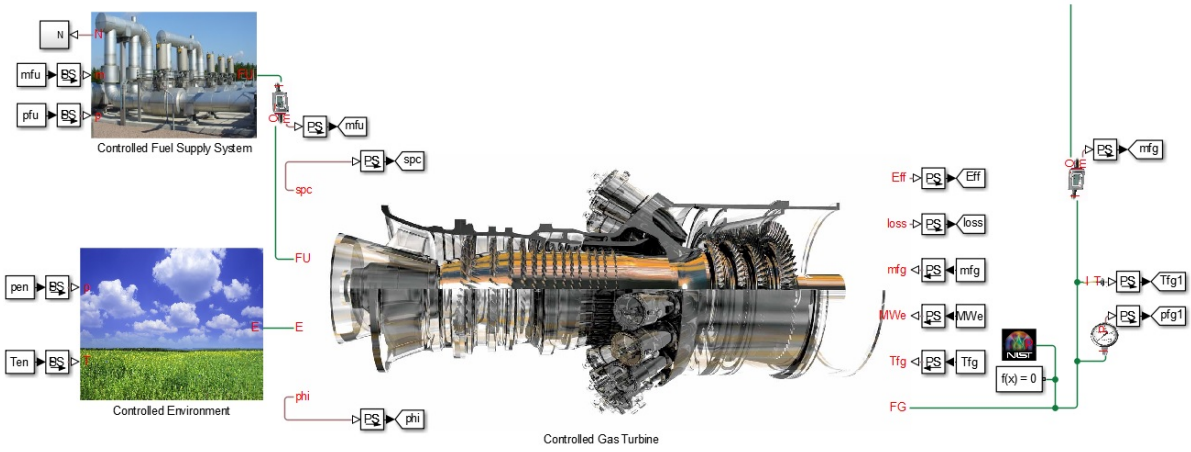

Figure 3.15: The GT sub-model in the Simulink^{TM} dynamic model

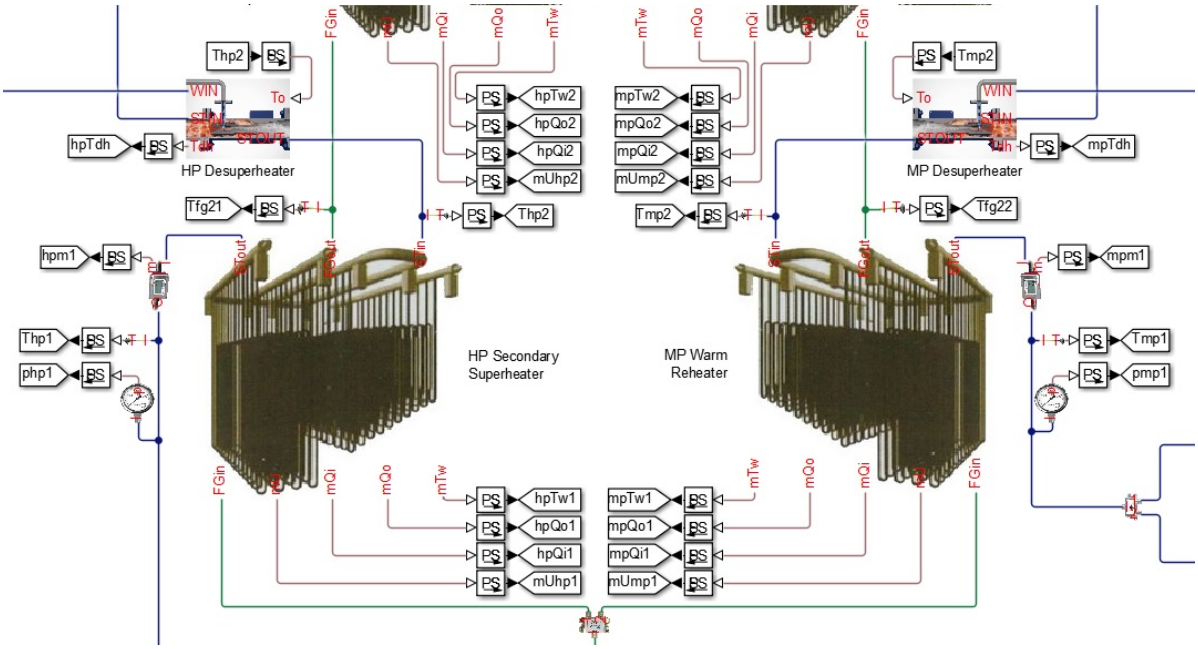

Figure 3.16: The hot section of the HRSG sub-model in the Simulink^{TM} dynamic model

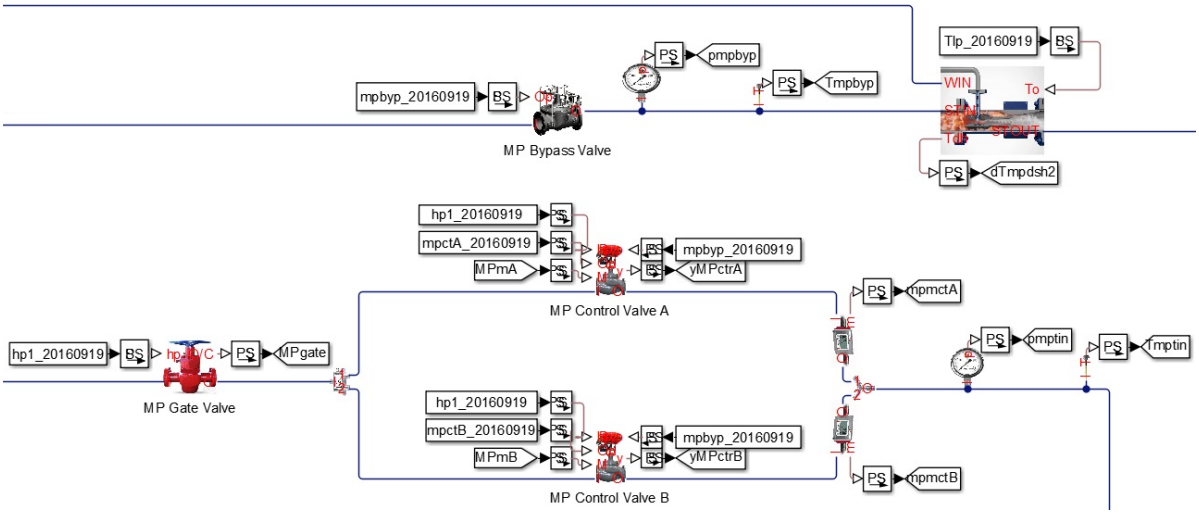

Figure 3.17: The MP part of the VALVES sub-model in the Simulink^{TM} dynamic model

The simulation of the dynamic model leads to the validation of the physical reality reproduced by the physical components, and the prediction of specific trends not shown in the real control panel (stress, valves flows, condensation, etc.). In order to carry out a stable simulation, three main preparation steps have to be performed, which are described in the following list.

1. the sources of experimental data have to be checked;
2. the desired initial values for the turbine temperatures and shaft speed have to be provided;
3. the beginning values for the temperatures and flows in the heat exchangers have to be set.

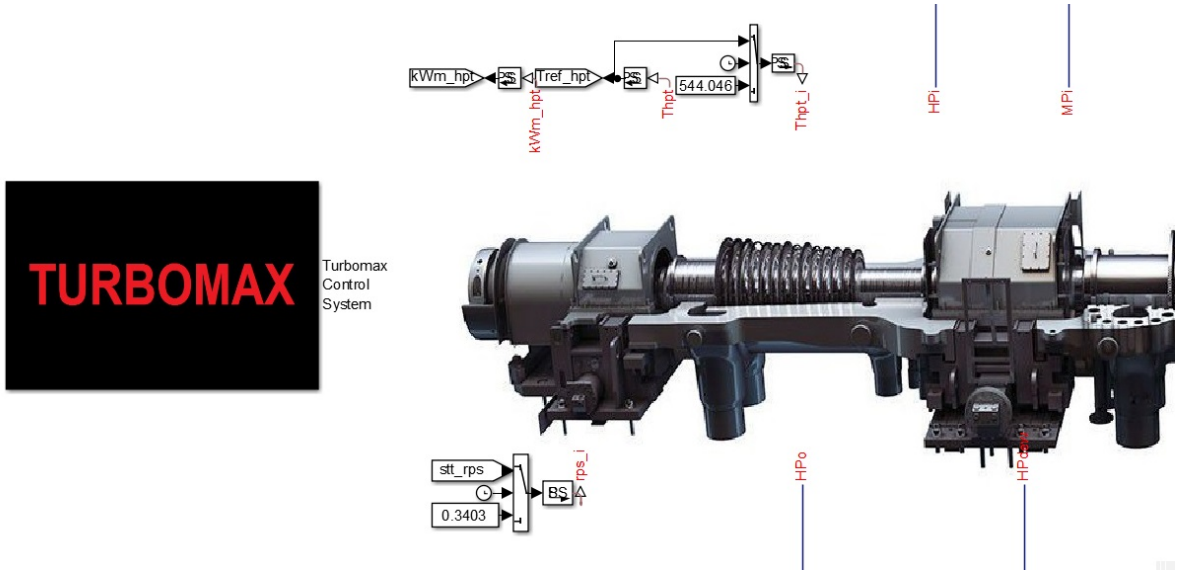

Figure 3.18: The HP turbine and stress controller block in the ST sub-model in the Simulink^{TM} dynamic model

The first preparation step involves the check of all the experimental data imported for the simulation. The data are stored in specific data-sheets, which gather the process data related to each start-up analysed. The data are imported to MATLAB^{TM} and converted in time-series vectors, which are interpolated by the Simulink^{TM} solver. The list of experimental inputs of the dynamic model is available in Table 3.9.

Table 3.9: Experimental data provided as simulation input

Data	Description	Unit
p_{en}	Environment pressure	bar
T_{en}	Environment temperature	K
p_{fu}	Fuel pressure	bar
$\dot{m}_{fu}$	Fuel mass flow rate	kg/s
MWe	GT generator output	MW
T_{fg}	GT exhaust flue gas temperature	K
$\dot{m}_{fg}$	Fuel pressure	bar
p_{hp}	HP drum pressure	bar
T_{dsh}	HP desuperheater outlet temperature	K
byp_{hp}	HP bypass valve opening	%
A_{hp}	HP control valve A opening	%
B_{hp}	HP control valve B opening	%
p_{mp}	MP drum pressure	bar
T_{drh}	MP desuperheater outlet temperature	K
byp_{mp}	MP bypass valve opening	%
A_{mp}	MP control valve A opening	%
B_{mp}	MP control valve B opening	%

Regarding the second preparation step, the beginning values of the turbine surface temperatures and shaft speed have to be provided. This can be done directly from the steam turbines system internal interface, as shown in Figure 3.19. In this way, the dynamic model can simulate any type of start-up. The beginning values of the rotor shell temperatures in the stress controllers also have to be set.

The last preparation step involves the identification of the right set of beginning values for the most

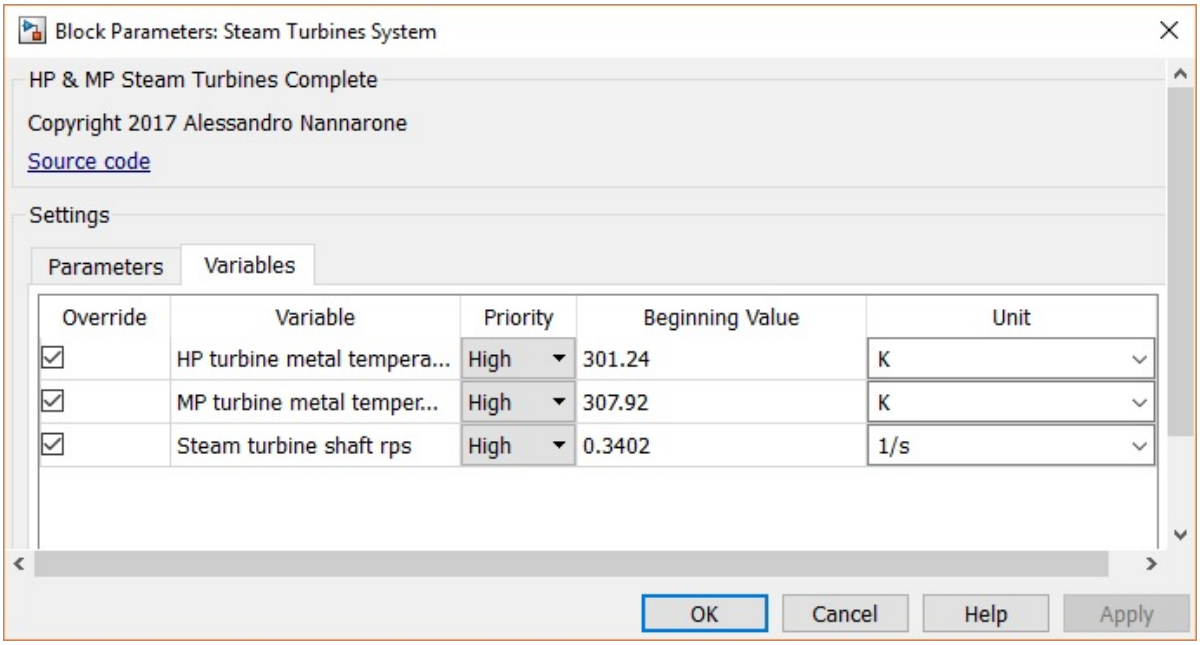

Figure 3.19: Variables begining values in the *Steam Turbines System* internal interface

important variables of the HRSG sub-model: temperatures and flows. These values must be sufficiently close to the values which lead to a stable simulation start. As a consequence, they can be found by setting up an additional MATLAB^{TM} model aimed at the solution of the first simulation step only. The list of variables whose beginning values have to be properly assigned is provided in Table 3.10.

Table 3.10: Experimental data provided as simulation input

Data	Description	Unit
$T_{fg,o}(HP, ssh)$	*HP Secondary Superheater* flue gas outlet temperature	K
$T_{fg,o}(MP, wrh)$	*MP Warm Reheater* flue gas outlet temperature	K
$T_{fg,o}(HP, psh2)$	*HP Primary Superheater 2* flue gas outlet temperature	K
$T_{fg,o}(MP, crh)$	*MP Cold Reheater* flue gas outlet temperature	K
$T_{fg,o}(HP, psh1)$	*HP Primary Superheater 1* flue gas outlet temperature	K
$\dot{m}_{st}(HP, ev)$	*HP Evaporator* vapour production	kg/s

3.6. Model simulation

The simulation in Simulink^{TM} divides into 6 major phases, listed below. In the simulation phases, the solver performs different actions, such as model structure validations and computations.

1. Model validation;
2. Network construction;
3. Equations construction;
4. Initial conditions;
5. Transient initialization;
6. Transient solve.

During the first phase, the solver checks the component codes and the connection of all the ports in the network, which have to respect the domain type conditions. Afterwards, the solver constructs the physical network by setting the equality of all the stream variables related to two or more connected ports. In the third phase, the solver constructs the system of equations characterizing the model.In the fourth phase, the initial conditions for the simulation are computed by the solver by trying to find a solution to the system of equation. Once a solution is found, the solver fixes all the variables and computes the time derivative of the dynamic variables, needed for the numerical integration of the differential equations. The variable step numerical integration is performed in the sixth phase, computing all the variables as a function of time. The results of the transient solve become the initial condition of the transient solve corresponding to the following time step. If an event takes place, such as a valve opening or sudden GT ramp-up, the solver returns to the transient initialization phase, in order to recalculate the initial conditions for te transient solve. This cycle continues until the end of the simulation, and the trends of the model variables can be viewed in the model control room scopes. A flow diagram of the simulation phases is depicted in Figure 3.20.

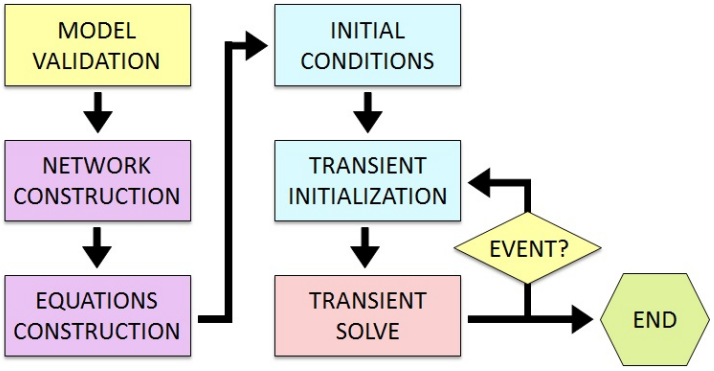

Figure 3.20: Flow diagram of the simulation phases

Regarding the solver configuration, the solver chosen is the `ode23t`, already implemented in Simulink^{TM}. The simulation time step is variable and the error relative tolerances are set to the automatic value of 10^{-3}. Starting from a maximum time step of 10 ms, the solver reduces it id the error exceeds the previous tolerances. The `ode23t` carries out the integration of the system of ordinary differential equations according to the trapezoidal rule, used to approximate the definite integral of the differential equations in the variable time step. The details of the solver configuration are summarized in Table 3.11.

Table 3.11: Details of the solver configuration options chosen for the simulation

Option	Choice
Solver type	`ode23t`
Numerical integration	Trapezoidal
Time-step	Variable
Maximum time-step	10 ms
Error relative tolerance	0.001 (10%)

3.7. Validation

The dynamic model is validated against data from real start-ups, in order to prove its accuracy. The accuracy of the model mainly depends on the results concerning the 8 most important operating variables, which are: HP superheating temperature, MP reheating temperature, HP and MP steam

flows, HP and MP turbine surface temperatures, ST generator output and shaft speed. The input data used for the validation regard the RoCa3 cold start on October, 10^{th}, 2016, and the warm start on September, 19^{th}, 2016. The results of the validation are discussed in this section.

3.7.1. Cold start

The cold start on October 10^{th}, 2016 is characterized by extremely low turbine reference temperatures: 28°C for the HP and 30° for the MP turbine. The start-up time is slightly longer than average, and equal to 4:37h. The general start-up data are provided in Table 3.12

Table 3.12: Data of the RoCa3 cold start carried out on October 10^{th}, 2016

Data	Description	Unit	Value
T_{hpt}	HP turbine reference temperature at process start	°C	28
T_{mpt}	MP turbine reference temperature at process start	°C	30
t	Start-up time	min	277

After the comparison with real process data, it is possible conclude that the model reproduces the cold starts with extremely high accuracy. In order to prove this, the comparison of the results concerning the HP superheating temperature, MP turbine surface temperature, MP steam mass flow and ST generator output are shown respectively in Figures 3.21, 3.22, 3.23 and 3.24. The results are commented, in order to highlight the nature of the errors.

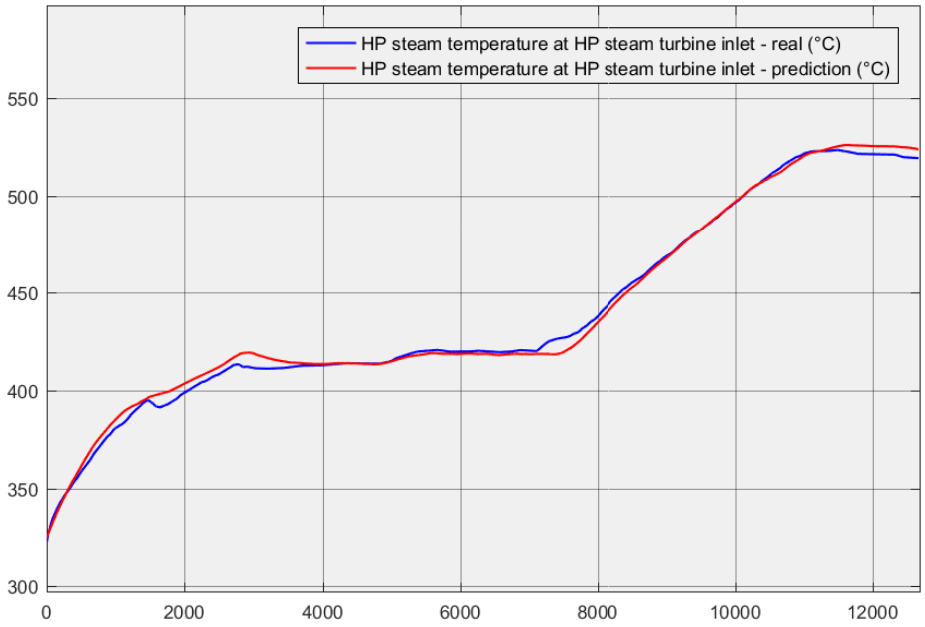

Figure 3.21: HP superheating steam temperature validation

Figure 3.21 shows the trends of the HP superheating temperature, which corresponds to the steam temperature at the exit of the last superheater. The percentage error is below 3% during the entire simulation, and it mainly depends on the metal-steam LMTD assumption and internal pressure drop.

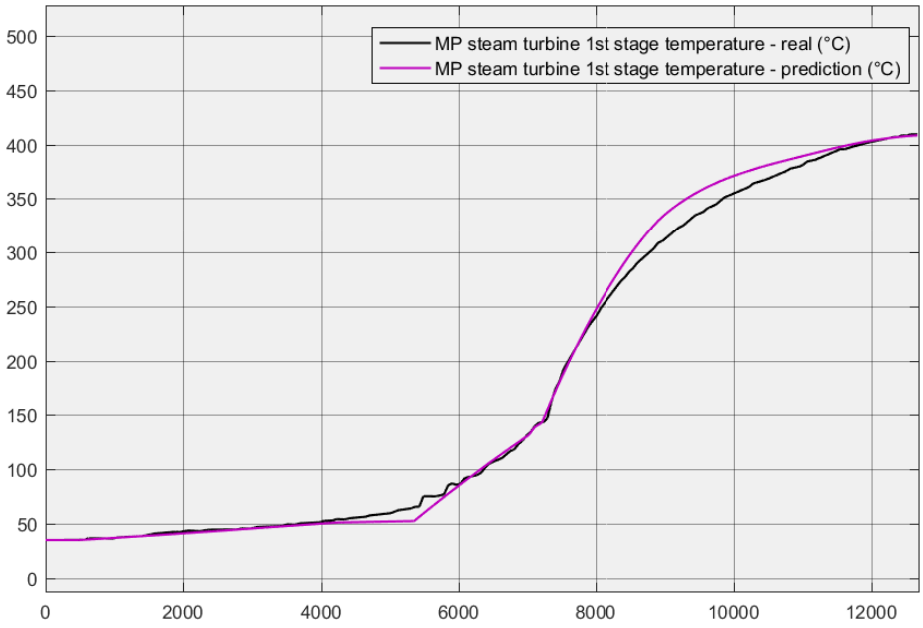

Figure 3.22: MP turbine surface temperature validation

The trends of the 1st stage surface temperature of the MP turbine are shown in Figure 3.22. Except for the very first part of the turbine heating up, the percentage error is always lower than 7%. This error is mainly due to the difficult evaluation of the heat transfer during the expansion.

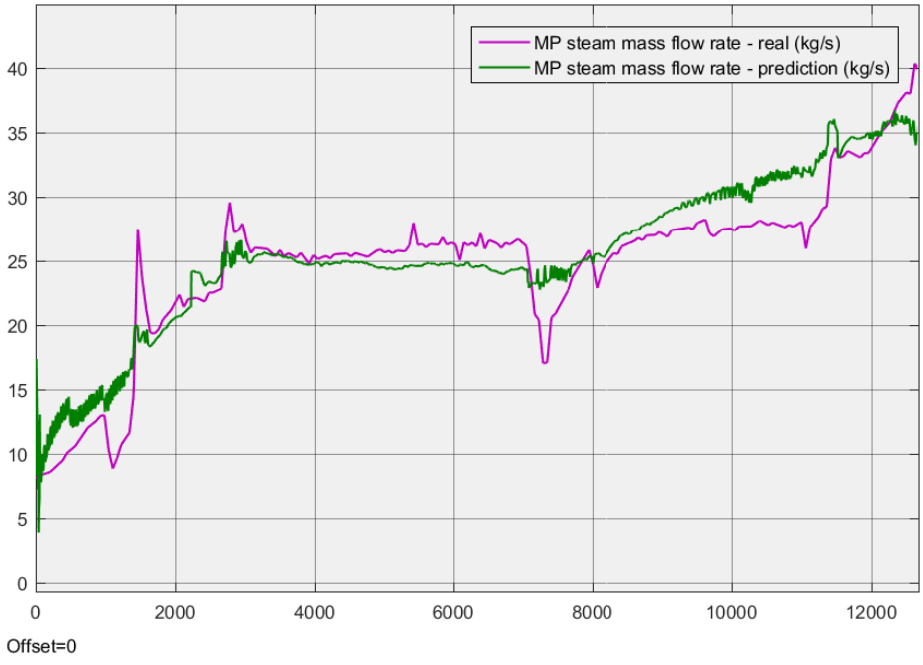

Figure 3.23: MP steam mass flow rate validation

The trends of the MP steam mass flow rate at HRSG exit are shown in Figure 3.23. The steam flow is the most sensible variable of the start-up, since it depends on many other operating variables such as the desuperheaters flow and pressure drop. In this case, the average percentage error is lower than 15%, but the accuracy decreases when bypass valves suddenly change opening position.

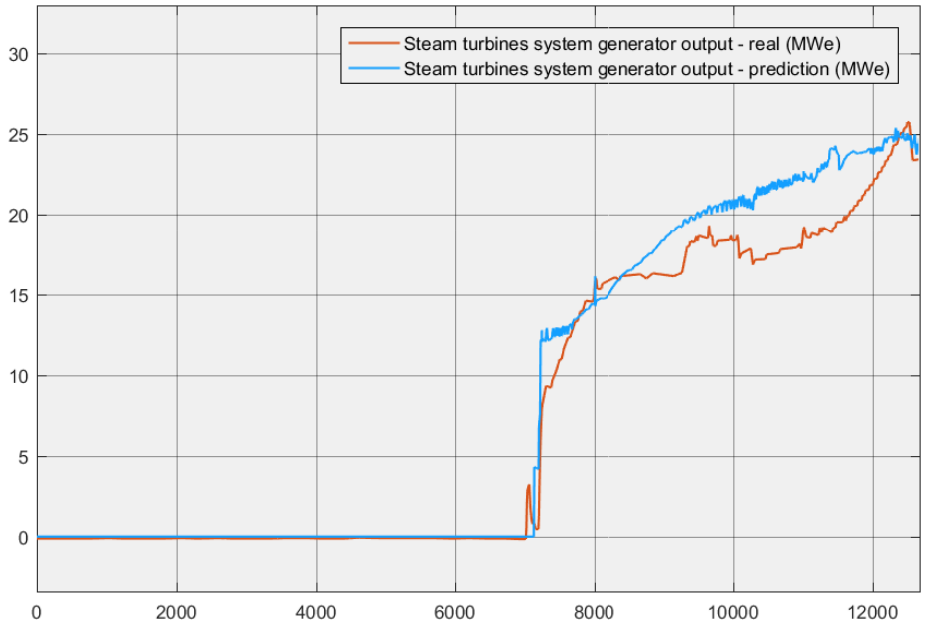

Figure 3.24: ST generator output validation

The trends of the ST generator output are shown in Figure 3.24. Neglecting the variable trends right after synchronization, the percentage error for the ST generator output is never higher than 20%.

3.7.2. Warm start

The warm start on September, 19^{th}, 2016 is characterized by a HP turbine reference temperature of 272°C and a HP turbine reference temperature of 335°C. The start-up time is equal to 1:25h. The general start-up data are provided in Table 3.13

Table 3.13: Data of the RoCa3 warm start carried out on September, 19^{th}, 2016

Data	Description	Unit	Value
T_{hpt}	HP turbine reference temperature at process start	°C	272
T_{mpt}	MP turbine reference temperature at process start	°C	335
t	Start-up time	min	85

The validation against real process data shows very good results in terms of accuracy, though slightly lower for some variables compared to the cold start validation results. In this case, the real and predicted trends concerning the other 4 main operating variables (MP reheating temperature, HP turbine surface temperature, HP steam mass flow and ST shaft speed) are compared respectively in Figures 3.25, 3.26, 3.27 and 3.28. The results of the comparisons are also described and discussed.

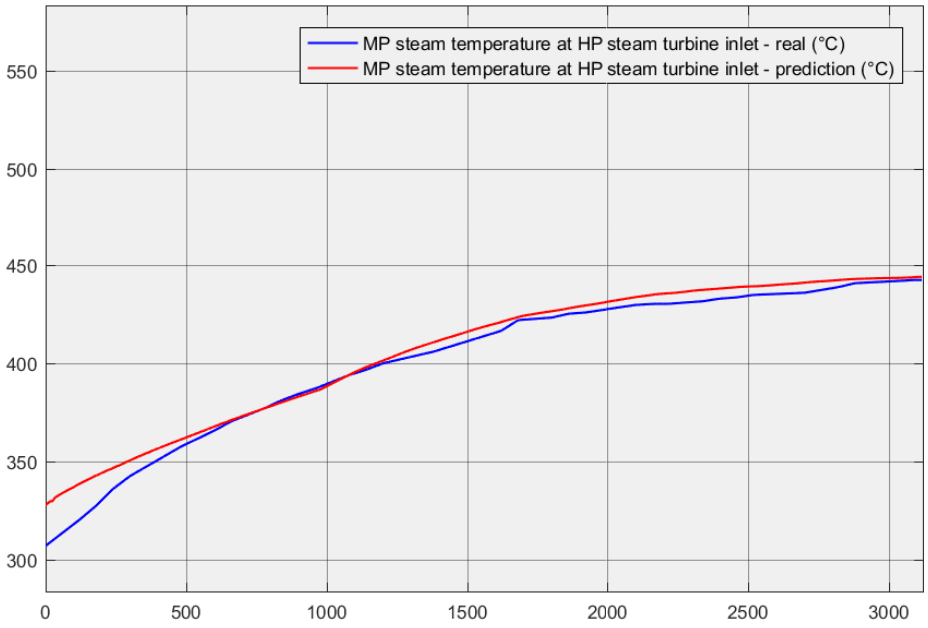

Figure 3.25: MP reheating steam temperature validation

Figure 3.25 shows the trends of the MP reheating temperature, which corresponds to the steam temperature at the exit of the warm reheater. Except for the simulation start, the percentage error is always lower than 2%. This error is still produced mainly by the assumption made for the internal LMTD, and the neglecting of the flow pressure drop.

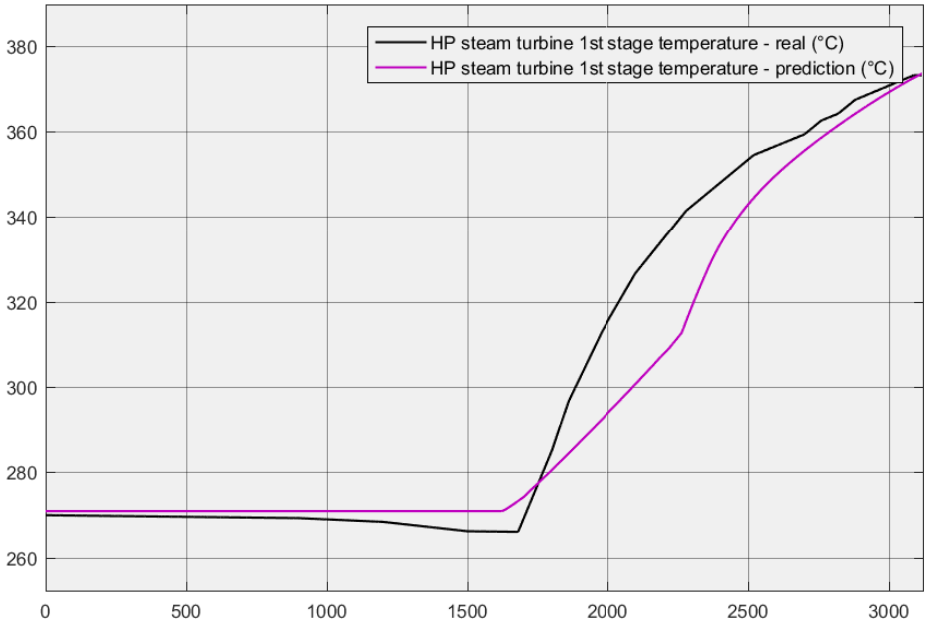

Figure 3.26: HP turbine surface temperature validation

The trends of the 1st stage surface temperature of the HP turbine are shown in Figure 3.26. The first heat transfer period inside the machine is not predicted in an excellent way, with a maximum percentage error of 8%.

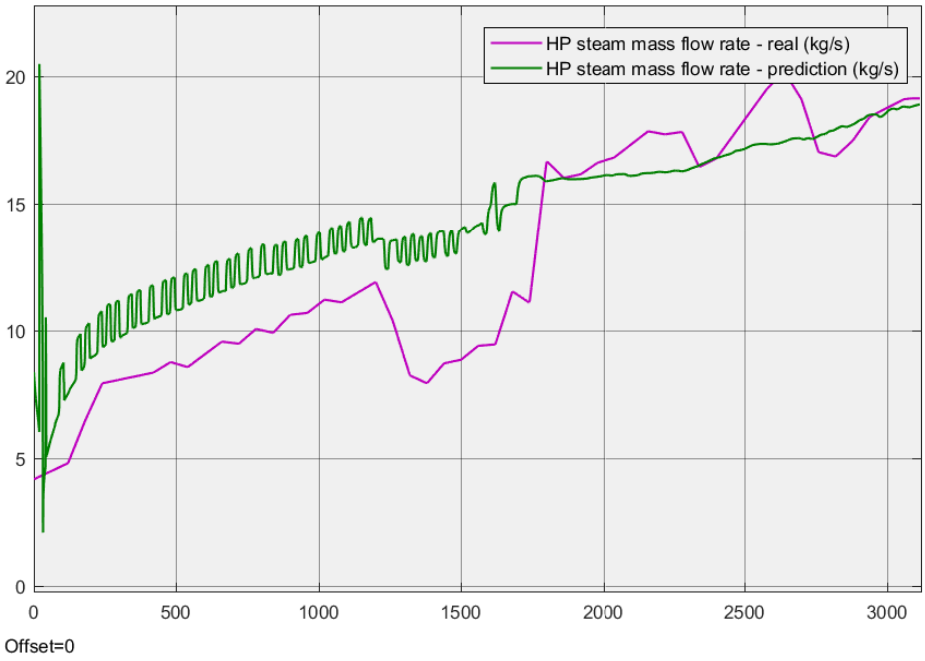

Figure 3.27: HP steam mass flow rate validation

The trends of the HP steam mass flow rate are shown in Figure **??**. Also in the warm starts, the effect of the rapid changes of the bypass opening on the steam production is not predicted accurately. Except for this, the maximum percentage error is always lower than 30%.

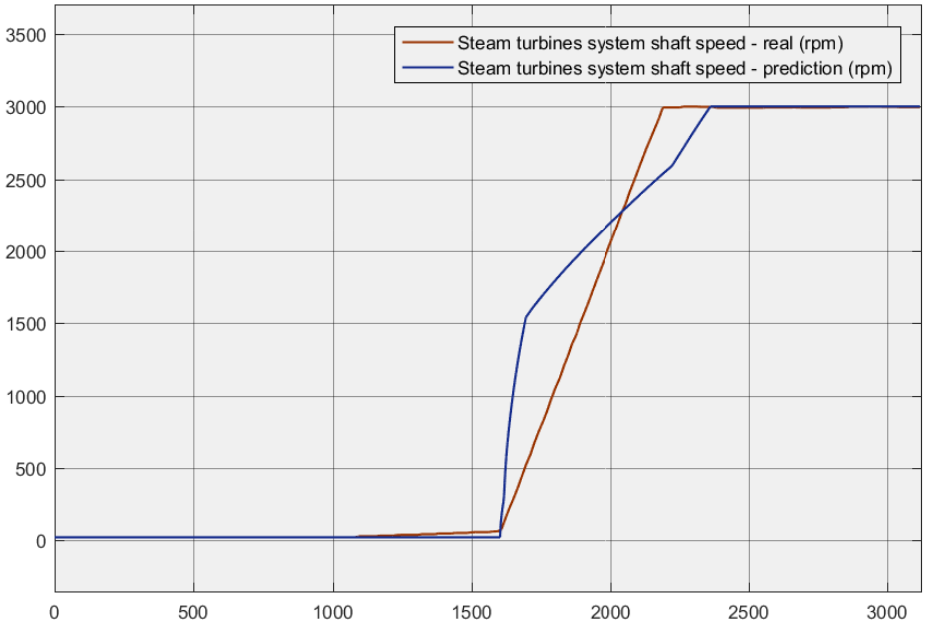

Figure 3.28: ST shaft speed validation

The trends of the steam turbines shaft speed output are shown in Figure 3.28. Although the model is capable to reproduce the shaft acceleration trend, very high percentage errors are reached at the beginning of the process.

4

Start-up Optimization

4.1. Optimization theory

The key of any start-up optimization is the control of the heat supply to the turbines. Depending on the variable to be optimized, different strategies for the heat supply to the turbine can be adopted. In the case of the RoCa3 power station, the start-up optimization was aimed at the shortening of the start-up time, keeping the maximum stress level in the steam turbines unchanged. As a consequence, it is important to analyse the mathematical expression describing the heating up of the turbines, which is conveniently provided below.

$$Q_{tot} = \int_{t_i}^{t_f} \dot{Q}_{hpt}(t)\ dt + \int_{t_i}^{t_f} \dot{Q}_{mpt}(t)\ dt; \qquad \text{Total heat absorbed} \quad (4.1)$$

Three variables mainly affect the heating-up of the machines until acceptable surface temperature values: the time t_i at which the heating-up starts, and the heat flows involved in the process, respectively $\dot{Q}_{hpt}$ and $\dot{Q}_{mpt}$. As a result, the optimization actions must regard these 3 variables.

4.1.1. Stop valves opening

According to the previous introduction, the first optimization action coincides with the shortening of the turbines start-up time $t_{i,hpt}$ and $t_{i,mpt}$. By optimizing these two variables, it is possible to obtain remarkable results even without manipulating the turbine heat flows. A heat flow optimization would further extend the reduction of the start-up time already enabled by this first optimization action. Considering the trends for the heat flows equal to the non-optimized case, the heating up process is characterized by a constant duration Δt. As a result, if the process starts earlier, it will also terminate earlier. The previous optimization action can be described by the following expression:

$$t_f = t_i + \Delta t; \qquad \text{Start-up time} \quad (4.2)$$

$$t_{i,new} << t_{i,old} \quad \rightarrow \quad t_{f,new} << t_{f,old} \qquad 1^{st} \text{ optimization action} \quad (4.3)$$

The start of the heating up process in the turbines depends on the opening of the stop valves. It should take place as soon as possible, and the waiting time considered by the control system should be reduced. In order to perform this optimization action, the opening condition of the stop valves has to be analysed. In the control system, this condition implies the pipe wall temperature right before the stop valves to be at least 20^C above the steam saturation temperature corresponding to the current HP pressure. However, in the start-up process, the quick increase of the HP pressure leads to a quick increase of the saturation pressure, and the reaching of the previous condition is delayed.

As a result, the optimization action involves the change of the pressure setpoint in the HP circuit, which is set constant to 10 bar until the meat temperature satisfies the opening condition. After the waiting time, conveniently reduced to 1 min, the HP bypass valve ensures a safe pressure increase of 0.5 bar/min, which later prevents the closing of the stop valves. Once the pressure reaches 40 bar, the HP bypass valve position is adjusted to keep the pressure constant at this value. The optimization action can be described by the following mathematical expression:

$$\begin{aligned} p_{hp} &= 10\ bar; && [T_m < T_{sat} + 20°C \wedge \Delta t \leq 1\ min] \\ &= 10\ bar + \int_{t_i+\Delta t}^{t} \frac{0.5\ bar}{min}\ dt; && [p_{HP} < 40\ bar \wedge T_m \geq T_{sat} + 20°C] \\ &= 40\ bar; && [p_{HP} \geq 40\ bar \wedge T_m \geq T_{sat} + 20°C] \end{aligned} \qquad \text{Optimal HP pressure} \quad (4.4)$$

4.1.2. GT manual control

The second optimization action concerns the identification of the optimal trends of the heat flows $\dot{Q}_{hpt}\,(t)$ and $\dot{Q}_{mpt}\,(t)$, to which the thermal stresses in the steam turbines are linked. According to the optimization goal, the maximum thermal stress characterizing the standard start-up procedure can still be reached. However, the heat flows should be controlled so that, while the thermal stress smoothly decreases, the heating up of the turbine is kept at an acceptable value. Being the heat flows function of the steam-turbine temperature difference $\Delta T_{st,t}$, the control of the heat flows implies the control of the steam inlet temperature $T_{st,i}$ in function of the turbine surface temperature T_1. The steam temperatures can be controlled by both the GT plant and the desuperheaters. However, for fuel saving reasons, the latter should not be used to decrease the steam temperatures when this action can be performed by the gas turbine.

As already discussed in Chapter 2, the DCS control of the gas turbine ramp-up leads to too high values for the heat flows. As a consequence, the ramp-up is manually controlled by the operators, who control the heat flows to the turbines by monitoring the flue gas, steam and turbine temperatures. Earlier than the stop valves opening, there is no reason why the GT output has to be high. In order to reduce the fuel consumption, it should be kept constant at the minimum value MWe_{min}, which depends on the type of start-up. As soon as the stop valves open, the GT ramp-up should be carried out in order to keep the $\Delta T_{st,t}$ constant at an optimum value, which must be determined by means of an optimization tool.

4.1.3. Desuperheaters opening

The third optimization action coincides with the identification of the optimal time when the quick reduction of the heat flows has to take place. In this way, once the steam turbines are sufficiently warm, the values of the heat flows can be decreased in order to reduce the $\Delta T_{st,t}$ temperature difference and the thermal stress. However, the setpoint for the $\Delta T_{st,t}$ must still ensure a smooth heating up of the machines. Under this condition, the control system can proceed with the further opening of the control valves, which leads to the gradual closing the bypass. The optimal time at which this optimization action is carried out depends on the steam turbine temperatures. Considering the expression of the heat flows, the optimization action can be described by the following expression:

$$\begin{aligned} \dot{Q} &= h\ A\left(\Delta T_{st,t,opt}\right); && \left[T_1 < T_{opt}\right] \\ &= h\ A\left(\Delta T_{st,t,min}\right); && \left[T_1 \geq T_{opt}\right] \end{aligned} \qquad \text{Turbine heat flow} \quad (4.5)$$

The desuperheaters, designed for conveniently decreasing the steam temperature during design operation, can be used to carry out this last optimization action. Closed during the first phases of the start-up, they open once the setpoint for the steam turbine temperatures are reached. As a result, the steam temperature is controlled to be $\Delta T_{st,t,min}$ higher than the turbine surface temperature. However, for the same reason explained in the previous section, this value for the $\Delta T_{st,t,min}$ has to be deter-

mined through an optimization tool. If this value does not satisfy the minimum superheating condition, the steam temperature is set equal to the minimum acceptable value. The optimal operation of the desuperheaters is described by the following expression:

$$\begin{aligned} T_{o,dh} &= T_{i,dh}; && [T_1 < T_{opt}] \\ &= T_{st,min}; && [T_1 \geq T_{opt} \wedge T_1 + \Delta T_{st,t,min} < T_{st,min}] \\ &= T_1 + \Delta T_{st,t,min}; && [T_1 \geq T_{opt} \wedge T_1 + \Delta T_{st,t,min} \geq T_{st,min}] \end{aligned} \quad \text{Desuperheaters outlet temperature} \tag{4.6}$$

4.2. Model extension

An tool capable to predict the effects of the optimization actions is needed to prove the reliability and the improvement in terms of start-up time reduction. For this purpose, the dynamic model described in Chapter 3 is extended by implementing the control systems logics in the network.

4.2.1. Extended structure

The general structure of the extended dynamic model is based on the one presented in the previous Chapter, and is upgraded by modelling the RoCa3 control systems, and an innovative feedback loop controlled GT plant. The structure of the four sub-models (GT, HRSG, VALVES and ST) remain the same, and the simulation results are still monitored by the model control room. The model is completely automatic, thanks to the presence of the control logics: only the pressure trends have to be provided externally, since the pressure control by means of the bypass valves is not modelled. A scheme of the structure of the extended dynamic model is provided in Figure 4.1.

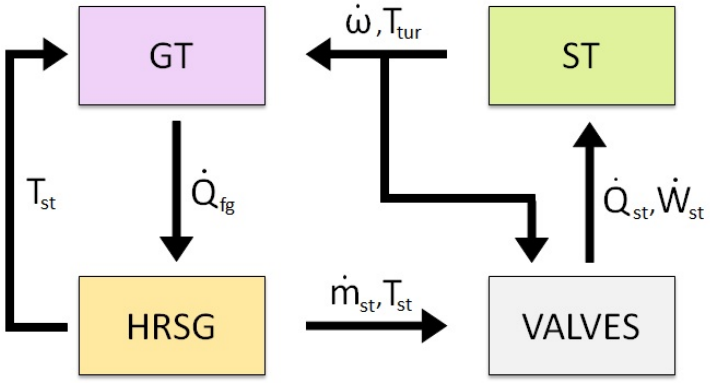

Figure 4.1: Scheme of the general structure of the extended dynamic model

The GT sub-model operates as heat source to the steam cycle depending on the data it receives from the HRSG and ST sub-models. Furthermore, the ST sub-model sends signals to the HRSG and VALVES sub-models, according to which the desuperheaters operation and the control valves opening is adjusted. Like the standard one, the extended dynamic model is composed by more than 110 components, and includes the same gas and water streams.

4.2.2. Controls modelling

The modelling of the control systems leads to the upgrade of the standard dynamic model. Due to the lack of data, experimental studies are conducted in order to identify trends and setpoints implemented in the main control logics. Starting from the two control valves per circuit, they divide into *leading* and *following*. The opening position of the *leading* valve is determined in function of the thermal stress in the turbine, while the other one is controlled in function of the former. Since no measurements

are available regarding the stress, it is possible to assume the $\Delta T_{st,t}$ temperature difference to be the unique control variable. According to this approach, the experimental correlation developed for the HP Control Valve A, the leading control valve in the HP circuit, is depicted in Figure 4.2.

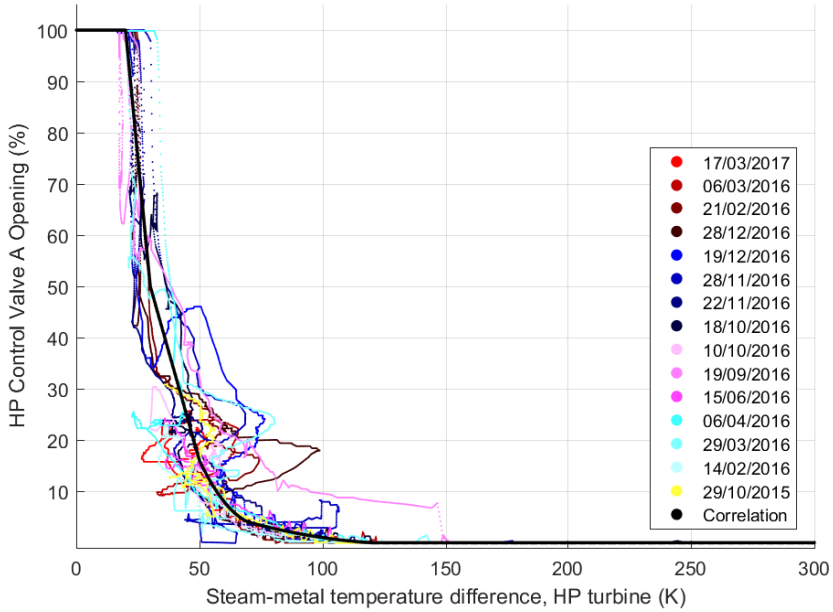

Figure 4.2: Scheme of the general structure of the extended dynamic model

Regarding the HP Control Valve B, a different correlation is developed by assuming the opening of the previous valve as unique control variable. The correlation is shown in Figure 4.3.

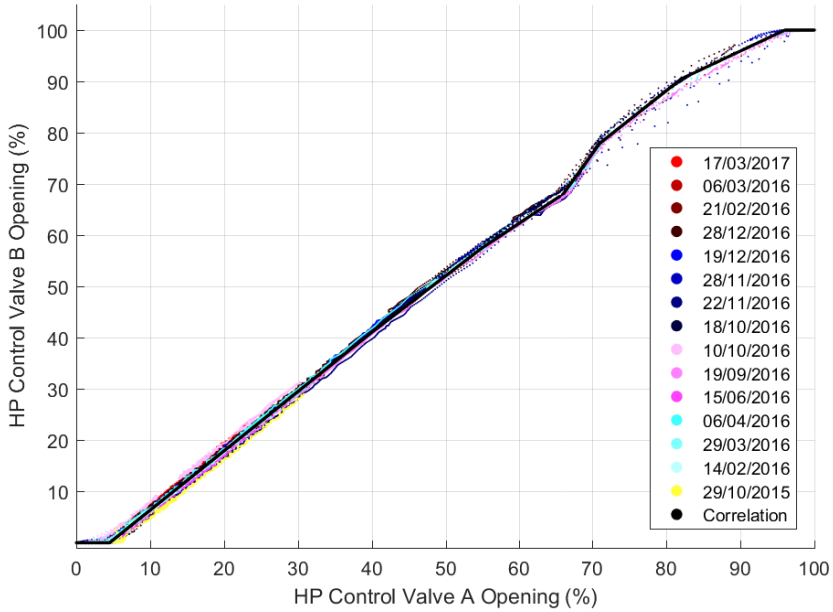

Figure 4.3: Scheme of the general structure of the extended dynamic model

The modelling of the Automatic GT equipped with feedback loop control implies the modification of the component structure and interface. The number of internal variables increases, as well as the parameters, through which is now possible to determine the IGV trend during the start-up. This affects the GT ramp-up, which is carried out automatically in function the steam turbine temperatures. As a result, the flue gas temperature and accordingly the steam temperature are gradually increased, in order to ensure a nearly constant $\Delta T_{st,t}$ temperature difference. Starting from the IGV control modes, they are described in Table 4.1.

Table 4.1: IGV control modes of the Automatic GT model

Control mode	Settings	Description
Combined Cycle - Manual IGV	$IGV_{ctr} = 1$	IGV position at IGV_{fix}
Combined Cycle - Anti-surge IGV	$IGV_{ctr} = 2$	IGV position at anti-surge value
Flexible IGV	$IGV_{ctr} = 3,\ pr_{max} = 0$	IGV position variable
Open Cycle - Maximum IGV	$IGV_{ctr} = 3,\ pr_{max} = 1$	IGV position at IGV_{max}

Once the desired IGV control is chosen, the GT ramp-up is controlled automatically in function of the feedback loop data from the steam turbines and HRSG. However, if the Flexible IGV option is chosen, a gradual closing of the IGV until the anti-surge value is carried out in order to increase the flue gas temperature. The GT ramp-up starts as soon as these initial conditions are satisfied:

1. the customizable $\Delta T_{st,t}$ setpoint is reached for the first time in the start-up;

2. the customizable $T_{hpt,min}$ setpoint is exceeded by the surface temperature of the HP turbine;

The control of the GT ramp-up is discrete, in order to represent the manual control carried out by the process operators. As a consequence, two customizable steps are used by the automatic control to increase the power output with regard to the HP turbine heating up. The former, the ramp-up step ΔMWe_i, determine how much the power output is increased at every manual change. The latter, the HP turbine surface temperature step $\Delta T_{hpt,i}$, determines the surface temperature increase after which the GT is ramped up by ΔMWe_i. As a result, the power output is increased by ΔMWe_i every time the HP turbine surface temperature rises of $\Delta T_{hpt,i}$, starting from the minimum value of $T_{hpt,min}$. The discrete control is described by the following mathematical expression.

$$MWe_{opt1} = MWe_{min} + i \cdot \Delta MWe_i; \quad \left[T_{hpt} > \left(T_{hpt,min} + (i-1)\ \Delta T_{hpt,i}\right) \wedge T_{hpt} \leq \left(T_{hpt,min} + i\ \Delta T_{hpt,i}\right)\right]$$

Optimized GT output 1 (4.7)

This ramp-up control is carried out until the MP turbine surface temperature reaches the customizable $T_{mpt,min}$ setpoint. At this point, due to the lower heat transfer in the HP turbine, the control considers also the trend of the surface temperature in the MP turbine. As a result, the power output is increased by ΔMWe_i every time the HP turbine surface temperature rises of $\Delta T_{hpt,i}$ or the MP turbine surface temperature rises of $\Delta T_{mpt,i}$. The GT ramp-up is described by the expression provided below.

$$\begin{aligned} MWe_{opt2} &= MWe_{opt1}; && \left[T_{mpt} \leq T_{mpt,min}\right] \\ &= MWe_{opt1} + i \cdot \Delta MWe_i; && \left[T_{mpt} > \left(T_{mpt,min} + (i-1)\ \Delta T_{mpt,i}\right) \wedge T_{mpt} \leq \left(T_{mpt,min} + i\ \Delta T_{mpt,i}\right)\right] \end{aligned}$$

Optimized GT output 2 (4.8)

All the component and stream variables are calculated by the physical model at the current operating conditions. In case the Flexible IGV control mode is selected, a IGV ramp-down is carried out before the first increase of the GT power output, which starts as soon as the position of the IGV reaches the minimum value, equal to the anti-surge value. However, this GT control represents an innovation for the RoCa3 installation, since the GT control system does not allow to control the IGV manually. The optimized IGV ramp-down is described by the following expression:

$$IGV_{opt} = \begin{cases} 57; & [T_{hpt} \le T_{hpt,min}] \\ 57 - i; & [T_{hpt} > (T_{hpt,min} + (i-1)\ \Delta T_{hpt,i}) \wedge\ T_{hpt} \le (T_{hpt,min} + i\ \Delta T_{hpt,i})] \\ IGV_{an,su}; & [IGV_{opt} \le IGV_{an,su}] \end{cases}$$

Optimized IGV position (4.9)

The control of the HP and MP Desuperheaters is simpler than one modelled for the Automatic GT. Depending on the signals received from the steam turbines, a PI controller regulates the water input from the economizers. The PI controller is tuned through a simple trial and error approach, and ensures high stability and accuracy in the temperature control. The control strategy can be selected by the user by modifying the set of customizable parameters directly from the component interface. The components include three different control modes, presented in Table 4.2.

Table 4.2: IGV control modes of the Automatic GT model

Control mode	Settings	Description
Maximum opening	$DH_{ctr} = 1$	Outlet steam temperature at minimum value
Always closed	$DH_{ctr} = 2$	No desuperheating
Optimized	$DH_{ctr} = 3$	Outlet steam temperature at optimized value

In the Optimized control mode, the desuperheaters are kept closed until the setpoint value of the $DeltaT_{set}$ of the corresponding turbine is reached. This setpoint value appears as customizable parameter in the parameters interface, so that different opening conditions can be tested. Once open, the desuperheater injects water in function of the steam temperature to be obtained at steam turbine inlet. The expressions of the temperature error and the PI control algorithm are described by the expressions provided below.

$$\Delta T_{err} = T_{opt} - T_{ssh,o};$$ Actual temperature difference (4.10)

$$\Delta T_{err,PI} = 0.5\ \Delta T_{err} + 0.05 \int_0^t \Delta T_{err}\ dt;$$ PI controller error (4.11)

$$T_o = \begin{cases} T_{st,i} + \Delta T_{err,PI}; & [T_{st,i} + \Delta T_{err,PI} \ge T_{sat} + dT_{sh,min}] \\ T_{sat} + dT_{sh,min}; & [T_{st,i} + \Delta T_{err,PI} < T_{sat} + dT_{sh,min}] \end{cases}$$ PI controller error (4.12)

4.3. Results from real start-ups

The optimization actions proposed are tested in real RoCa3 start-ups, and the results are compared with the ones obtained in the standard start-up procedure. In particular, the effective improvements in terms of start-up time and fuel saving are evaluated. The tests for the cold and warm starts are carried out on July 18^{th} 2017, after which the installation is shut down and not kept synchronized to the grid.

4.3.1. Cold start test

The test of the optimized start-up procedure for the cold starts takes place in the morning of July 18^{th}. Due to the long shut-down period, the values of the turbine temperatures at process start are equal to 30°C. These values exactly correspond with the ones related to the October 10^{th} 2016 start,

used for the validation of the standard model. As a result, the comparison between the two cold starts is done at the same conditions, and the estimation of the improvements is precise. The beginning values of the most important operating variables for the two start-ups is provided in Table 4.3.

Table 4.3: Variables beginning values at process start

Variable	18/07/2017 - Beginning value	10/10/2016 - Beginning value
HP turbine surface temperature	30°C	28°C
MP turbine surface temperature	30°C	30°C
Steam turbines shaft speed	20 rpm	20 rpm

The start-up test shows remarkable results in comparison with the non-optimized start-up process. Starting from the start-up time, the test lasts for 187 minutes, exactly 90 minutes shorter than the one characterizing the October 10^{th} cold start. The start-up time reduction is equal to 32.5%, which represents a relevant improvement for the operation of the RoCa3 power station. The result is depicted in Figure 4.4 by showing the opening trend of the MP bypass, whose closing, since the other conditions are satisfied, determines the end of the start-up process.

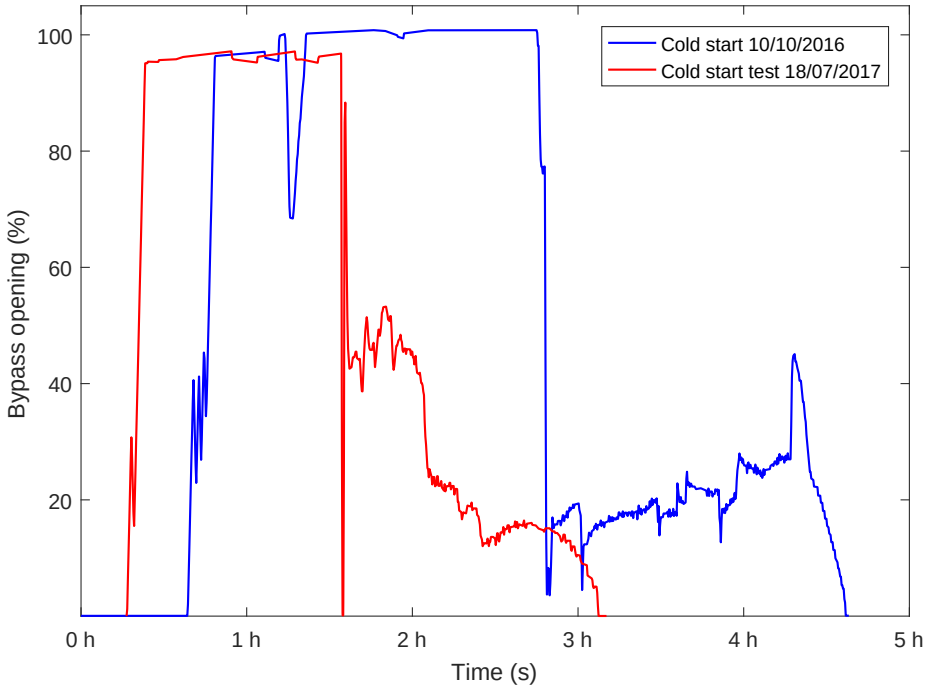

Figure 4.4: Start-up time reduction

The remarkable reduction of the start-up time, combined with the smart operation of the GT plant, leads to a strong reduction of the fuel consumption as well. In the October 10^{th} cold start, the GT plant burnt 69955.0 Nm^3 of natural gas, while the test required the consumption of 37421.4 Nm^3 of this fuel only. As a result, the optimized start-up process leads to a fuel saving of 46.5 %, to which a relevant economical improvement of the asset is linked. The trends for the fuel consumption in the two cold starts is shown in Figure 4.5.

In the end, through the simulation in the standard dynamic model, it is possible to compare the trends of the stress in the steam turbines for the two cold starts. Regarding the HP turbine, the maximum stress reached in the start-up test is equal to 362.9 MPa, exactly 10.0% lower than the value reached during the October 10^{th} cold start, equal to 403.5 MPa. The maximum stress reduction is higher for the MP turbine. During the start-up test, a maximum stress of 275.1 MPa, 17.6% lower than the 333.9 MPa

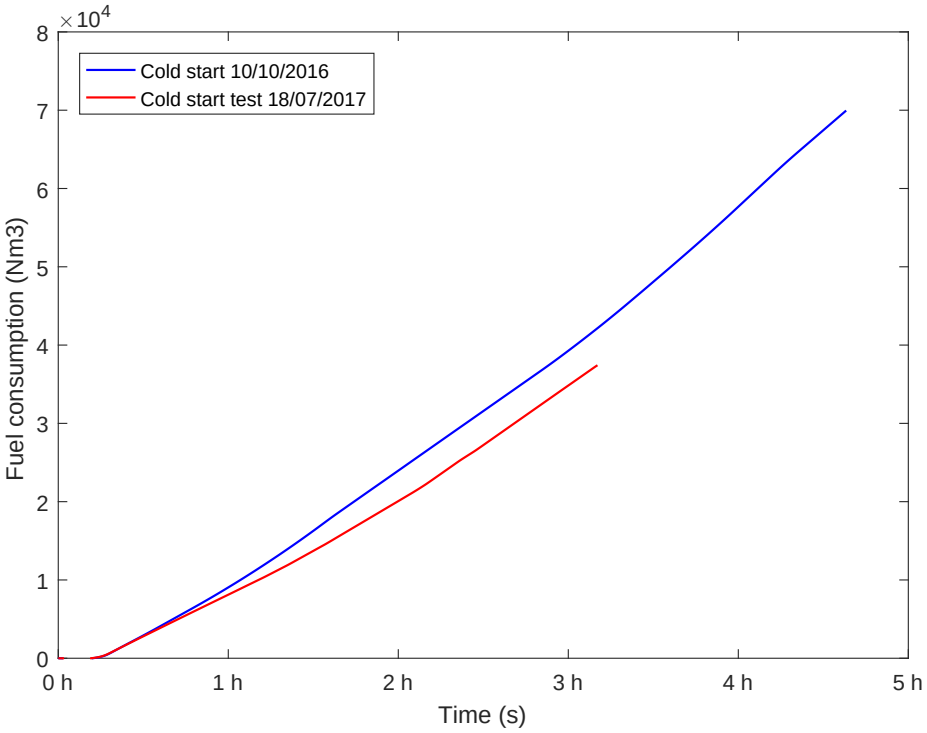

Figure 4.5: Fuel consumption 0.77

reached in the October 10^{th} cold start. The comparison of the maximum stress trends in the HP and MP turbines are respectively shown in Figures 4.6 and 4.7.

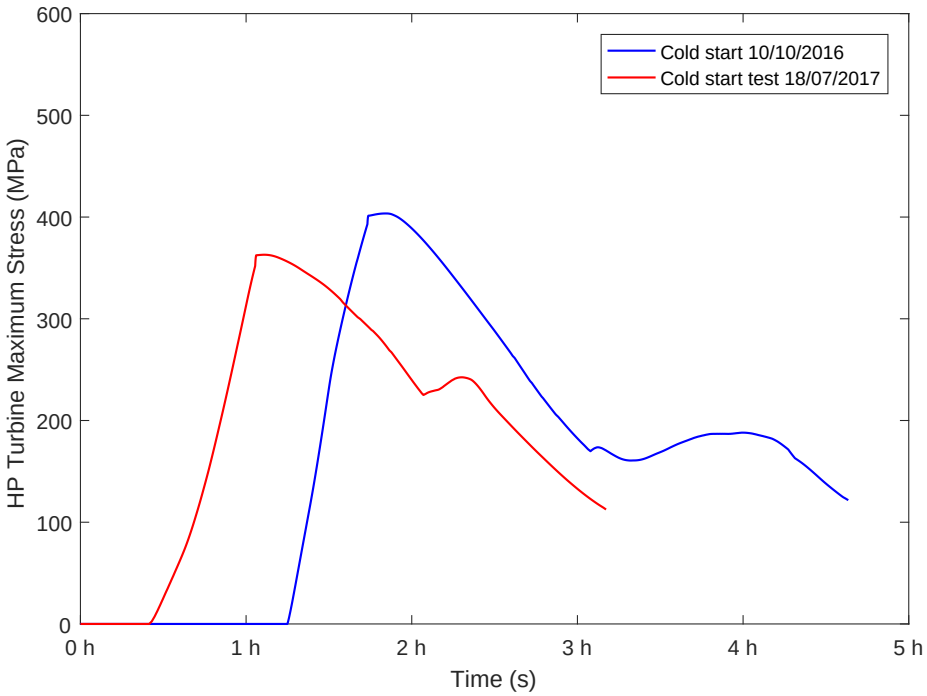

Figure 4.6: Stress level HP reduction

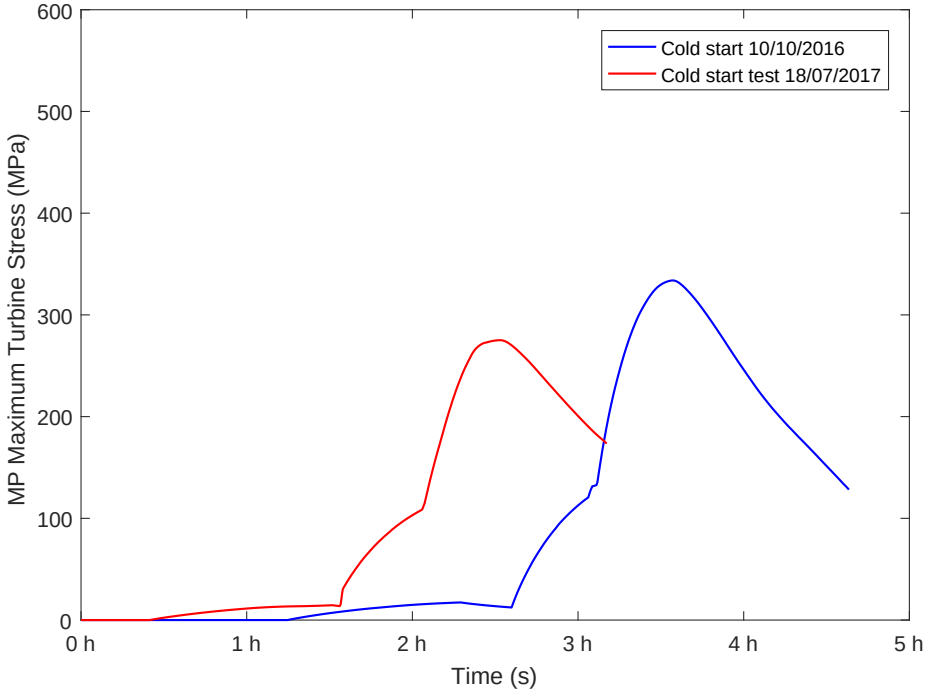

Figure 4.7: Stress level MP reduction

4.3.2. Warm start test

Once the cold start test is complete, the installation is shut down for nearly two hours before carrying out the warm start test. In this way, the test begins with HP and MP turbine temperatures respectively of 351°C and 312°C. Although these beginning values do not exactly correspond to the ones from September 19^{th} 2016, it is still possible to evaluate the improvements produced by the optimization actions. The reason why the data do not match well relies on the different ways through which the beginning values are obtained: very short shut-down period of warm turbines in the former, longer shut-down period of hot turbines in the latter. The values assumed by the main operating variables at the beginning of the start-ups are provided in Table 4.4.

Table 4.4: Variables beginning values at process start

Variable	18/07/2017 - Beginning value	10/10/2016 - Beginning value
HP turbine surface temperature	351°C	272°C
MP turbine surface temperature	312°C	336°C
Steam turbines shaft speed	20 rpm	20 rpm

The warm start test is characterized by a start-up time of 58 minutes, while the September 19^{th} warm start lasts for 85 minutes. This results in a start-up time reduction of 31.8%, very close to the one achieve in the cold start tests. The improvement in terms of start-up time is shown in Figure 4.8.

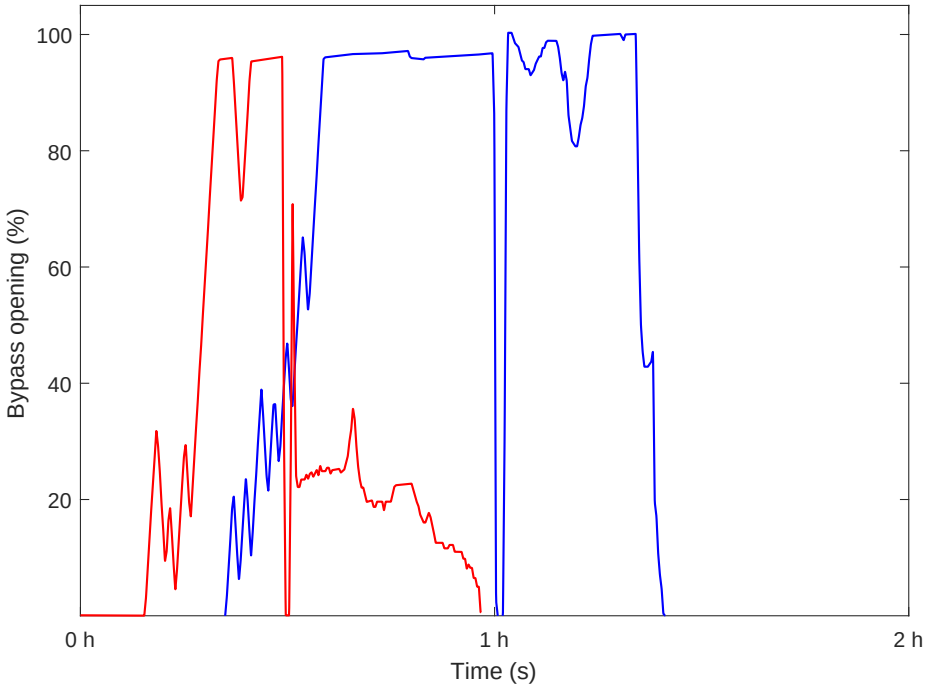

Figure 4.8: Start-up time

Due to the lower duration of the process, the reduction in the fuel consumption is lower than for the cold starts. During the test, 10070.94 Nm^3 of natural gas are burnt, while the standard warm start is characterized by a fuel consumption of 14909.84 Nm^3. As a result, the optimized process enables the saving of the 32.45% in fuel, important for the calculation of the cycling operation costs. The comparison between the trends for the fuel consumption in time is shown in FIgure 4.9.

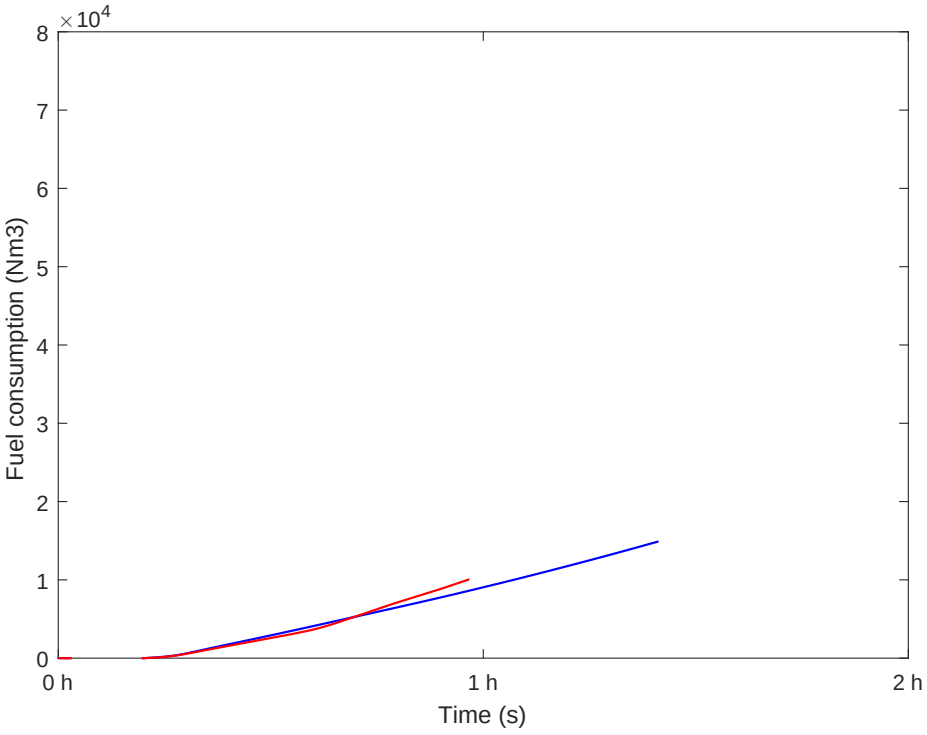

Figure 4.9: Fuel consumption

The thermal stress in the HP turbine is characterized by a reduction of 41.1%, from the 220.2 MPa reached in September 19^{th} to 129.0 MPa. However, the initial conditions of the two warm starts are not the same, and the stress reduction just described must be confirmed through additional test starts. Regarding the MP turbine, the stress reduction is negligible, as well as the stress itself. The maximum stress trends for the HP and MP turbines are respectively shown in Figures 4.10 and 4.11.

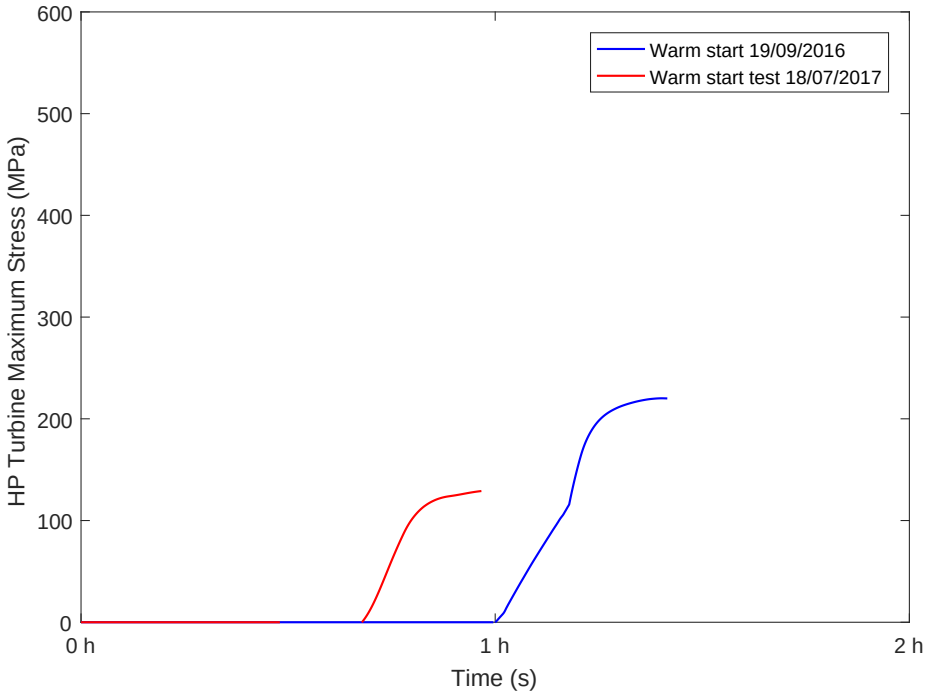

Figure 4.10: Stress level HP reduction

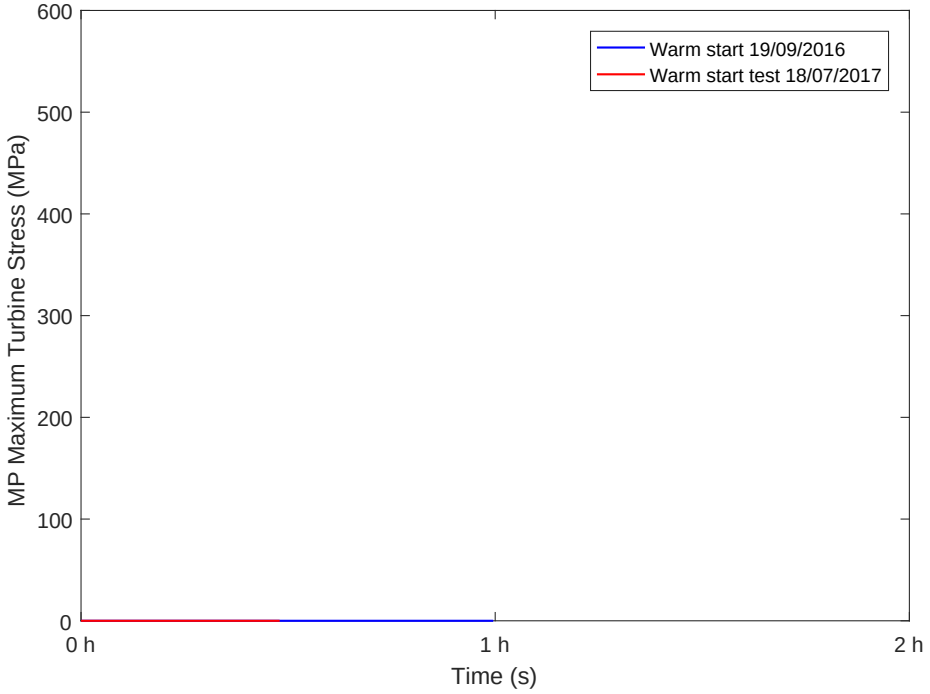

Figure 4.11: Stress level MP reduction

4.4. Recommendations for further optimization

The implementation of the previous optimization actions to the start-up process, thanks to the collaboration of the process operator team, produces many benefits in terms of flexibility and economic operation. However, further improvements can be achieved through the investigation and test concerning new optimization actions and control upgrades. Automatic GT control PI controller

4.4.1. Steam condensation

The steam condensation in the HP turbine limits the further improvement of the start-up process, since it negatively affects the stress, which reaches its maximum value at condensation end, and the shaft acceleration, limited by the low mechanical power. Analysing the condensation phenomenon, it takes place as long as the turbine surface temperature is lower than the saturation temperature of the steam at the existing pressure. Since the turbine pressure is slightly higher than the environment pressure at the beginning of the starts, condensation certainly occurs in the turbines below around 110°. In this way, the vacuum reaches the machines, and the steam transfers heat to the metal without turning into liquid. The best solution to solve the condensation problem is to conveniently decrease the turbines temperature by connecting the machines to the condenser. However, this action requires an additional investment, which has to be supported by a proper cost-benefit analysis.

4.4.2. Maximum IGV opening

An optimization action tested in the extended model, but not yet implemented, is to operate the GT plant at maximum IGV position. The flue gas temperature is accordingly the lowest possible according to the control system, and the GT efficiency increases thanks to the higher mass flow through compressor and turbine. As a consequence, the ramp-up is steeper in order to reach the minimum part-load as soon as possible. The theoretical results from the extended dynamic model suggests that an additional 5% could be achieved in terms of start-up reduction. On the other hand, the steeper GT ramp-up is linked to a higher fuel consumption, which has to be considered in the operations planning. After a thorough investigation, this optimization action can be implemented to the start-up process with no additional investment. For this reason, it represents the most convenient step to be done to further reduce the start-up time.

4.4.3. Flexible IGV opening

The flexible control of the IGV opening would lead to a further start-up reduction, keeping the fuel consumption low. According to the steam turbine temperatures, the IGV gradually close until the minimum value (anti-surge) is reached. As a consequence, this optimization action is an upgrade of the previous one. In this case, the control should be completely automatic, and this implies the implementation of an additional controller. The automatic control can also regard the GT ramp-up, which is currently discrete. The theoretical results from the extended dynamic model support the positive impact of this potential investment, and the tool can be also used to develop the controller logics.

5

Conclusions

5.1. Project summary

Before providing the conclusions of the present work, it is important to summarize the milestones which has led to the start-up optimization of the RoCa3 installation. The work has involved different activities, from start-up monitoring from the control room with the operators to experimental investigations and the dynamic modelling of the power station. All of them have been fundamental for the achievement of very good optimization results during the real start-up tests. The project milestones are summarized in the list provided below.

1. The physical reality of the RoCa3 start-up process is deeply analysed;
2. The main bottlenecks of the process are identified;
3. A dynamic model capable to reproduce the RoCa3 start-ups is developed and validated;
4. The dynamic model is extended to include the RoCa3 control loops and a feedback loop;
5. A set of optimization actions is conceived and tested through the extended dynamic model;
6. The optimization actions are tested during real start-ups, and the improvements are evaluated;
7. Additional optimization actions are proposed as recommendations for the future optimization.

5.2. Conclusions

The dynamic modelling of the RoCa3 power station represents a fundamental step for the start-up optimization. The extended dynamic model developed allows to virtually start up the installation anytime, and thoroughly study the effects of potential optimization actions before their implementation to the real system. The low errors shown by the model validation ensure the very high accuracy of the model in reproducing the RoCa3 start-up process. The flexibility achieved thanks to the implementation in Simulink^{TM} enables the simulation of new equipments as well, and its user-friendly interface allows any user to easily interact with the model. The use of the extended dynamic model, combined with the deep understanding of the physical reality of the process, allows to conceive effective optimization actions, which lead to the significant improvement of the RoCa3 start-up process. The strong reduction in start-up time, fuel consumption and turbine stress for both cold and warm starts also translates into operational and economical benefits for Uniper Benelux. The company is also informed regarding further optimization actions, such as the flexible IGV control mode, which also imply new economical investments. On the other hand, the results of the simulations can support the feasibility studies, providing interesting information concerning the potential benefits that a certain investment would produce.

5.3. Recommendations

An important upgrade of the extended dynamic model would be the modelling of the pressure control, which is now set by external sources. This upgrade would make the model capable to operate autonomously, with the setpoints of the control logics to be given only. Furthermore, the extended dynamic model can be further improved by modelling the phenomena which are now accurately reproduced through experimental correlations, such as the heat transfer in the steam turbines and the pressure at steam turbines inlet. In the end, additional upgrades can be the modelling of the GT components, in order to investigate the start-up time reduction of the GT plant, compressor surge and the emissions. The previous recommended actions are summarized in the list provided below.

- Modelling of the pressure controls;
- Modelling of the phenomena currently reproduced through experimental correlations;
- Modelling of the GT components and emissions;

Bibliography

[1] California ISO *Renewables Watch*,
http://content.caiso.com/green/renewrpt/20170409_ DailyRenewablesWatch.pdf.

[2] P. K. Nag *Power Plant Engineering*,
McGraw Hill Education (India) Ltd., Green Park Extension, New Delhi 110 016, India,
2015,
53.

[3] M. R. Kolhe et Al. *Thermal Stress Analysis in Steam Turbine Rotor - A Review*,
IOSR Journal of Mechanical and Civil Engineering (IOSR-JMCE)
2014,
83-86.

[4] H. Pour-mohamadian *Transient Inelastic Thermal Stresses in a Solid Cylinder With Temperature Dependent Properties*,
Louisiana State University, LSU Historical Dissertations and Theses, Baton Rouge, Louisiana 70803, USA
1982,
Chapter IV, 38-39.

[5] Fisher Controls International, Inc. *Control Valve Handbook, Third Edition*,
Marshalltown, Iowa 50158 U.S.A.
2001,
Chapter 5, 118.

[6] VDI, Gesellschaft Verfahrenstechnik und Chemieingenieurwesen (GVC) *VDI Heat Atlas, Second Edition*,
VDI-Platz 1, 40468 Duüsseldorf, Germany
2010,
Chapter G1, 693-697.

[7] VDI, Gesellschaft Verfahrenstechnik und Chemieingenieurwesen (GVC) *VDI Heat Atlas, Second Edition*,
VDI-Platz 1, 40468 Duüsseldorf, Germany
2010,
Chapter G1, 725-728.

[8] VDI, Gesellschaft Verfahrenstechnik und Chemieingenieurwesen (GVC) *VDI Heat Atlas, Second Edition*,
VDI-Platz 1, 40468 Duüsseldorf, Germany
2010,
Chapter H3.4, 813-827.